INSTITUTE
FOR
AEROSPACE STUDIES

UNIVERSITY OF TORONTO

AN ANALYTICAL AND NUMERICAL STUDY OF THE INTERACTION OF RAREFACTION WAVES WITH AREA CHANGES IN DUCTS

PART 2: AREA ENLARGEMENTS

by

O. Igra, J. J. Gottlieb and T. Saito

December 1984

UTIAS Report No. 273
CN ISSN 0082-5255

AN ANALYTICAL AND NUMERICAL STUDY OF THE INTERACTION OF RAREFACTION WAVES WITH AREA CHANGES IN DUCTS

PART 2: AREA ENLARGEMENTS

by

O. Igra, J. J. Gottlieb and T. Saito

Submitted August 1984

December 1984

UTIAS Report No. 273
CN ISSN

Acknowledgements

The authors would very much like to thank Mr. P. M. Ostaff for his capable assistance with the quasi-steady flow analysis. Thanks are also due to Mr. T. W. Crouch for helping with one of the random-number generator algorithms, Mr. H. S. I. Sadek for handling part of the work processing involved with the manuscript, Mr. C. P. T. Groth for his proof reading of the manuscript, and Mr. C. Basdeo for the printing, collating and stapling of this report.

The encouragement received from Professor I. I. Glass was very helpful and much appreciated.

The financial support received mainly from the Defence Research Establishment Suffield, Ralston, Alberta, Canada, and partly from the Natural Sciences and Engineering Council of Canada is also very gratefully acknowledged.

Abstract

The interaction of a rarefaction wave with a gradual monotonic area enlargement of finite length in a duct or pipe is studied both analytically and numerically. A quasi-steady flow analysis that is analytical for an inviscid flow of a perfect gas is presented first, to obtain asymptotic solutions for the flow at late times, after all transient disturbances from the interaction process have subsided. Analytical results are given and discussed for the boundary between the two possible asymptotic wave patterns that are predicted and the corresponding asymptotic strengths of the transmitted, reflected and other waves, all as a function of both the incident rarefaction-wave strength and area-enlargement ratio. This was done for both perfect diatomic gases and air with $\gamma = 7/5$ and perfect monatomic gases with $\gamma = 5/3$. Finally, numerical results obtained by employing the new random-choice method to solve the nonstationary equations of motion are presented and discussed for the complete unsteady rarefaction-wave interaction with the area enlargement, for numerous different combinations of rarefaction-wave strengths and area-enlargement ratios. These results show clearly how the transmitted, reflected and other waves develop and evolve with time, until they eventually attain constant strengths at late times, in good agreement with the quasi-steady flow predictions for the asymptotic wave patterns.

Table of Contents

Notation

a	speed of sound $[a = (\gamma RT)^{1/2} = (\gamma p/\rho)^{1/2}]$
C_p	specific heat at constant pressure
C_v	specific heat at constant volume
e	total energy per unit volume $[p/(\gamma-1) + \rho u^2/2]$
h	specific enthalpy (C_pT)
M	flow Mach number (u/a)
N	total number of grid points for the flow field
p	static pressure $(p = \rho RT)$
R	gas constant
s	specific entropy $[s = -(\gamma-1)^{-1} R \ln(p/\rho^\gamma)]$
S	local cross-sectional area of a duct or pipe
S_d	duct area downstream of the area enlargement
S_u	duct area upstream of the area enlargement
t	time
t_c	characteristic time for the nonstationary flow to settle down and become quasi-steady
Δt	time interval between successive spatial distributions of pressure, flow velocity, density, and entropy
T	static temperature
u	flow velocity
x	distance along the duct or through the area change

Notation (continued)

α	$(\gamma + 1)/(\gamma - 1)$
β	$(\gamma - 1)/(2\gamma)$
γ	specific heat ratio (C_p/C_v)
δ	length of the area enlargement or transition in the duct
ρ	static density
τ_c	nondimensional characteristic time for the nonstationary flow to become quasi-steady $(\tau_c = a_1 t_c/\delta)$
$\Delta\tau$	nondimensional time interval between successive spatial distributions of pressure, flow velocity, density, and entropy $(\Delta\tau = a_1 \Delta t/\delta)$

1. INTRODUCTION

Moving shock and rarefaction waves that interact with area changes are a common feature of nonstationary gas flows encountered in engineering practice and research. For example, they occur in the piping system of reciprocating engines and pumps, in gas transportation pipelines, and in various shock tubes and blast-wave simulators that have an area change in the driver or channel (or at the diaphragm location). In early work the method of characteristics was employed to predict nonstationary one-dimensional flows in ducts.[1-4] Because most of the tedious calculations had to be done by hand, the simple flows in constant-area duct segments could usually be handled as nonstationary but the flow across each area change between the constant-area segments was normally treated simply as being steady. Modern high-speed digital computers have now eliminated such approximation. Although modern gasdynamic computer codes based on the method of characteristics, finite-difference or finite-element methods, and the random-choice method can now be employed to solve such nonstationary internal flow problems,[5-7] it is important to study separately the simple and straightforward interactions of shock and rarefaction waves with an area change in a duct. Fundamental knowledge gained from these studies is invaluable in interpreting the behavior of more complex flows.

The interaction of shock waves with area changes of finite length in ducts has been studied fairly thoroughly during the past three decades. Most of the early research incorporated a quasi-steady flow analysis,[3-4,8-16] with the most comprehensive and detailed approach being presented in a paper by Oppenheim, Urtiew, and Laderman[12], although a couple of papers used a nonstationary flow analysis.[3,15] Only more recent research specifically unites and exploits both types of analyses.[17] By contrast, no work of a similar nature is available for the case of the interaction of a rarefaction wave with an area change, although previous research[1-4,9,14] certainly contain relevant basic information.

It should be mentioned here that approximate analytical methods are also available for shock waves moving in variable area ducts,[18-23] but such methods do not apply to the case of rarefaction waves. In any case, these methods of approximate analysis, although valuable, are not of interest in this report.

The aim of this study is to use both the quasi-steady and nonstationary flow analyses to obtain basic detailed results that apply in general to the case of a rarefaction wave interacting with an area enlargement. Attention is devoted to understanding the nature of the transient flow phenomena that will eventually establish the quasi-steady flow at late times, after all transient disturbances from the interaction process have subsided. This work is a sequel to recent studies involving the interaction of a rarefaction wave with an area reduction.[24-25] These studies are complementary, providing a clear picture of the nonstationary interaction process from early to late times for rarefaction waves passing through both gradual monotonic area reductions and enlargements.

2. ANALYTICAL AND NUMERICAL ANALYSES

2.1 Quasi-Steady Flow Analysis

A rarefaction wave moving in a quiescent gas toward an area enlargement in a duct or pipe is illustrated in Fig. 1. Spatial distributions of pressure and flow velocity are both shown at the top of the figure, and it can be seen that

this wave produces a flow that moves in the opposite direction to its motion. Depending on the magnitudes of the area-enlargement ratio (S_d/S_u) and incident rarefaction-wave strength (i.e., pressure ratio p_2/p_1 across this wave), the rarefaction wave interaction with the area enlargement will result in one of only two different possible postulated wave patterns shown schematically in Fig. 2. A transmitted rarefaction wave and a reflected shock wave appear in wave patterns A and B. Owing to the existence of the shock wave, a contact surface or contact region also occurs in both patterns. An upstream-facing rarefaction wave appears only in wave pattern B, just downstream of the area change. Its head is stationary at the flow outlet of the area enlargement (where the outflow is sonic), and the remainder of this wave is swept downstream by the ensuing supersonic flow.

The boundary between pattern A and B is defined simply in the following manner. This boundary is where the outflow from the area change is just sonic and the upstream-facing rarefaction wave is a Mach wave (with no pressure or flow velocity change). That is, the head and tail of this wave coincide - the fan is not spread out but vertical - and they are stationary at the flow outlet of the area change.

The interaction of the incident rarefaction wave with the area enlargement is initially a nonstationary or an unsteady flow process. However, as local disturbances subside or disappear, through both wave reflection and coalescing processes, the flow will eventually become quasi-steady or steady. That is, the rarefaction and shock waves will eventually develop constant strengths and, at this stage, these waves and the contact region will separate fully developed regions of steady flow. The solution for the quasi-steady flow properties for asymptotic wave patterns A and B can be obtained analytically, and the solution procedure is outlined herein.

For an inviscid flow of a perfect gas, the flow properties in regions 1 and 6 on either side of the transmitted rarefaction wave (see Fig. 2) are connected by an equation for a negatively sloped characteristic line that crosses a simple rarefaction or expansion wave,[4,26]

$$\frac{2}{\gamma-1}\,a_6 - u_6 = \frac{2}{\gamma-1}\,a_1 - u_1 \qquad (1)$$

(with $u_1 = 0$), and the isentropic relations

$$p_6/p_1 = [T_6/T_1]^{\gamma/(\gamma-1)} = [a_6/a_1]^{2\gamma/(\gamma-1)} = [\rho_6/\rho_1]^{\gamma}. \qquad (2)$$

The symbols p, T, a, ρ, u, and γ denote pressure, temperature, sound speed, density, flow velocity, and specific-heat ratio, respectively. If the strength p_6/p_1 of the transmitted rarefaction wave is specified, for convenience instead of p_2/p_1 of the incident rarefaction wave, all of the flow properties in region 6 can be obtained directly from Eqs. 1 and 2, because the flow properties in region 1 are known initial conditions.

For a one-dimensional, isentropic, steady flow in the area enlargement, from region 6 to region 5, the basic continuity and energy equations,[4,26]

$$\rho_5\, u_5\, S_d = \rho_6\, u_6\, S_u\,, \qquad (3)$$

$$h_5 + u_5^2/2 = h_6 + u_6^2/2\,, \qquad (4)$$

along with the sound-speed relation $a = (\gamma RT)^{1/2} = (\gamma p/\rho)^{1/2}$ and the enthalpy

$h = C_pT = \gamma RT/(\gamma-1)$, yield

$$p_5/p_6 = [T_5/T_6]^{\gamma/(\gamma-1)} = [a_5/a_6]^{2\gamma/(\gamma-1)} = [\rho_5/\rho_6]^{\gamma}$$

$$= \left[\frac{M_6}{M_5}\frac{S_u}{S_d}\right]^{2\gamma/(\gamma+1)} = \left[\frac{2 + (\gamma-1)M_6^2}{2 + (\gamma-1)M_5^2}\right]^{\gamma/(\gamma-1)} . \quad (5)$$

The symbols h, R and M denote the specific enthalpy, gas constant and flow Mach number (u/a), respectively. Because M_6 is dictated by previously determined information (u_6 and a_6) and the duct cross-sectional areas upstream (S_u) and downstream (S_d) of the area enlargement are specified, M_5 can be obtained from the latter part of Eq. 5. Values of the flow properties p_5, T_5, a_5 and ρ_5 then follow from the former part of Eq. 5, and u_5 is obtained quite simply from the product a_5M_5.

For the moment, consider only pattern A (Fig. 2), which does not have a downstream-swept rarefaction wave. Pattern B will be considered later but only briefly. The contact region in pattern A then separates regions 3 and 4 or 5. Regions 4 and 5 are coexistent or the same for pattern A. Because the pressure and flow velocity remain unchanged across the contact region, the values of these flow properties in region 3 follow from $p_3 = p_5$ and $u_3 = u_5$. Other flow properties in region 3, such as the temperature T_3 and the density ρ_3, are not generally equal to those in region 5 (T_5 and ρ_5). They can be calculated in the following manner.

Region 2 lies between the tail of the incident rarefaction wave and the reflected shock wave. The flow properties in this region are related to those in region 3 by the well-known Rankine-Hugoniot or shock relations,[4,26]

$$u_3 = u_2 - a_2(p_3/p_2 - 1)/[\gamma^2\beta(1 + \alpha p_3/p_2)]^{1/2} , \quad (6)$$

$$a_3 = a_2[(p_3/p_2)(\alpha + p_3/p_2)]^{1/2}\,[1 + \alpha p_3/p_2]^{-1/2} , \quad (7)$$

in which $\alpha = (\gamma+1)/(\gamma-1)$ and $\beta = (\gamma-1)/2\gamma$. Furthermore, the flow properties in region 2 can be related to the known initial conditions in region 1, by using the following isentropic equations for the incident rarefaction wave,[4,26]

$$\frac{2}{\gamma-1}a_2 - u_2 = \frac{2}{\gamma-1}a_1 - u_1 \quad (8)$$

(with $u_1 = 0$), and

$$p_2/p_1 = [T_2/T_1]^{\gamma/(\gamma-1)} = [a_2/a_1]^{2\gamma/(\gamma-1)} = [\rho_2/\rho_1]^{\gamma} . \quad (9)$$

These two expressions are simply Eqs. 1 and 2 with subscript 6 replaced by 2.

Equations 6 to 9 permit all of the flow properties in regions 2 and 3 to be determined, and thus the strength p_2/p_1 of the incident rarefaction wave, because values of the properties p_3 and u_3 are already known from previously described calculations for pattern A. The relevant equations can be combined to yield

$$\left[\frac{p_2}{p_1}\right]^{\beta} = 1 + \gamma\beta\frac{u_3}{a_1} + \beta^{1/2}\left[\frac{p_2}{p_1}\right]^{\beta}\left[\frac{p_3}{p_1}\frac{p_1}{p_2} - 1\right]\left[1 + \alpha\frac{p_3}{p_1}\frac{p_1}{p_2}\right]^{-1/2} , \quad (10)$$

from which p_2/p_1 can be obtained readily by iteration. Values of T_2, a_2, ρ_2 and u_2 then follow from Eqs. 8 and 9. Finally, a_3 is obtained from Eq. 7, T_3 follows from a_3 by the sound-speed relation, and ρ_3 follows from p_3 and T_3 by means of the equation of state. This then completes the development of the equations required for obtaining the flow properties and wave strengths for pattern A.

For the case of pattern B, the equations already introduced for pattern A simply need be supplemented to account for the additional downstream-swept rarefaction wave (see pattern B in Fig. 2). The two supplemental equations that now connect regions 4 and 5 across this rarefaction wave are given simply as [4,26]

$$\frac{2}{\gamma-1}\, a_4 - u_4 = \frac{2}{\gamma-1}\, a_5 - u_5, \tag{11}$$

$$p_4/p_5 = [T_4/T_5]^{\gamma/(\gamma-1)} = [a_4/a_5]^{2\gamma/(\gamma-1)} = [\rho_4/\rho_5]^{\gamma}, \tag{12}$$

which are Eqs. 1 and 2 with subscripts 6 and 1 becoming 4 and 5, respectively. Although these equations introduce additional variables, other variables simply disappear because the outflow from the area change for pattern B is now sonic ($M_5 = -1$), resulting in a similar but slightly modified calculation procedure with the same degree of difficulty as that for pattern A. Hence, any further explanation is not required. This completes the development of the procedure required for pattern B.

The procedure for obtaining a complete set of flow properties for wave patterns A and B, for some specified area ratio, is now outlined. The solution for pattern A covers a limited range of strengths of the incident and transmitted rarefaction waves. For the transmitted wave, the ratio p_6/p_1 takes on values from unity, for which there is no flow and all waves are Mach waves, to a minimum value of $\{p_6/p_1\}_{min}$, when the transmitted wave is strongest. This minimum value corresponds to the condition when the flow is choked at the flow outlet of the area change ($M_5 = -1$). The value of $\{p_6/p_1\}_{min}$ depends on the area-enlargement ratio, because it is equal to $[1 - (\gamma-1)M_6/2]^{-1/\beta}$ from Eqs. 1 and 2, with M_6 given implicitly from $S_u/S_d = -M_6^{-1}[2/(\gamma+1) + M_6^2/\alpha]^{\alpha/2}$ from the latter part of Eq. 5 (with $M_5 = -1$). Hence, a complete set of flow properties and the strength of the incident rarefaction wave can be obtained for pattern A by first specifying p_6/p_1 over the entire range from unity to $\{p_6/p_1\}_{min}$ and then by using the equations presented for pattern A, in the manner described previously.

The set of flow properties for pattern B, for a specified area ratio, can be calculated in the following manner. For this case the flow is always choked as it just leaves the area change ($M_5 = -1$), and the strength of the transmitted rarefaction wave and the values of the flow properties in regions 5 and 6 are fixed. These limiting conditions with $M_5 = -1$ and $p_6/p_1 = \{p_6/p_1\}_{min}$ are obtained from calculations for pattern A, by making use of Eqs. 1 to 5. For subsequent calculations of the flow properties in regions 2, 3 and 4, it is now most convenient to specify the strength of the downstream-swept rarefaction wave (p_4/p_5), instead of p_2/p_1 for the incident rarefaction wave. All of the flow properties in region 4 can be now obtained from Eqs. 11 and 12. The flow properties in regions 2 and 3, as well as the strength of the incident rarefaction wave, then follow from equations 6 to 10. Note that, as p_4/p_5 for the

downstream-swept rarefaction wave is varied in the range from unity (Mach wave) to zero (strongest and a complete expansion wave), then p_2/p_1 for the incident rarefaction wave decreases from its upper value, corresponding to $\{p_6/p_1\}_{min}$, to zero, which also corresponds to a complete expansion wave.

2.2 Nonstationary Flow Analysis

The continuity, momentum, and energy equations for one-dimensional, nonstationary, inviscid gas flows, written in conservation form, are given as[4,26]

$$\frac{\partial}{\partial t}(\rho) + \frac{\partial}{\partial x}(\rho u) = -\frac{1}{S}\frac{dS}{dx}(\rho u) , \tag{13}$$

$$\frac{\partial}{\partial t}(\rho u) + \frac{\partial}{\partial x}(\rho u^2 + p) = -\frac{1}{S}\frac{dS}{dx}(\rho u^2) , \tag{14}$$

$$\frac{\partial}{\partial t}(e) + \frac{\partial}{\partial x}(ue + up) = -\frac{1}{S}\frac{dS}{dx}(ue + up) , \tag{15}$$

where the new symbols x, t, S and e denote distance, time, duct cross-sectional area and total energy per unit volume, respectively. The total energy is the sum of both the internal energy $\rho C_v T$ and kinetic energy $\rho u^2/2$, which is often expressed as $p/(\gamma-1) + \rho u^2/2$ for a perfect gas. Finally, this set of equations is completed by the thermal equation of state for a perfect gas, which is given by $p = \rho RT$.

For computations for the problem of a rarefaction wave interacting with an area enlargement in a duct or channel, the specific variation of area S(x) is required. For this study the area change between two constant-area ducts of upstream area S_u and downstream area S_d is specified by

$$S(x) = S_d \exp[\ln(S_u/S_d)^{1/2}(1 - \cos\{\pi x/\delta\})] , \tag{16}$$

for which $x = 0$ at the small end (S_d) and $x = \delta$ at the large end (S_u). This particular area change of finite length δ has a monotonic transition and can be used for both an enlargement and a reduction. It was chosen because

$$\frac{1}{S}\frac{dS}{dx} = (\pi/2\delta)\ln(S_u/S_d)\sin(\pi x/\delta) \tag{17}$$

is a symmetric, sinusoidal transition, which is advantageous over asymmetrical area-change variations in reducing numerical noise in the computed flow-field properties.

Equations 13 to 17 are solved numerically in the present study, by using the random-choice method (RCM) invented by Glimm[27] and first applied successfully by Chorin,[28] which is well suited for solving such problems. Shock waves and contact surfaces are well defined with sharp fronts in this method, unlike finite-difference methods in which they are normally smeared out over many mesh zones, owing to the detrimental effects of explicit artificial and implicit numerical viscosities. The operator-splitting technique introduced to the RCM by Sod,[29] in order that one-dimensional flow problems with area changes could be solved, is also employed in this study. Note that the RCM is a first-order, explicit, numerical scheme that repeatedly solves a Riemann or extended shock-tube problem between two grid points, and details of this method can be found elsewhere[7,27-29].

3. RESULTS AND DISCUSSION

3.1 Quasi-Steady Flow

For the interaction of a rarefaction wave with an area enlargement in a duct (Fig. 1), two different wave patterns shown schematically in Fig. 2 were postulated. Based on the quasi-steady flow analysis presented earlier, the domains and boundary for these two patterns can be calculated as a function of the incident rarefaction-wave strength p_2/p_1 and the duct area ratio S_d/S_u. As mentioned earlier in section 2.1, the boundary corresponds to the conditions when the flow is choked ($M_5 = -1$) and the downstream-swept rarefaction wave is just a Mach wave ($p_4 = p_5$). Results obtained for perfect diatomic gases and air with $\gamma = 7/5$ are given in Fig. 3. Additional results for monatomic gases with $\gamma = 5/3$ and a polyatomic gas with $\gamma = 11/10$ are also shown, to illustrate the effects of different specific-heat ratios. Patterns A and B are the only two wave patterns that can exist for the entire range of values of p_2/p_1 and S_d/S_u (between 0 and 1).

Expressions to give values of p_2/p_1 for the two end points of the boundary between patterns A and B can be derived from the previous equations, by finding the two limiting conditions when S_d/S_u goes to both unity and zero. The final results are

$$\frac{p_2}{p_1} = \left[\frac{2}{\gamma + 1}\right]^{2\gamma/(\gamma-1)} \tag{18}$$

and

$$\frac{1 - \frac{\gamma - 1}{2}\left[\frac{2}{\gamma + 1}\right]^{1/2}}{\left[\frac{p_2}{p_1}\right]^{\beta}} = \frac{\frac{p_2}{p_1} - \left[\frac{2}{\gamma + 1}\right]^{\gamma/(\gamma-1)}}{\left[\frac{1}{\beta}\frac{p_2^2}{p_1^2} + \frac{\alpha}{\beta}\frac{p_2}{p_1}\left[\frac{2}{\gamma + 1}\right]^{\gamma/(\gamma-1)}\right]^{1/2}} - 1 \tag{19}$$

for the two end points at the top and bottom borders, respectively. Note that the limiting value of p_2/p_1 for the boundary at the bottom border can only be obtained by iteration from the last equation.

The strength p_6/p_1 of the transmitted rarefaction wave is shown in Fig. 4, in terms of the incident rarefaction-wave strength p_2/p_1 and area-enlargement ratio S_d/S_u, for perfect diatomic gases and air with $\gamma = 7/5$. The domains corresponding to patterns A and B are also indicated and separated by a dashed line. As p_2/p_1 decreases from unity to zero, for a particular value of S_d/S_u, p_6/p_1 first decreases from unity to $\{p_6/p_1\}_{min}$ in region A and then remains constant at this latter value throughout region B. Because the flow at the outlet of the area change is choked for region B, the strength of the transmitted wave remains constant. The transmitted rarefaction wave is weaker than the incident rarefaction wave, for a fixed area ratio, because p_6/p_1 is larger than p_2/p_1. For a fixed strength of the incident wave, an increase in the area-enlargement ratio results in a stronger transmitted wave. For a fixed strength p_2/p_1 of the incident wave, an increase in the area-enlargement ratio S_d/S_u results in a stronger transmitted wave. The transmitted wave is merely a Mach wave when the area ratio S_d/S_u is zero (i.e., S_u is infinitely larger than S_d), and it is strongest when $S_d/S_u = 1$ (i.e., no change in duct area). For

this case with pattern A, the incident rarefaction wave merely becomes the transmitted rarefaction wave, resulting in p_6/p_1 being equal to p_2/p_1 (as one would, of course, expect for a constant-area duct). For the case of pattern B, the first part of the incident wave from its head, where there is no flow, to the point within the wave, where the flow is sonic, becomes the transmitted wave, and the remainder from the sonic point to the tail (where the flow is supersonic) then becomes the upstream-facing but downstream-swept rarefaction wave.

The strength p_3/p_2 of the reflected shock wave is shown in Fig. 5, also as a function of both the incident rarefaction-wave strength and area-enlargement ratio. For no change in cross-sectional area ($S_d/S_u = 1$) the reflected shock wave is merely a Mach wave or nonexistent ($p_3/p_2 = 1$). As the change in area becomes more severe (i.e., S_d/S_u decreases) and the incident rarefaction wave becomes stronger (p_2/p_1 decreases), the strength p_3/p_2 of the reflected shock wave increases, as could be expected.

It can be observed that the reflected shock wave is generally quite weak (i.e., p_3/p_2 is less than 1.5), unless the incident rarefaction wave is almost a complete expansion wave with a strength p_2/p_1 very close or equal to zero. Results from the quasi-steady analysis also indicated that changes in density, temperature, and entropy across the contact region were negligibly small. This means that a reflected compression wave instead of a reflected shock wave could have been used in the quasi-steady flow analysis, provided that values of p_2/p_1 were not too close to zero or equal to zero, and the calculated flow properties would have been virtually the same. For all practical purposes, therefore, it is inconsequential as to whether the weak reflected wave is taken to be a shock or compression wave in the quasi-steady flow analysis, provided that p_2/p_1 is greater than 0.01.

The strength p_4/p_5 of the downstream-swept rarefaction wave of pattern B is shown in Fig. 6, again as a function of p_2/p_1 and S_d/S_u. For a fixed area ratio, p_4/p_5 decreases almost linearly with decreasing values of p_2/p_1, from unity (at the boundary between patterns A and B) to zero when $p_2/p_1 = 0$. For a fixed incident rarefaction-wave strength, the downstream-swept rarefaction wave is stronger when the area change is more severe. However, the downstream-swept rarefaction wave is always weaker than the incident rarefaction wave. This, no doubt, should be expected since the origin of this downstream-swept rarefaction wave is the latter part of the incident rarefaction wave. Although this part of the wave passes through the reflected shock wave and contact region, being somewhat altered in the process, it cannot move forward against the supersonic flow (in region 5) and into the area enlargement.

For the case of a rarefaction wave interacting with an area enlargement when the gas is monatomic with $\gamma = 5/3$, graphical results for the strengths of the transmitted rarefaction wave, reflected shock wave, and downstream-swept rarefaction wave are presented in Figs. 7, 8, and 9, respectively. These new results are, in general, very similar to those just presented in Figs. 4 to 6 for the case of diatomic gases with $\gamma = 7/5$, and further discussion is therefore curtailed.

The listing of the computer program for the quasi-steady flow analysis for the interaction of a rarefaction wave with an area enlargement consists of two basic programs and is given in appendix A for interest and completeness. This program was used to obtain all of the data needed for producing Figs. 3 to 9. The first basic program listing is for the standard case of a reflected shock

wave from the interaction process. For the second one the reflected wave is taken to be a compression wave. Because the reflected wave is relatively weak, as mentioned earlier, it is inconsequential as to which one is actually used to compute the quasi-steady flow-field properties, and this is especially true if the incident rarefaction-wave strength p_2/p_1 is greater than 0.01. The second program was used to verify this fact.

3.2 Nonstationary Flow

Numerical results obtained by using the RCM for solving the interaction of a rarefaction wave with an area enlargement are now presented graphically and discussed, in order to illustrate clearly how the transmitted, reflected, and other waves form, evolve with time, and eventually attain constant strengths as they become quasi-steady, in agreement with quasi-steady flow predictions for the asymptotic wave patterns. Computations were made for numerous different combinations of values of the incident rarefaction-wave strength p_2/p_1 and area-enlargement ratio S_d/S_u, and numerical results for ten different cases are presented and discussed herein. A convenient summary of the locations of the ten cases in the S_d/S_u-versus-p_2/p_1 plane is presented in Fig. 10. This figure will be very helpful later, in quickly locating the positions of a particular case; that is, in determining quickly and easily whether it is in the center of one of the two particular domains or near the boundary between them.

Numerical results obtained for the ten cases are given in Figs. 11 to 20, in the form of separate sets of spatial distributions at successive time levels for nondimensional pressure p/p_1 and flow velocity u/a_1. Each successive distribution in Figs. 11 to 20 is displaced upward slightly from the previous one, both for clarity and to produce the effect of a time-distance diagram. The nondimensional time interval between adjacent or successive distributions is given by $\Delta\tau = a_1\Delta t/\delta$, and the nondimensional value of $\Delta\tau$ for each case is given in the caption of the figure. The location of the area enlargement of length δ in the flow field is well indicated by the two closely spaced vertical dashed lines in each set of spatial distributions.

The incident rarefaction wave is specified initially, in the first or bottom distribution of each set, just to the left of the area enlargement. In each case it is distributed over a distance of nine-tenths of the length of the area change or $9\delta/10$. The initial flow velocity is specified to change linearly over this spatial interval, and all other flow properties can, of course, be derived from this variation and the specification of the strength p_2/p_1 of the incident rarefaction wave. Such a specification of the spatial properties of the incident rarefaction wave simply means that it was originally a centered rarefaction wave at some earlier distance and time. The flow field is computed with a total of 720 grid zones, of which 20 zones are specifically allocated to the area enlargement and another 18 are allocated to the incident rarefaction-wave profile.

Graphical results for density, temperature and entropy are not presented, because they do not provide significant additional information, for the following reasons. In each example the flow is essentially isentropic and changes in the flow properties across the contact region are negligibly small, because the reflected shock wave is relatively weak. Hence, the entropy is essentially constant throughout the flow field, and sets of spatial distributions for density and temperature are very similar to those for the pressure. In fact, the density and temperature can be obtained easily from the pressure, for most

practical purposes, by using the usual isentropic equations like those given by Eq. 2.

The first set of numerical results for the pressure and flow velocity is given in Fig. 11, for the case of $p_2/p_1 = 0.80$ and $S_d/S_u = 0.50$, corresponding to a point near the center of the domain of pattern A (Fig. 10). The incident rarefaction wave is shown clearly in the bottom distribution, just prior to its impingement on the area enlargement. Its subsequent interaction with the area change can be observed in the following distributions, where the formation and evolution of the transmitted rarefaction wave and reflected shock wave can be seen clearly, as well as the eventual development of steady subsonic flow in and on both sides of the area change. It is evident that the reflected wave is initially a compression wave, whose front becomes steeper as it propagates away from the area enlargement, and it is obvious that a steep-fronted shock wave will eventually be formed (not shown in this figure). Note that the steady flow in the area change at later times is the expected subsonic nozzle flow. As the gas flows through the convergence in area (i.e., from right to left) the pressure decreases and the flow speed increases (becomes more negative). The flow velocity is negative simply because the flow is moving in the negative x direction.

The second set of numerical results is presented in Fig. 12, for the case when $p_2/p_1 = 0.50$ and $S_d/S_u = 0.80$, corresponding to a point in the upper part of the domain of pattern A. These results are similar to those of the previous case, but with one main difference. In this case the change in area is less severe and, although the incident rarefaction wave is stronger, the reflected wave is now weaker (by about 25%). This can be seen best from the quasi-steady flow results given in Fig. 5. Consequently, the steepening of the reflected compression wave to form a steep-fronted shock wave procedes much more slowly in this latter case, as is evident from the results in Fig. 12. Note that the reflected wave is less noticeable in Fig. 12 than Fig. 11, not only because this wave is 25% weaker, but also primarily because this wave is weak relative to the others and the pressure scale has therefore been suitably compressed by about 60%.

The third set of numerical results is given in Fig. 13, for the case when $p_2/p_1 = 0.50$ and $S_d/S_u = 0.20$, corresponding to a point in the lower part of the domain of pattern A. For this case with a fairly strong incident rarefaction wave and severe change in area, the reflected wave is now relatively strong. Therefore, the steepening of the compression wave into a steep-fronted shock wave occurs more quickly, as shown. Note that the spatial distributions contain more numerical noise than those for the last two cases, mainly because the change in area is more severe. This noise is typical of RCM calculations for flows through rapidly changing areas, and the noise level can generally be reduced by using a finer grid or more appropriate random-number algorithm (see section 3.3).

Numerical results for three additional cases for which p_2/p_1 and S_d/S_u correspond to different points in the domain of pattern A are shown in Figs. 14 to 16 (see these figures and Fig. 10). Besides substantiating a number of the previous comments, these results provide additional insight into the nature of the transient flow behavior. Again, the results obtained for the large area changes (Fig. 14 for which $S_d/S_u = 0.10$) have a fairly high level of numerical noise, whereas those for small area changes (Fig. 16 for which $S_d/S_u = 0.90$) are practically free of noise. As one might expect, the reflected wave is clearly noticeable in Fig. 14 for a severe area change ($S_d/S_u = 0.10$), and this

compression wave steepens into a shock wave, whereas the compression wave shown in Fig. 16 for a small area change ($S_d/S_u = 0.90$) is barely visible and it also steepens very slowly.

It is apparent from the numerical results presented in Figs. 11 to 16 that the wave pattern that emerges at late times is always pattern A. This was also true for other numerical results for values of p_2/p_1 and S_d/S_u that correspond to points in the domain of quasi-steady wave pattern A, even when points are taken very close to the boundary to pattern B. Furthermore, pattern A emerges fairly quickly in the numerical results, and both the computed flow properties in various quasi-steady flow regions and the wave strengths converge fairly rapidly to those predicted by the quasi-steady flow analysis. This occurs after the tail of the incident wave enters the area change and shortly after the tails of the transmitted and reflected waves leave the vicinity of the area change, afterwhich quasi-steady flow regions of increasing spatial extent begin to develop on either side of the area change. The flow properties in these growing regions are generally within 5% of the quasi-steady flow predictions by the time the tail of the last wave leaving the area change has moved about three area-transition lengths (3δ) away from the area change. These observations illustrate that the simple quasi-steady flow analysis can be used in practice to determine the quasi-steady flow properties and the transmitted and reflected wave strengths for pattern A, not only at late times but also at fairly early times.

The seventh set of numerical results is presented in Fig. 17, for the case of $p_2/p_1 = 0.10$ and $S_d/S_u = 0.50$, corresponding to a point near the center of the domain of pattern B (see Fig. 10). The incident rarefaction wave is again shown in the bottom distribution, just prior to its impingement on the area enlargement. Its subsequent interaction with the area change can be observed in the following distributions, where the formation and evolution of the transmitted and downstream-swept rarefaction waves can be clearly observed. Both of these waves are spreading out at later times, and a quasi-steady flow region of increasing lateral extent develops between the transmitted wave and the area change. The reflected compression wave is just noticeable, mainly because the other waves are much stronger and the pressure scale has been highly compressed. Any steepening of this compression wave in the computed flow field is barely visible.

In this seventh example, the strong incident rarefaction wave produces a sufficiently low pressure just downstream of the area change such that the flow is first accelerated to sonic or choked conditions at the flow outlet of the area change. This flow is then further accelerated to supersonic speeds as it moves through the downstream-swept rarefaction wave (being supersonic in quasi-steady flow region 4 of pattern B.

Two additional sets of numerical results are presented in Figs. 18 and 19, for the sets of conditions given by $p_2/p_1 = 0.10$ and $S_d/S_u = 0.80$ and finally $p_2/p_1 = 0.20$ and $S_d/S_u = 0.20$, corresponding to points in the upper and lower parts of the domain of pattern B, respectively. These results are similar to those for the previous example, but they differ somewhat in detail. In the results shown in Fig. 18 the reflected compression wave is barely visible, and the quasi-steady flow region between the transmitted wave and area change forms fairly late and also grows slowly in lateral extent. In Fig. 19, the reflected compression wave that is steepening into a shock wave is now clearly observed. Furthermore, the transmitted wave is fairly weak and its rarefaction-wave fan therefore diverges slowly in this latter case.

The tenth and final set of numerical results is presented in Fig. 20, for the case of $p_2/p_1 = 0.30$ and $S_d/S_u = 0.50$, corresponding to a point that also lies in the domain of pattern B but fairly close to the boundary between patterns A and B (see Fig. 10). In this case the downstream-swept rarefaction wave is extremely weak and barely forms a fan that spreads out with time, as one would expect. Compare this case to that in Fig. 17, for which S_d/S_u also equals 0.50 but the incident rarefaction wave is stronger with $p_2/p_1 = 0.10$, to see a much wider spread downstream-swept rarefaction-wave fan. Because the downstream-swept rarefaction-wave fan is not spreading out much with time, the quasi-steady flow region that forms between this fan and the reflected wave is wide spread.

It is apparent from the numerical results given in Figs. 17 to 20 that wave pattern B always emerges at late times. This was also true for all other results for values of p_2/p_1 and S_d/S_u corresponding to points in the domain of pattern B, even when points were selected close to the boundary to pattern A. Furthermore, it can be seen that pattern B also emerges fairly quickly in the flow field, and both the computed flow properties and wave strengths were found to converge relatively rapidly to those predicted by the quasi-steady flow analysis.

However, the time required for pattern B to be established is always somewhat longer than that required to establish pattern A, for the following reason. The initial part of the incident rarefaction wave first establishes pattern A, which is then altered or extended to pattern B by the latter portion of the incident rarefaction wave. This alteration takes place rapidly, and pattern B does not take much longer to be established than pattern A. These observations illustrate that the quasi-steady flow analysis can be employed in practice to determine the quasi-steady flow properties and the transmitted and reflected wave strengths for pattern B, like those for pattern A, not only at late times but also at fairly early time.

The time for the nonstationary flow to become quasi-steady and establish pattern A and B has been discussed only qualitatively. In order to obtain some quantitative results, a definition of a characteristic time is needed. Let the characteristic time t_c be defined as the time interval measured from when the incident rarefaction wave first encounters the area enlargement until all of the nonstationary flow properties in 'quasi-steady' flow regions between distinct waves are within 5% of the quasi-steady flow predictions. Based on this simple definition, the nondimensional characteristic time $\tau_c = a_1 t_c/\delta$ obtained from many numerical results are shown versus the incident rarefaction-wave strength in Fig. 21. The characteristic times, shown as a band, increase for stronger incident rarefaction waves and decreasing values of p_2/p_1. This could have been expected because a stronger rarefaction wave has a wider fan of characteristics that would take longer to complete its interaction with the area enlargement.

The characteristic times are presented in the form of a band instead of a single or multiple curves for the following two reasons. Firstly, the choice of a characteristic time from numerically predicted results for the nonstationary flow properties to come within 5% of the quasi-steady flow predictions is somewhat arbitrary, because the numerical results contain numerical noise or random fluctuations that are characteristic of the RCM. For this reason alone, precise values could not be obtained in this investigation. Finally, the characteristic times were discovered to be weakly dependent on the area-enlargement ratio S_d/S_u, which could not be determined with precision from the numerical

results. However, the trend discovered was that the characteristic times were always slightly longer for more severe area enlargements, for a given value of the incident rarefaction-wave strength p_2/p_1.

For the numerical results presented in Figs. 11 to 20, the spatial extent of the incident rarefaction wave was always taken as nine-tenths of the length of the area enlargement. When the spatial extent of this wave was reduced, it was found that the transient-flow behavior did not change appreciably and the time to establish a particular pattern did not become significantly shorter. When the spatial extent was increased, however, the transient-flow behavior was again similar but extended proportionally in time.

The listing of the RCM computer program for the nonstationary computations of the interaction of a rarefaction wave with an area enlargement is not given in this reprort, because it is the same as that already presented in a sequel to this report[24], where it can be obtained easily. This computer program was used to generate all of the numerical results plotted in Figs. 11 to 25.

3.3 Numerical Noise Reduction in the RCM Results

During the presentation and discussion of the RCM numerical results in the previous section, it was noted on a couple of occassions that numerical noise of different severity occurred in the spatial distribution of the pressure and flow velocity and that the noise level was worse for more severe area changes. The severity of the numerical noise is dependent on the size or fineness of the grid and also on the particular algorithm of the random-number generator. By using a finer grid and a more suitable random-number algorithm, the level of the undesirable numerical noise can most often be reduced. The usual questions involve how much can the noise be reduced, how can this be accomplished, and what is the cost. The effects of grid size and the random-number algorithms are investigated in next two subsections, in order to get some answers to the above questions.

3.3.1 Effects of the Grid Size on the Noise Level

The effects of grid size on the level of the numerical noise can be rather extreme, if the grid is too coarse, as well as adversely affecting the accuracy of computational results, as most researchers involved in computational fluid dynamics already know. In this report the number of grid zones adopted for the flow field was 720, a fairly large number. In the authors' opinion this was sufficient to reduce numerical noise to an acceptable level and also maintain a reasonable accuracy, both of which are subjective assessments. The level of the numerical noise in some examples, such as the results given in Fig. 13 for the case of $p_2/p_1 = 0.50$ and $S_d/S_u = 0.20$, is still bothersome. Hence, this example was rerun with twice the number of grid zones (i.e., 1440), keeping all other factors constant, in order to illustrate how much the numerical noise could be reduced. The new set of results is shown in Fig. 22 for comparison. One can see clearly that the level of the numerical noise has been reduced, but the reduction is not highly significant even though it is quite beneficial. If the number of grid zones had instead been reduced by one-half from 720 to 360, then the numerical noise in the results (not shown here) would have increased by a much larger factor, making the numerical results unacceptable. From results such as these, the decision was made to use 720 grid zones to obtain results with an acceptably low numerical noise level, although the number of

grid zones could also have been selected in the range of 600 to 720, to obtain slightly worse but probably acceptable numerical results.

The detrimental effect of increasing the number of grid zones to reduce the level of numerical noise is an increase in the computational time and cost to obtain the numerical results. For example, the increase in the number of grid points by a factor of two, from 720 to 1440, for the previous results and discussion causes a large increase in the central processor unit (CPU) time by a factor of slightly less than four, which is fairly significant considering that this results in about a four-fold increase in cost. This is typical for doubling the number of grid points in the RCM, with times and costs increasing by a factor of 3.8 to 4. Hence, any reduction in the number of grid points, without markedly increasing the number of computations per unit cell or grid zone, is highly beneficial from the point of view of cost efficiency.

It is worth pointing out here that a second-order accurate RCM has been developed and used,[30-32] and similar quality results as those given in this report with 720 grid zones can be obtained with only 100 grid zones. However, the computer program logic is now markedly more complex and therefore difficult to learn how to use and change for solving different problems.[32] Furthermore, and most importantly, the increase in the number of calculations at each step or grid zone to make the method second order is approximately offset by the reduction in calculations from employing fewer grid zones, and the resulting computational time and cost are not reduced.[32] In other words, similar quality numerical results having the same level of numerical noise are obtained with both the first- and second-order RCM with approximately the same CPU time and computational cost. It is for this reason that we have avoided the increased complexity of using the second-order RCM and simply applied our version of the simpler first-order method.

3.3.2 Effects of the Random-Number Algorithm on the Noise Level

An inherent aspect of the RCM is the use of random numbers. Actually, the RCM uses pseudo-random numbers, because no algorithm known today produces truly random numbers.[33] However, in this report we will refer to pseudo-random numbers simply as random numbers for brevity. Tables of random numbers which have been well tested and approved do exist,[34,35] but these are seldom used today because the RCM is not applied by hand but rather by digital computer, although tables of random numbers on punched cards for digital computers are available.[34] Furthermore, these random numbers are not the best for the RCM because equidistributed random numbers are required[28,36-37] (see appendix B). The best method available today for use with digital computers is to employ some specified rule, scheme or algorithm to obtain the necessary sequence of random numbers (actually psuedo-random numbers), and many different algorithms are now available for a variety of different uses.[38] Good questions to ask are does it matter which random-number algorithm is used and, if it does, which one is best suited for the RCM?

These questions have been considered by Chorin[28] and also by Colella[36-37] and other researchers in Japan (no references available), although one would think that they would be unimportant, provided each algorithm gives a sequence of random numbers with statistical properties not deviating significantly from those of truly random numbers. However, this has been found to be untrue, it does matter which random-number generator is employed in the RCM computations. With all other conditions held equal, some random-number algorithms are much

better than others in producing results with less numerical noise. The results to be given in this section add some new information and confirm previous work.

Four different random-number algorithms are considered in this study. The names given to these sampling schemes are listed below:

i) Chorin's sampling scheme,

ii) IMSL sampling scheme,

iii) Lax's sampling scheme,

iv) Van der Corput's sampling scheme.

Information regarding these different random-number sampling schemes, and also the computer program listings of their FORTRAN statements, are given for both interest and reference in appendix B. It is worth noting here that Chorin's sampling scheme is the one that has been employed in the RCM to generate all previous numerical results for the interaction of a rarefaction wave with both the area reductions and enlargements. This is true despite the fact that in the previous report[24] the computer program listing contains van der Corput's sampling scheme. This latter sampling scheme was included in the previous report as an update, partly because it was used in the program just before the listing was included in the report and partly because it proved to be the best sampling scheme, which would be used henceforth.

Numerical results to be compared to evaluate the effects of different random number algorithms in the RCM are all for one specific case. The strength p_2/p_1 of the incident rarefaction wave is 0.50 and the area-enlargement ratio S_d/S_u is 0.20, which corresponds to a point in the domain of wave pattern A. Only the random number scheme is changed. The first set of numerical results has already been presented in Fig. 13. Chorin's sampling scheme, which gives stratified random numbers (see appendix B), was used in the RCM to obtain these results. As mentioned earlier in the previous section, there is noticeable jaggedness or some numerical noise contained in these results, on both sides of the area enlargement, as well as inside the area change.

The second set of numerical results is presented in Fig. 23. In this case the sampling scheme from the International Mathematical and Statistical Library or IMSL,[39] which gives the most truly random numbers (see appendix B), was used in the RCM. It is immediately obvious that the degree of the jaggedness or the numerical noise in these results is markedly enhanced as compared to that of the previous case for Chorin's sampling scheme. In fact, the numerical noise is so severe that these new results would likely be deemed unacceptable for most engineering and scientific purposes.

The third and fourth sets of numerical results are presented in Figs. 24 and 25, for which Lax's sampling scheme[40] was employed in the RCM for the first set of results (Fig. 24) and Van der Corput's sampling scheme[33,41] was used for the latter set (Fig. 25). Both sampling schemes produce equidistributed random numbers (see appendix B). It is clear that these two sets of numerical results are significantly better than the ones obtained by the IMSL sampling scheme, by having significantly less jaggedness or numerical noise. Furthermore, they are also better than the results obtained by using Chorin's sampling scheme. Even though the improvement is not as marked as the improvement over the second case with the IMSL sampling scheme, it is still deemed significant.

By comparing the results shown in Figs. 24 and 25 from Lax's and Van der Corput's sampling schemes, it is the opinion of the authors that the better results are obtained by using Van der Corput's sampling scheme. Hence, of the four random number algorithms tested herein, it can be concluded that the best one is Van der Corput's sampling scheme. Note that the worst algorithm was the IMSL sampling scheme that gave random numbers that were the most truly random, the next best one was Chorin's sampling scheme that gave stratified random numbers, and the best ones were Lax's and Van der Corput's sampling schemes that gave equidistributed random numbers. This is in agreement with the theory of random numbers for the RCM, which shows that the best random-number algorithms for the RCM should be those that produce both nonrandom and equidistributed numbers.[28,36-37] (Please see the presentation given in appendix B). Note that, because Van der Corput's sampling scheme has a lower order error in the placement of shock-wave fronts in the flow field than that for Lax's sampling scheme,[36-37] it should be better and thus more preferable for use in the RCM. However, it is not possible to determine if this is true directly from the numerical results that are presented in this report, and one has to rely almost totally on theory.

4. CONCLUDING REMARKS

The interaction of rarefaction waves with gradual, monotonic area enlargements in otherwise constant area ducts has been investigated by employing two complementary analyses. The quasi-steady flow analysis that describes the flow behavior at late times was instrumental in establishing the two asymptotic wave patterns, including the asymptotic values of the quasi-steady flow properties and the asymptotic strengths of the transmitted, reflected and other waves, as a function of both the incident rarefaction-wave strength and area-enlargement ratio. The nonstationary flow analysis was necessary for the determination of the transient flow behavior from early to late times, and it therefore showed how the quasi-steady flow was eventually established. Note that the random-choice method was found to be excellent for solving this nonstationary flow problem, as has also been found for other similar problems in our previous work.[24,25]

The nonstationary flow analysis showed that the asymptotic wave patterns were established fairly rapidly for pattern A and somewhat longer for pattern B (see Fig. 21). Consequently, the quasi-steady flow analysis can be used to give a good estimate of the flow properties and strengths of the transmitted, reflected and other waves at relatively early times, which would have practical implications. However, when a detailed study of the transient wave behavior is needed, the nonstationary flow analysis is required to obtain more accurate flow-field predictions.

The flow was assumed to be one-dimensional for both the quasi-steady and nonstationary flow analyses. This assumption is reasonable for flow-field calculations of the interaction of a rarefaction wave with an area enlargement, for the following reason. The flow in the area change is a typical subsonic nozzle flow in which flow separation is suppressed by a favorable pressure gradient. Although viscous effects would become important for severe area changes, especially if the downstream area becomes very small, these effects have simply been ignored here. Including such effects is beyond the scope of this type of study.

5. REFERENCES

1. Schultz-Grunow, F., 'Nichtstationaire, Kugelsymmetrische Gasbewegung und Nichtstationaire Gasstromung in Dusen und Diffusoren,' Ingenieur-Archiv, Vol. 14, No. 1, pp. 21-29, 1943.

2. Schultz-Grunow, F., 'Gas Dynamic Investigation of the Pulse-Jet Tube,' NACA TM 1131, National Advisory Committee for Aeronautics, February 1947.

3. Bannister, F.K. and Mucklow, G.F., 'Wave Action Following Sudden Release of Compressed Gas from a Cylinder,' Proceedings of Industrial and Mechanical Engineering, Vol. 159, pp. 269-300, 1948.

4. Rudinger, G., 'Wave Diagrams for Nonsteady Flow in Ducts,' D. van Nostrand Co., New York, 1955. Also, 'Nonsteady Duct Flow: Wave-Diagram Analysis,' Dover Publications, New York, 1969.

5. Jones, A.D. and Brown, G.L., 'Determination of Two-Stroke Engine Exhaust Noise by the Method of Characteristics,' Journal of Sound and Vibration, Vol. 82, pp. 305-327, June 1982.

6. Beam, R.M. and Warming, R.F., 'An Implicit Factored Scheme for the Compressible Navier-Stokes Equations,' AIAA Journal, Vol. 16, pp. 393-402, April 1978.

7. Saito, T. and Glass, I.I., 'Applications of Random-Choice Method to Problems in Shock and Detonation-Dynamics,' University of Toronto Institute for Aerospace Studies, UTIAS Report No. 240, October 1979.

8. Parks, E.K., 'Supersonic Flow in a Shock Tube of Divergent Cross-Section,' University of Toronto Institute for Aerophysics (now Aerospace Studies), UTIA Report No. 18, May 1952.

9. Kahane, A., Warren, W.R., Griffith, W.C., and Marino, A.A., 'A Theoretical and Experimental Study of Finite Wave Interactions with Channels of Varying Area,' Journal of Aeronautical Sciences, Vol. 21, pp. 505-525, August 1954.

10. Laporte, O., 'On the Interaction of a Shock with a Constriction,' LASL Report No. LA-1740, Los Alamos Scientific Laboratory, Los Alamos, New Mexico, U.S.A., August 1954.

11. Bird, G.A., 'The Effect of Wall Shape on the Degree of Reinforcement of a Shock Wave Moving into a Converging Channel,' Journal of Fluid Mechanics, Vol. 5, Part 1, pp. 60-66, January 1959.

12. Oppenheim, A.K., Urtiew, P.A., and Stern, R.A., 'Peculiarity of Shock Impingement on Area Convergence,' Physics of Fluids, Vol. 2, No. 4, pp. 427-431, July-August, 1959.

13. Chester, W., 'The Propagation of Shock Waves Along Ducts of Varying Cross Section,' Advances in Applied Mechanics, Vol. 6, pp. 119-152, Academic Press, New York, 1960.

14. Oppenheim, A.K., Urtiew, P.A., and Laderman, A.J., 'Vector Polar Method for the Evaluation of Wave Interaction Processes,' Archiwum Budowy Maszyn (The Archive of Mechanical Engineering), Vol. XI, No. 3, pp. 441-495, 1964.

15. Rudinger, G. 'Passage of Shock Waves through Ducts of Variable Cross Section,' Physics of Fluids, Vol. 3, No. 3, pp. 449-455, May-June 1960.

16. Russell, D.A., 'Shock-Wave Strengthening by Area Convergence,' Journal of Fluid Mechanics, Vol. 27, part 2, pp. 305-314, February 1967.

17. Greatrix, D.R. and Gottlieb, J.J., 'An Analytical and Numerical Study of a Shock Wave Interaction with an Area Change,' University of Toronto Institute for Aerospace Studies, UTIAS Report No. 268, November 1982.

18. Meyer, R.E., 'On Waves of Finite Amplitude in Ducts: Part I - Wave Fronts, Part II - Waves of Moderate Amplitude', Quarterly Journal of Mechanics and Applied Mathematics, Vol. 5, part 3, pp. 257-291, 1952.

19. Chester, W., 'The Propagation of a Shock Wave in a Channel of Non-Uniform Width,' Quarterly Journal of Mechanics and Applied Mathematics, Vol. 6, part 4, pp. 440-452, 1953.

20. Chester, W., 'The Quasi-Cylindrical Shock Tube,' Philosophical Magazine, Vol. 45, pp. 1293-1301, 1954.

21. Chisnell, R.F., 'The Motion of a Shock Wave in a Channel, with Application to Cylindrical and Spherical Shock Waves,' Journal of Fluid Mechanics, Vol. 2, part 3, pp. 286-298, May 1957.

22. Whitham, G.B., 'On the Propagation of Shock Waves Through Regions of Non-Uniform Area or Flow,' Journal of Fluid Mechanics, Vol. 4, part 4, pp. 337-360, 1958.

23. Rosciszewski, J., 'Calculations of the Motion of Non-Uniform Shock Waves,' Journal of Fluid Mechanics, Vol. 8, part 3, pp. 337-367, July 1960.

24. Gottlieb, J.J. and Saito, T., 'An Analytical and Numerical Study of the Interaction of Rarefaction Waves with Area Changes in Ducts -- Part 1: Area Reductions,' University of Toronto Institute for Aerospace Studies, UTIAS Report No. 272, November 1983.

25. Gottlieb, J.J. and Igra, O., 'Interaction of Rarefaction Waves with Area Reductions in Ducts,' Journal of Fluid Mechanics, Vol. 137, pp. 285-305, December 1983.

26. Owczarek, J.A., Fundamentals of Gasdynamics, International Textbook Co., Scranton, Pennsylvania, 1964.

27. Glimm, J., 'Solution in the Large for Nonlinear Hyperbolic Systems of Equations,' Communications of Pure and Applied Mathematics, Vol. 18, No. 4, pp. 697-715, November 1965.

28. Chorin, A.J., 'Random Choice Solution of Hyperbolic Systems,' Journal of Computational Physics, Vol. 22, No. 4, pp. 517-533, December 1976.

29. Sod, G.A., 'A Numerical Study of a Converging Cylindrical Shock,' Journal of Fluid Mechanics, Vol. 83, part 4, pp. 785-794, 1977.

30. Glimm, J., Marshall, G, and Plohr, B., 'A Generalized Riemann Problem for Quasi-One-Dimensional Gas Flows,' Advances in Applied Mathematics, Vol. 5,

No. 1, pp. 1-30, 1984.

31. Liu, T.P., 'Quasilinear Hyperbolic Systems,' Communications in Mathematical Physics,' Vol. 68, pp. 141-172, 1979.

32. Fok, S.K., 'Extension of Glimm's Method to the Problem of Gas Flow in a Duct of Variable Cross-Section,' Report No. LBL-12322, Lawrence Berkeley Laboratory, Physics, Computer Science and Mathematics Division, University of California, Berkeley, California, December 1980.

33. Hammersley, J.M. and Handscomb, D.C., 'Monte Carlo Methods,' Methuen and Company Limited, London, 1975.

34. Kendall, M.J. and Babington Smith, B., 'Tables of Random Sampling Numbers,' Tracts for Computers, Vol. 24, Cambridge University Press, 1939.

35. Anon., 'A Million Random Digits with 100,000 Normal Deviates,' RAND Corporation, Glencoe, Illinois, U.S.A., 1955.

36. Colella, P., 'Glimm's Method for Gas Dynamics,' Society for Industrial and Applied Mathematics, Journal of Scientific and Statistical Computing, Vol. 3, No. 1, March 1982.

37. Colella, P., 'An Analysis of the Effect of Operator Splitting and the Sampling Procedure on the Accuracy of Glimm's Method,' Report No. LBL-8874, Lawrence Berkeley Laboratory, Physics, Computer Science and Mathematics Division, University of California, Berkeley, California, U.S.A., December 1978.

38. Hull, T.E. and Dobell, A.R., 'Random Number Generators,' Society for Industrial and Applied Mathematics, Rev. 4, pp. 230-254, 1962.

39. Anon., 'International Mathematical and Statistical Library', International Mathematical and Statistical Libraries, Incorporated, Customer Relations, Sixth Floor, NBC Building, 7500 Bellaire Boulevard, Houston, Texas, U.S.A., June 1982.

40. Lax, P.D., 'Hyperbolic Systems of Equations and Computing,' Society for Industrial and Applied Mathematics, Review 11, pp. 7-19, 1969.

41. Van der Corput, 'Verteilungsfunktionen,' Proc. Kon. Adad. Wet., Vol. 38, pp. 813-821 and pp. 1058-1066, Amsterdam, 1935.

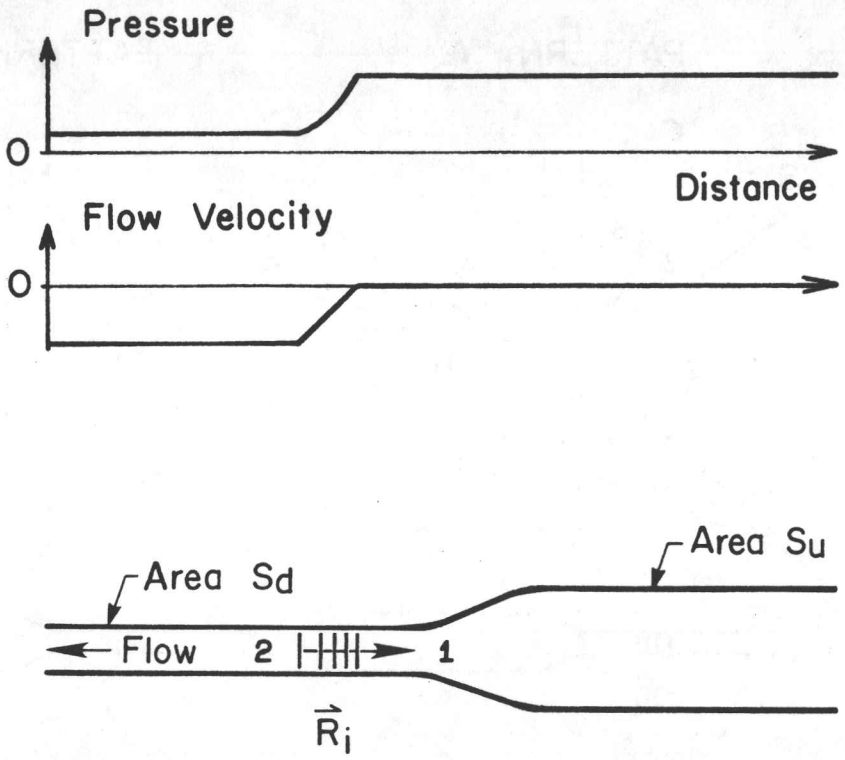

Fig. 1. Illustration of a rarefaction wave moving toward an area enlargement in a duct.

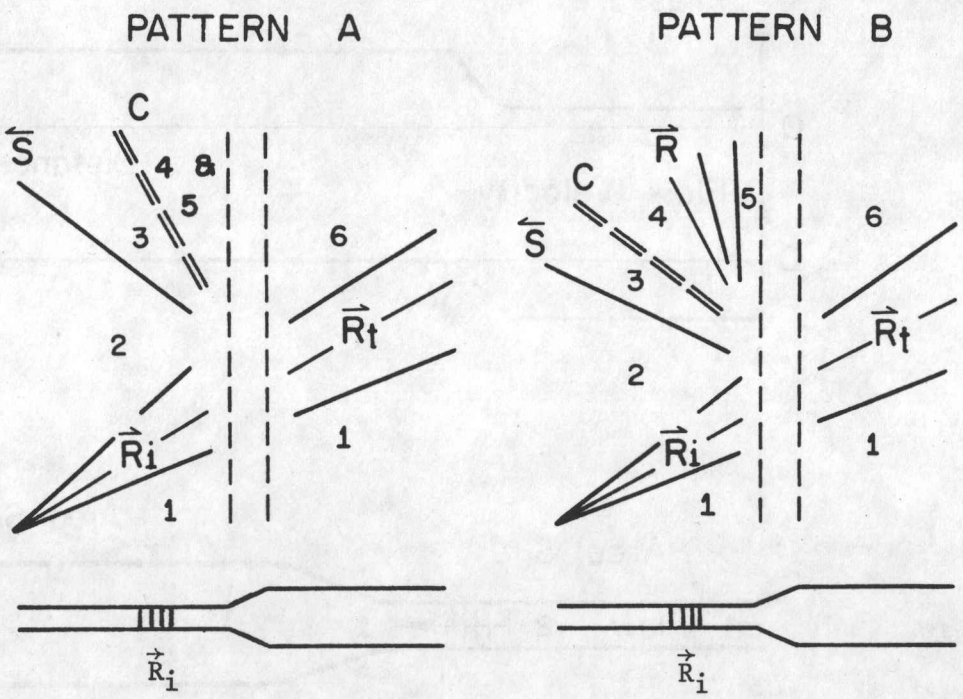

Fig. 2. Two different schematic quasi-steady wave patterns for the interaction of a rarefaction wave with an area enlargement in a duct. These are the only two possible wave patterns.

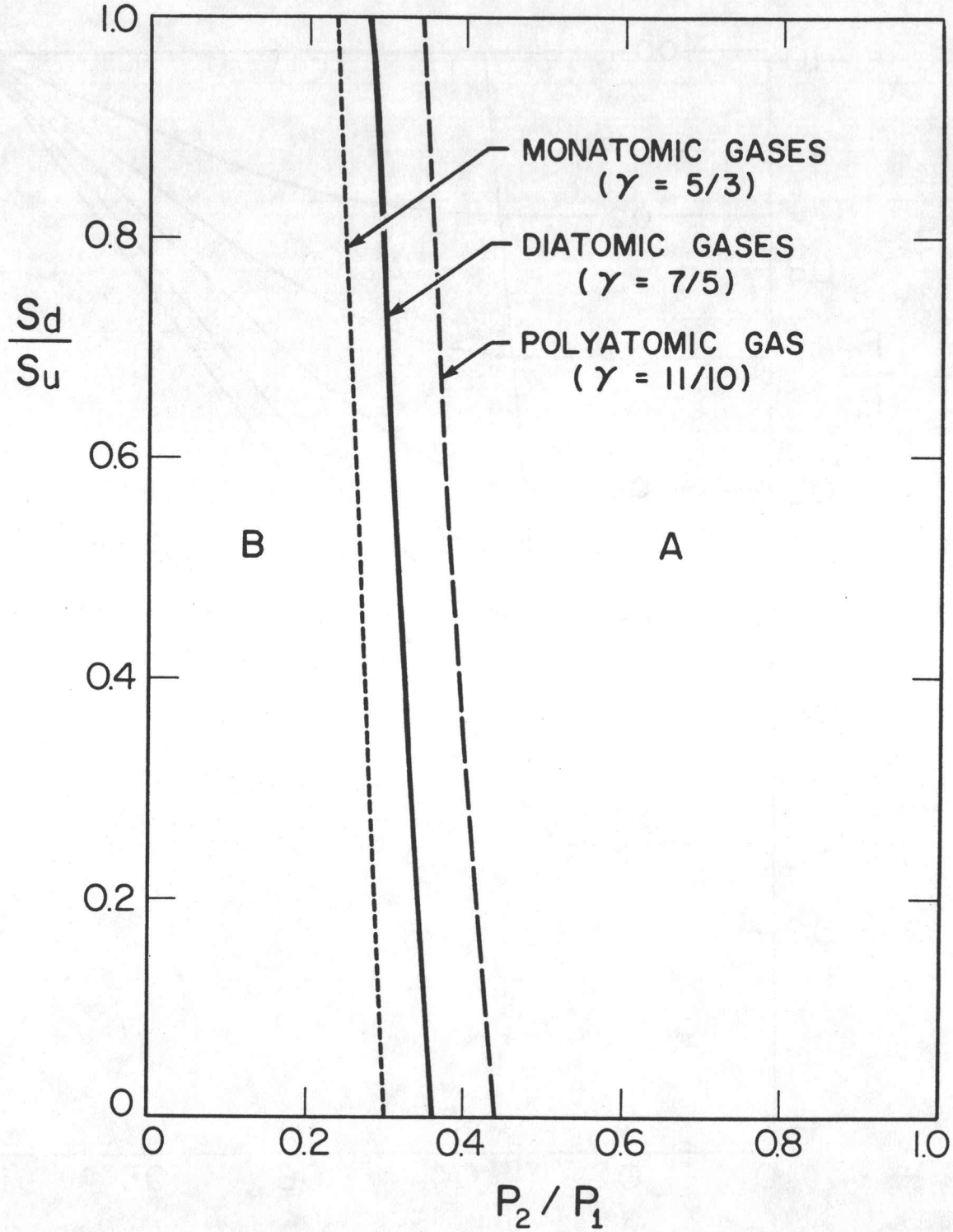

Fig. 3. Domains and boundary for wave patterns A and B for the interaction of a rarefaction wave of incident pressure ratio p_2/p_1 with an area enlargement of ratio S_d/S_u, for perfect gases.

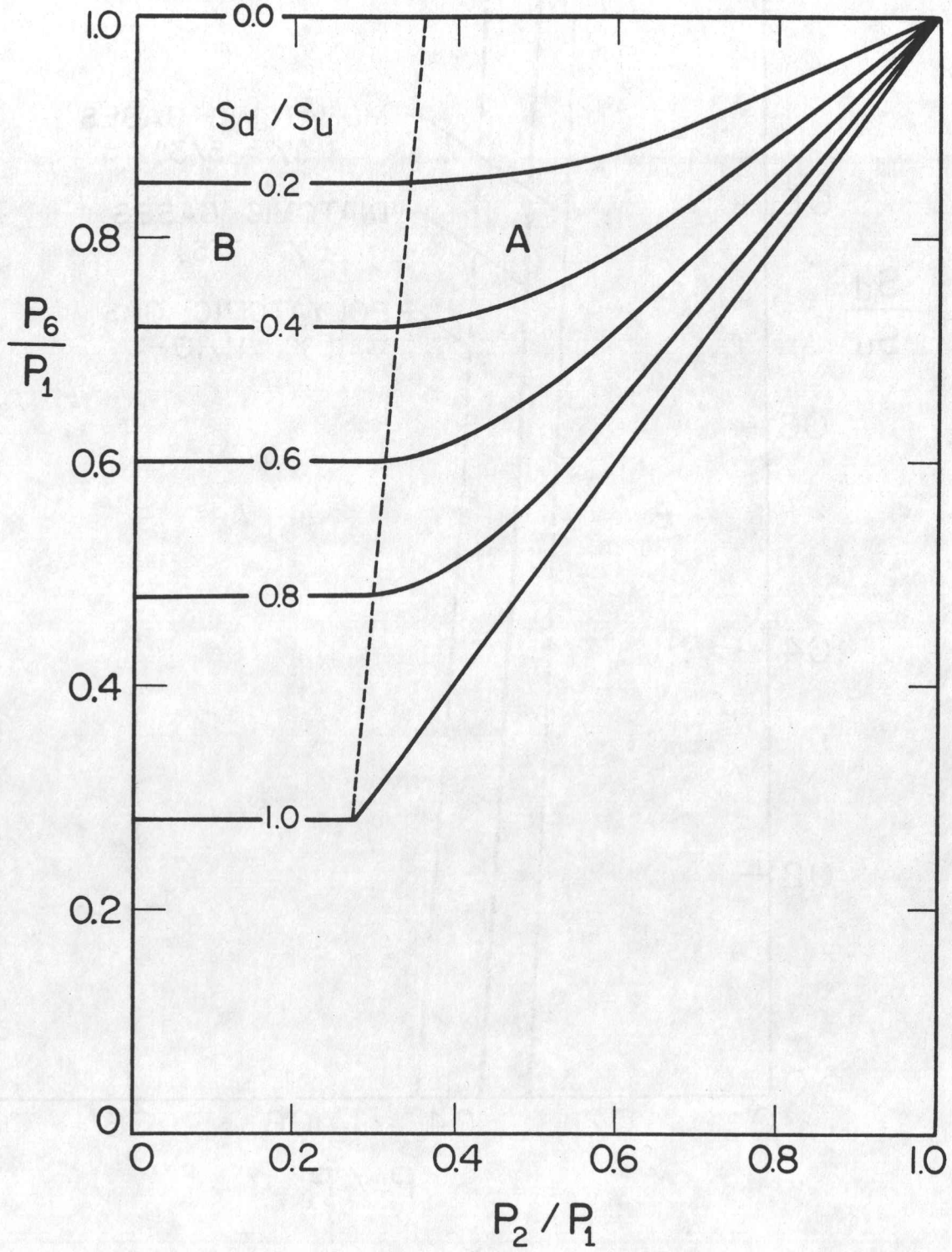

Fig. 4. Strength p_6/p_1 of the transmitted rarefaction wave, shown as a function of the incident rarefaction-wave strength p_2/p_1 and area-enlargement ratio S_d/S_u, for perfect diatomic gases and air with $\gamma = 7/5$.

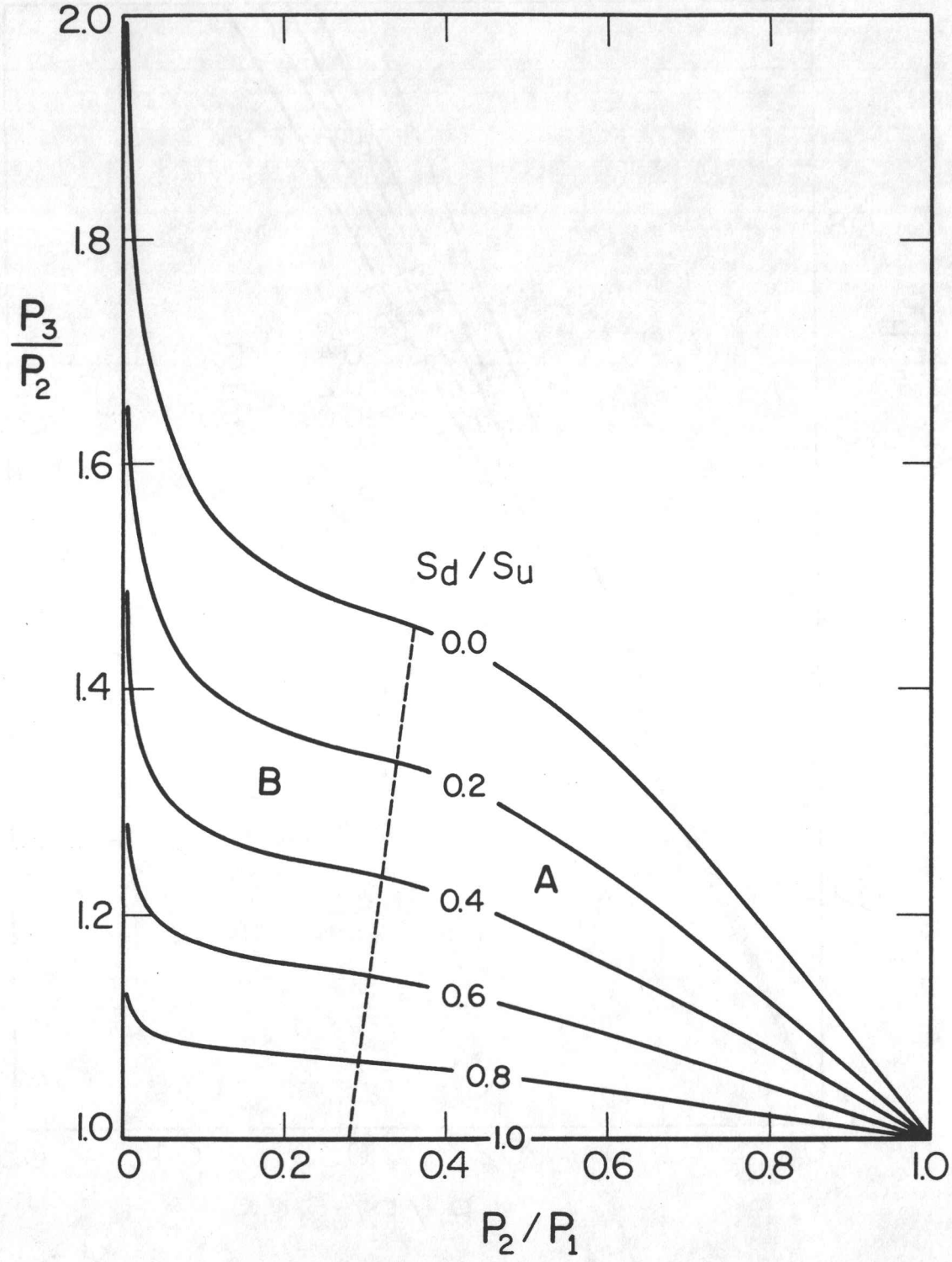

Fig. 5. Strength p_3/p_2 of the reflected shock wave, shown as a function of the incident rarefaction-wave strength p_2/p_1 and area-enlargement ratio S_d/S_u, for perfect diatomic gases and air with $\gamma = 7/5$.

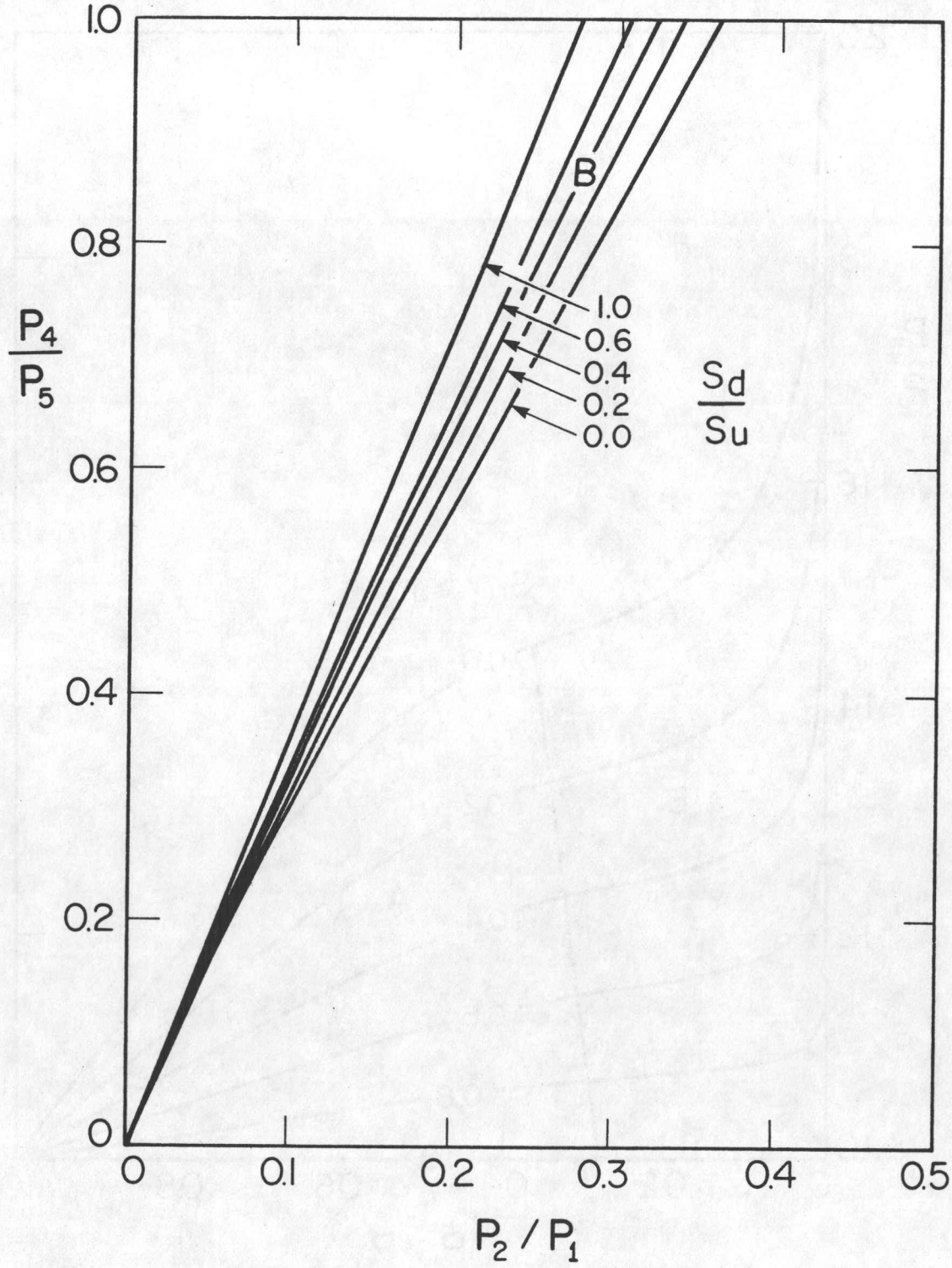

Fig. 6. Strength p_4/p_5 of the downstream-swept rarefaction wave of pattern B, shown as a function of the incident rarefaction-wave strength p_2/p_1 and area-enlargement ratio S_d/S_u, for perfect diatomic gases and air with $\gamma = 7/5$.

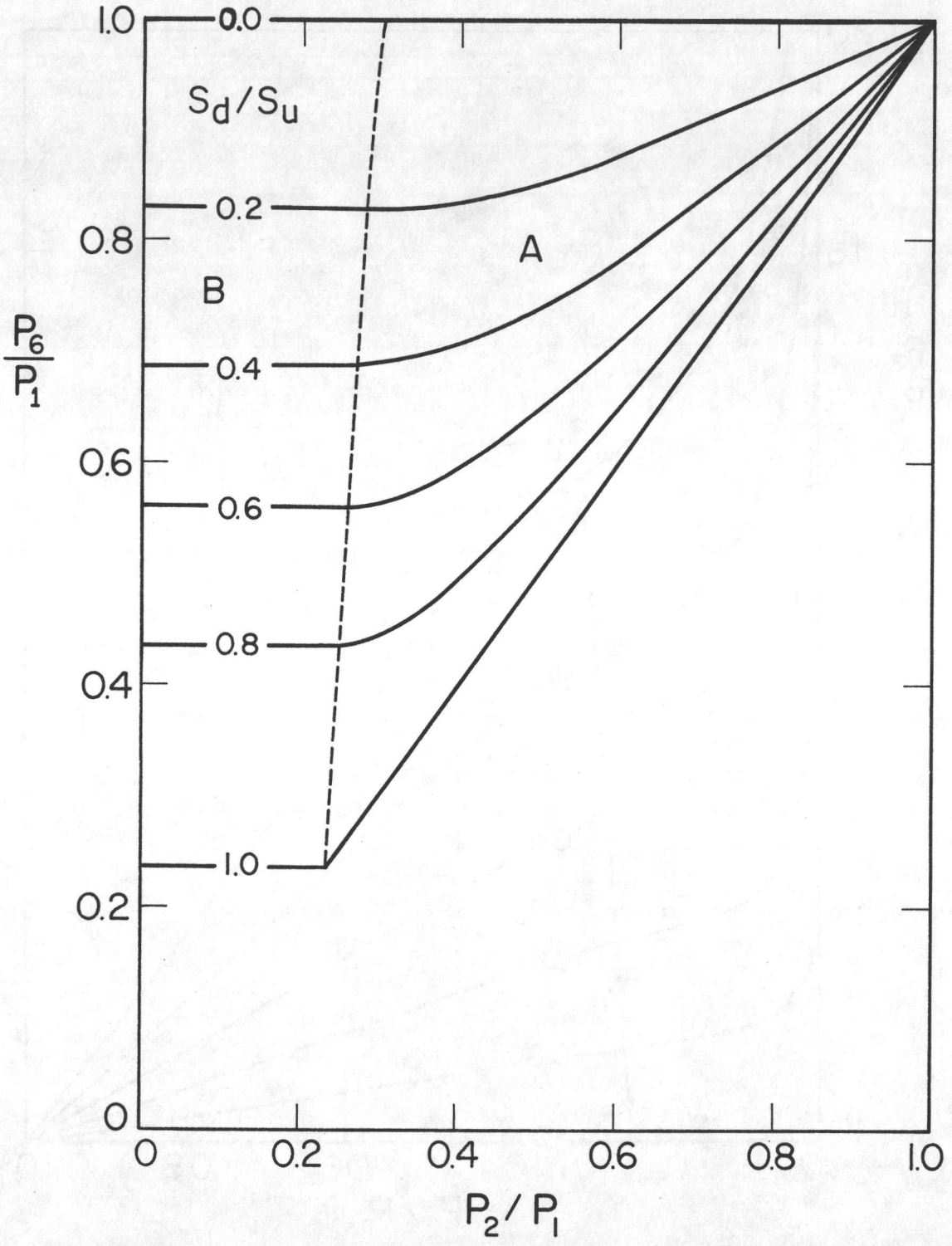

Fig. 7. Strength p_6/p_1 of the transmitted rarefaction wave, shown as a function of the incident rarefaction-wave strength p_2/p_1 and area-enlargement ratio S_d/S_u, for perfect monatomic gases and air with $\gamma = 5/3$.

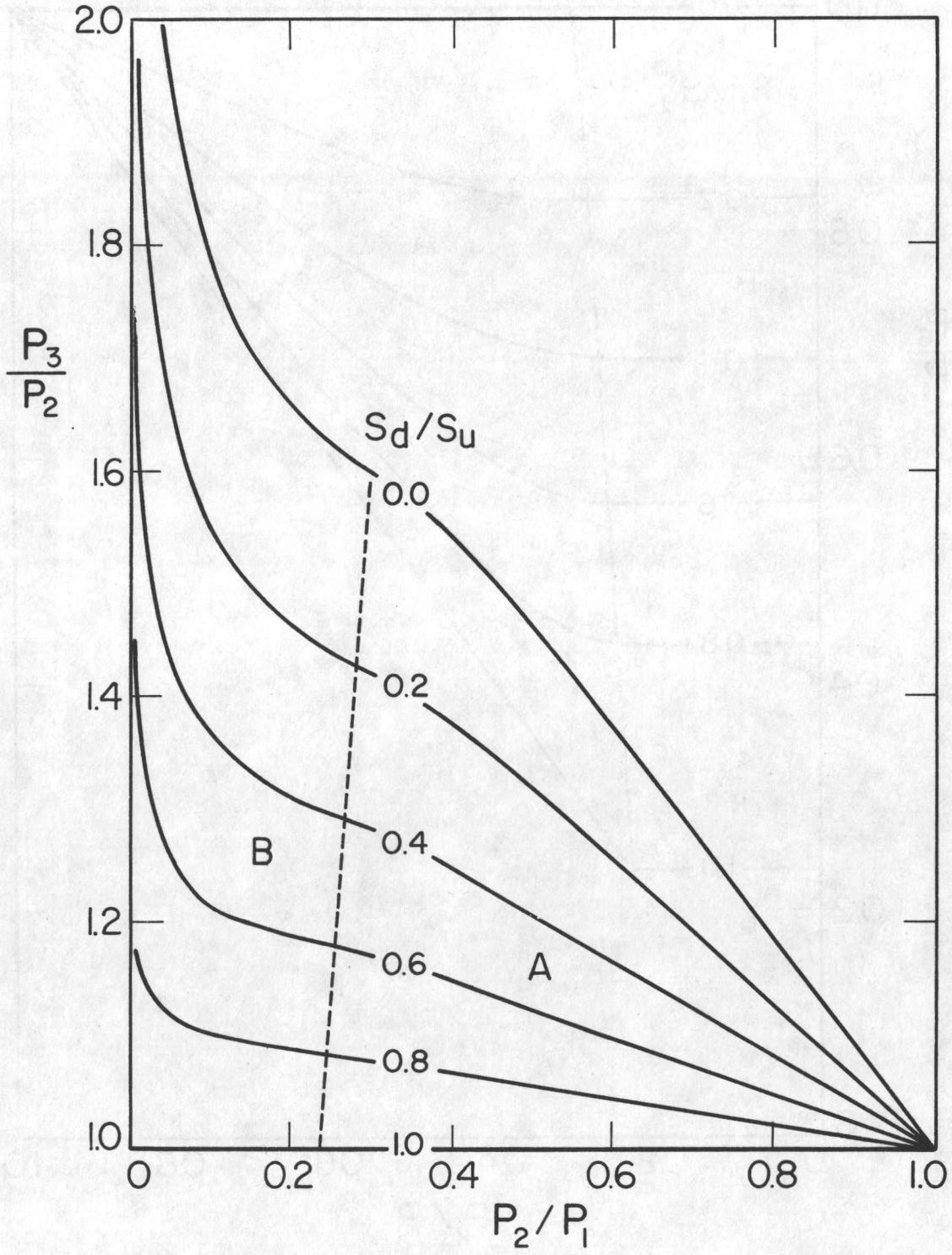

Fig. 8. Strength p_3/p_2 of the reflected shock wave, shown as a function of the incident rarefaction-wave strength p_2/p_1 and area-enlargement ratio S_d/S_u, for perfect monatomic gases and air with $\gamma = 5/3$.

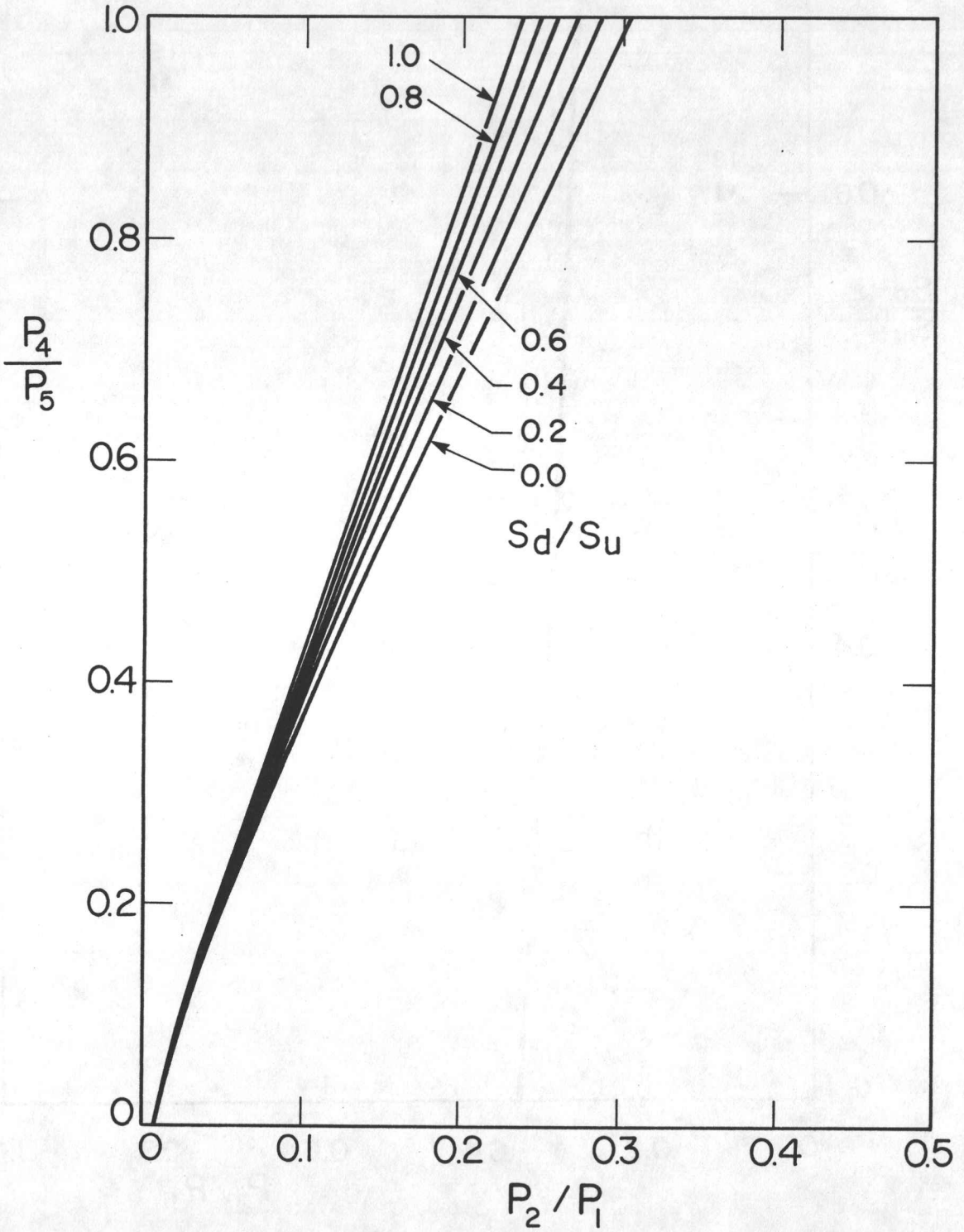

Fig. 9. Strength p_4/p_5 of the downstream-swept rarefaction wave of pattern B, shown as a function of the incident rarefaction-wave strength p_2/p_1 and area-enlargement ratio S_d/S_u, for perfect monatomic gases and air with $\gamma = 5/3$.

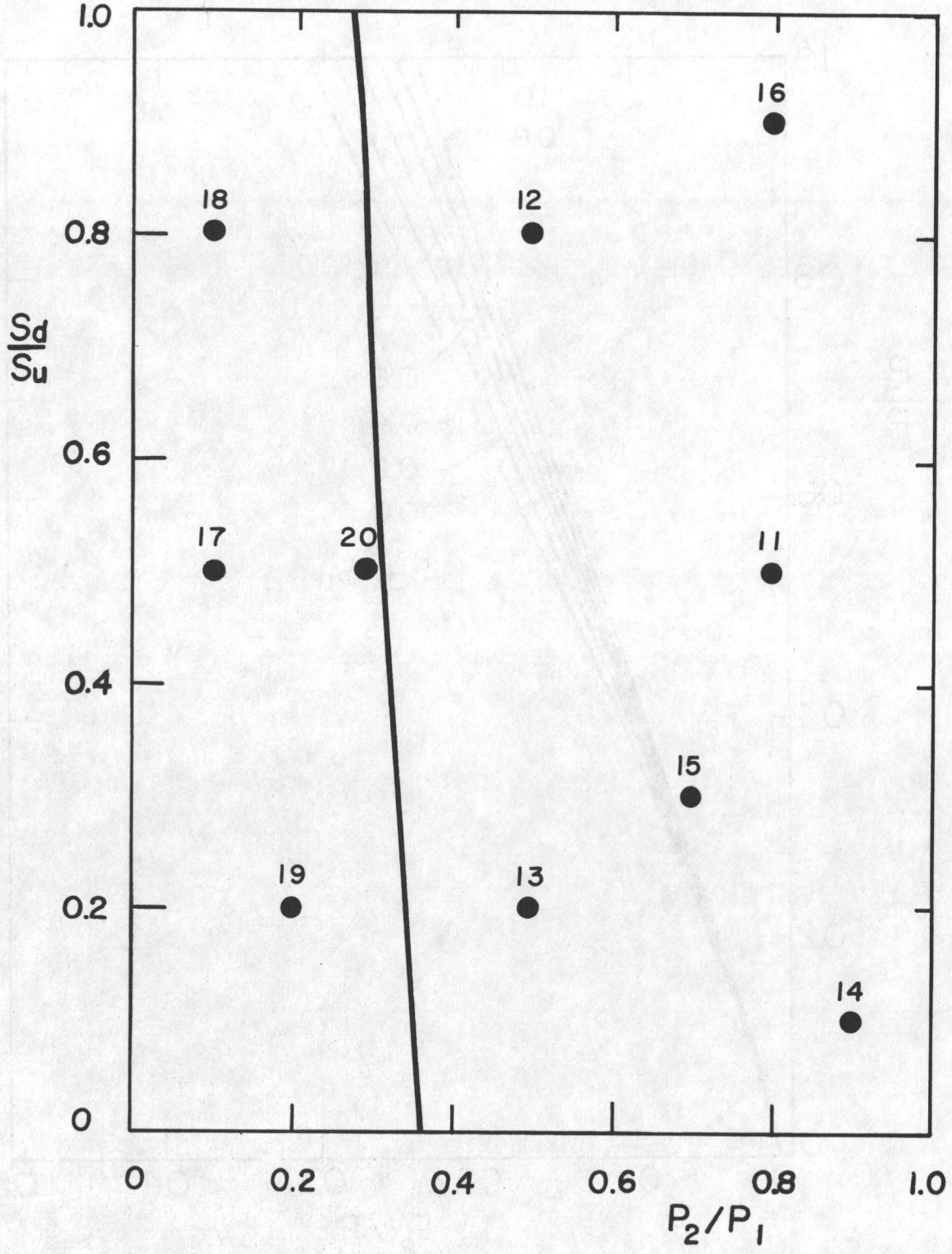

Fig. 10. Locations of points in the domains of wave patterns A and B for numerical results given in Figs. 11 to 20. The numbers shown here correspond directly to the figure numbers.

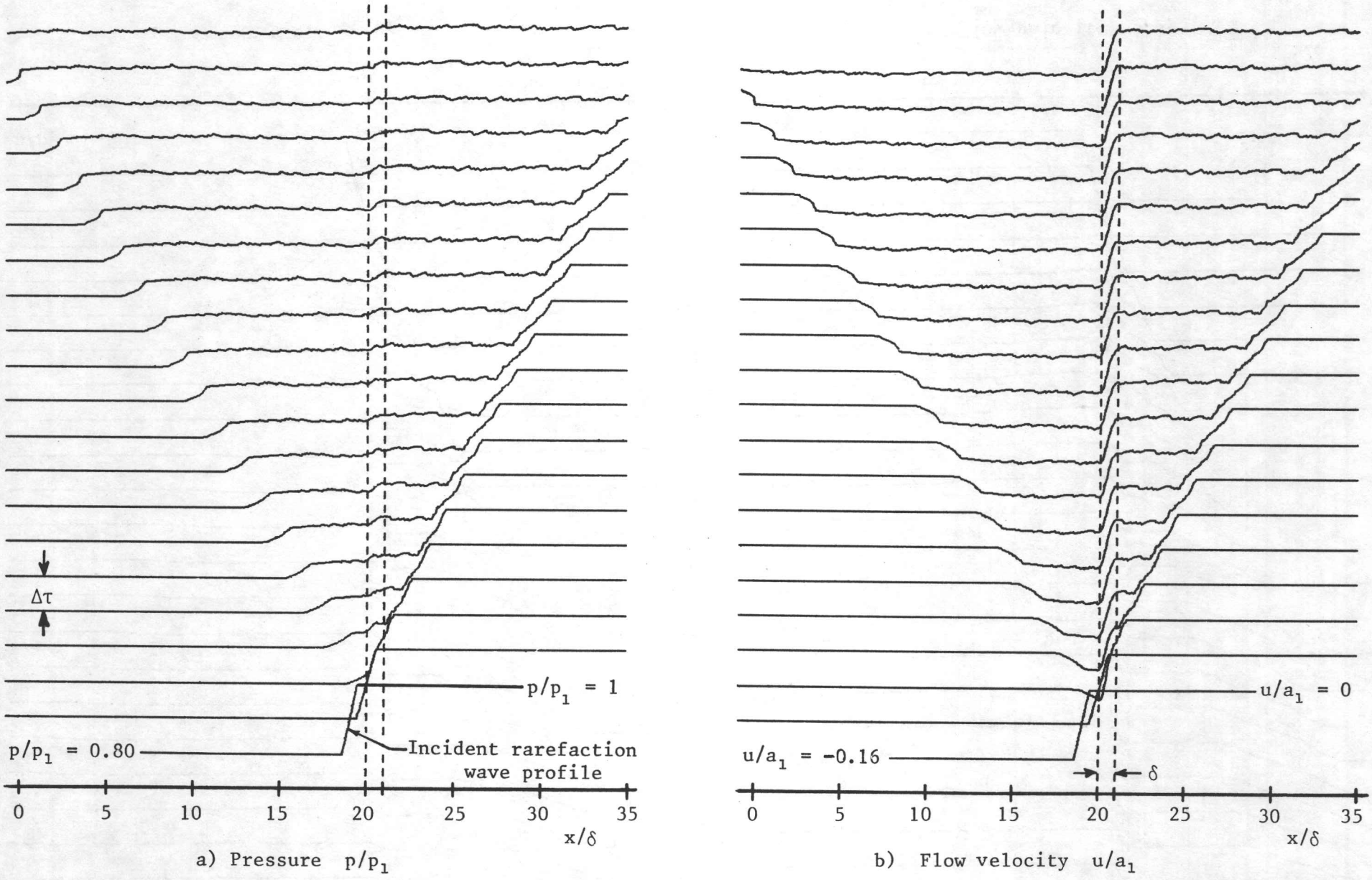

Fig. 11. Spatial distributions of pressure (a) and flow velocity (b) for the interaction of a rarefaction wave with an area enlargement ($p_2/p_1 = 0.80$, $S_d/S_u = 0.50$, $\Delta\tau = 1.04$, pattern A).

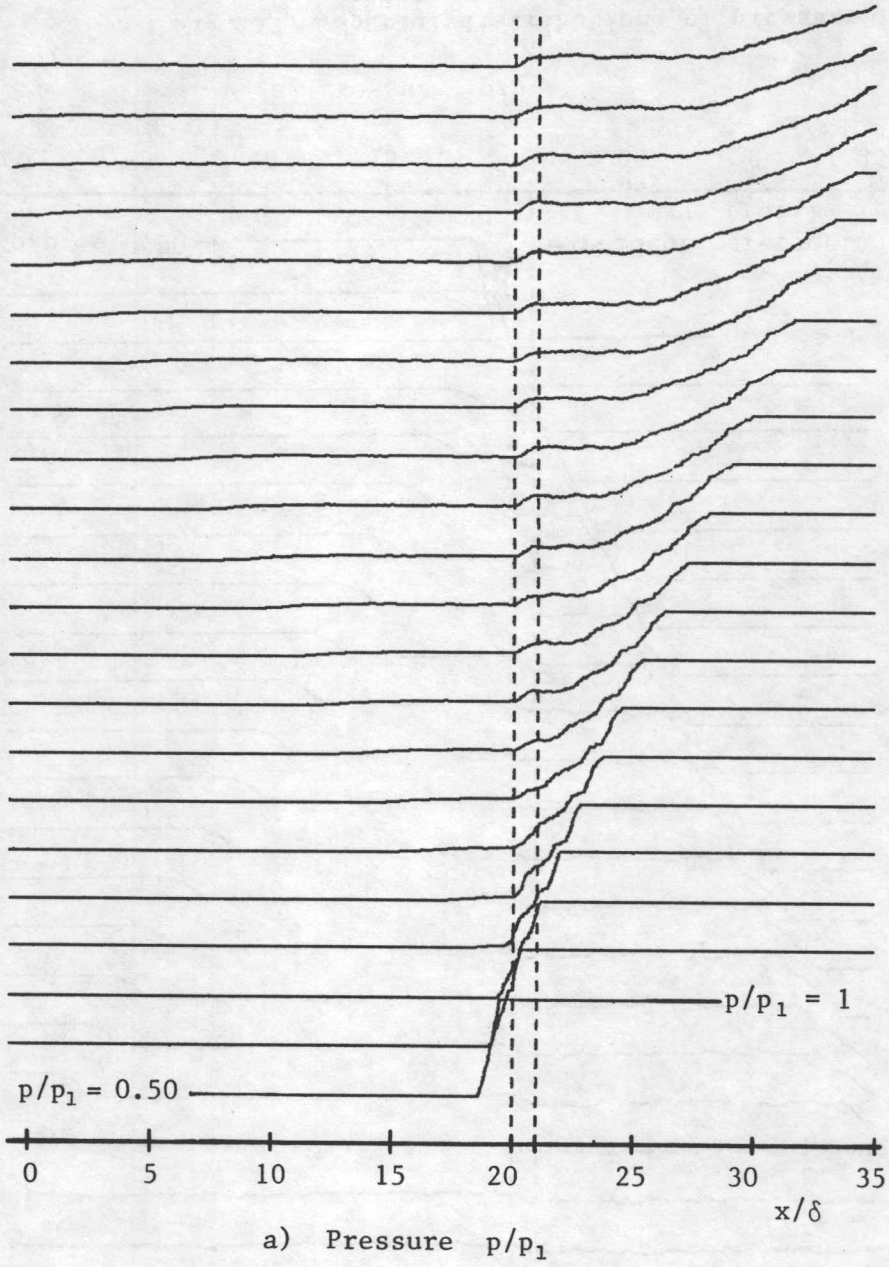

a) Pressure p/p_1

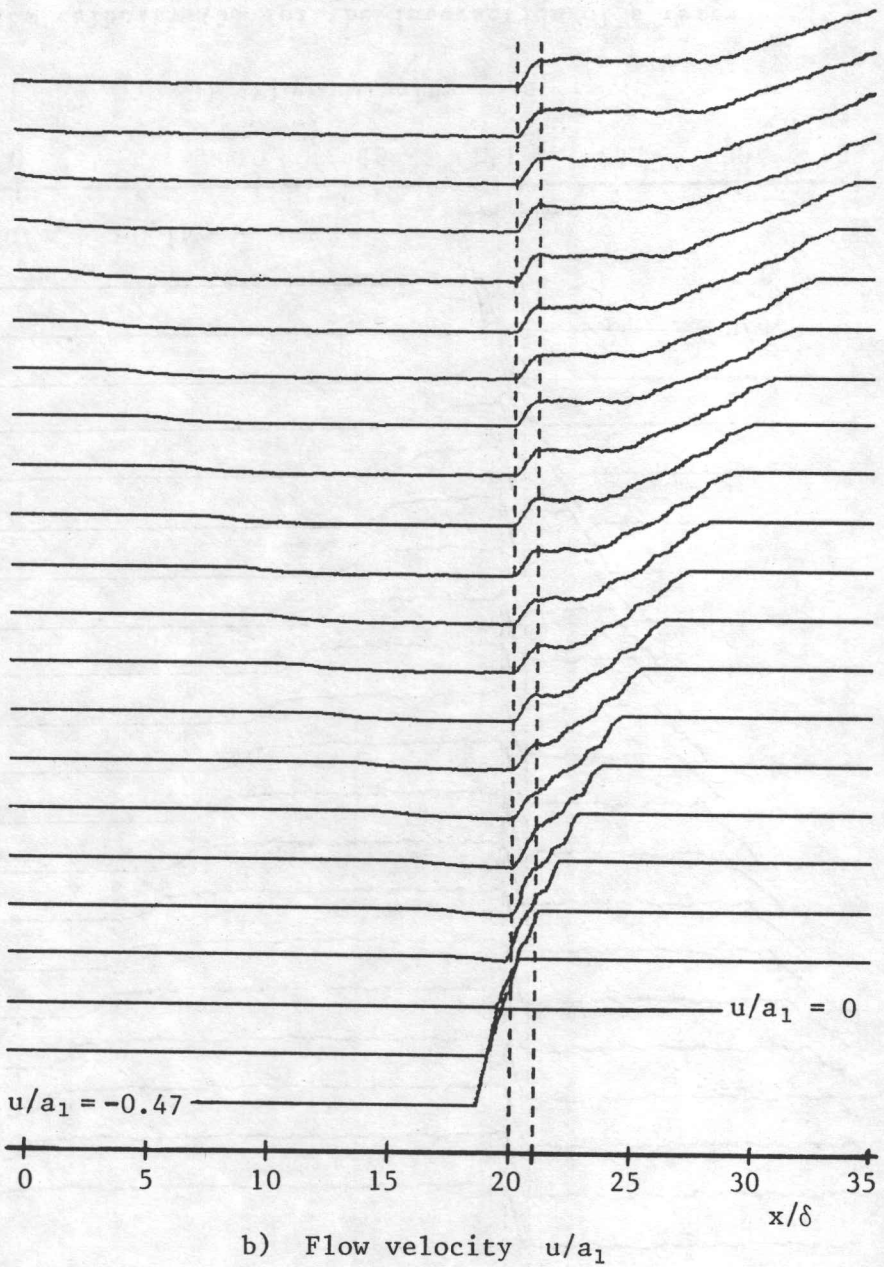

b) Flow velocity u/a_1

Fig. 12. Spatial distributions of pressure (a) and flow velocity (b) for the interaction of a rarefaction wave with an area enlargement ($p_2/p_1 = 0.50$, $S_d/S_u = 0.80$, $\Delta\tau = 0.88$, pattern A).

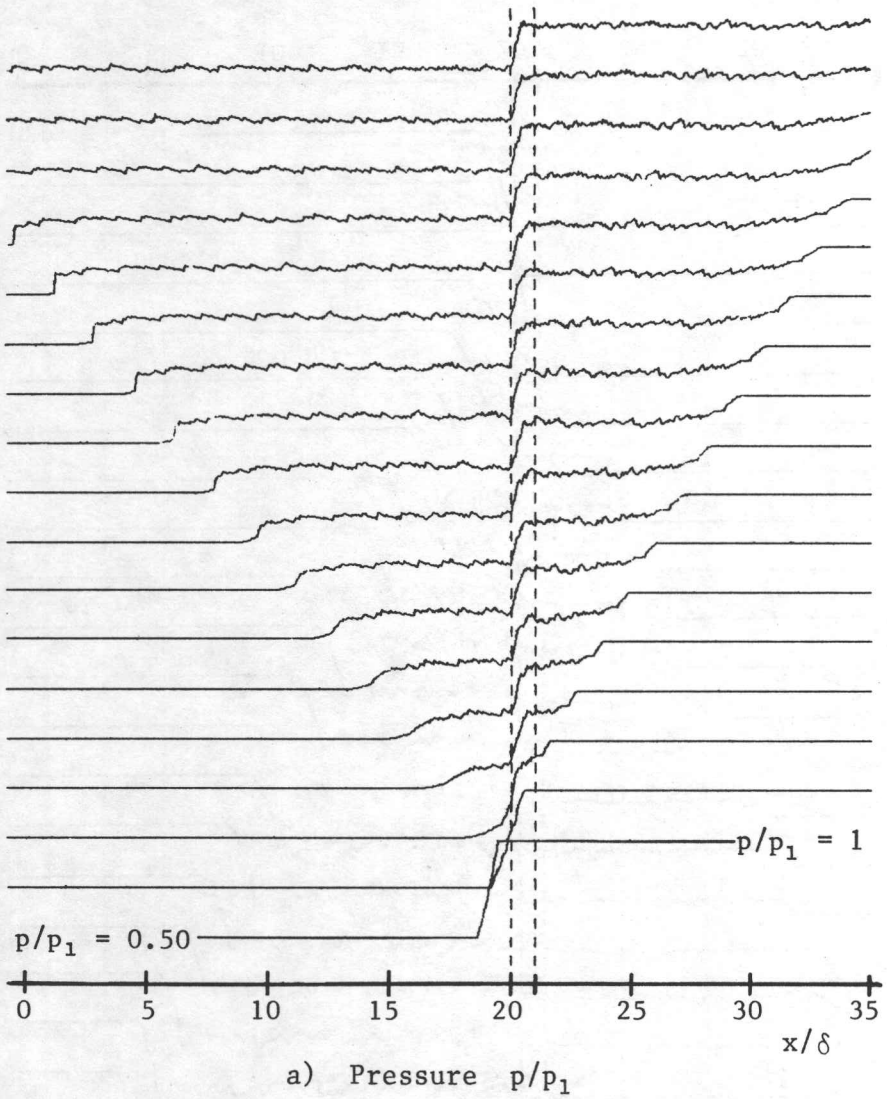

a) Pressure p/p_1

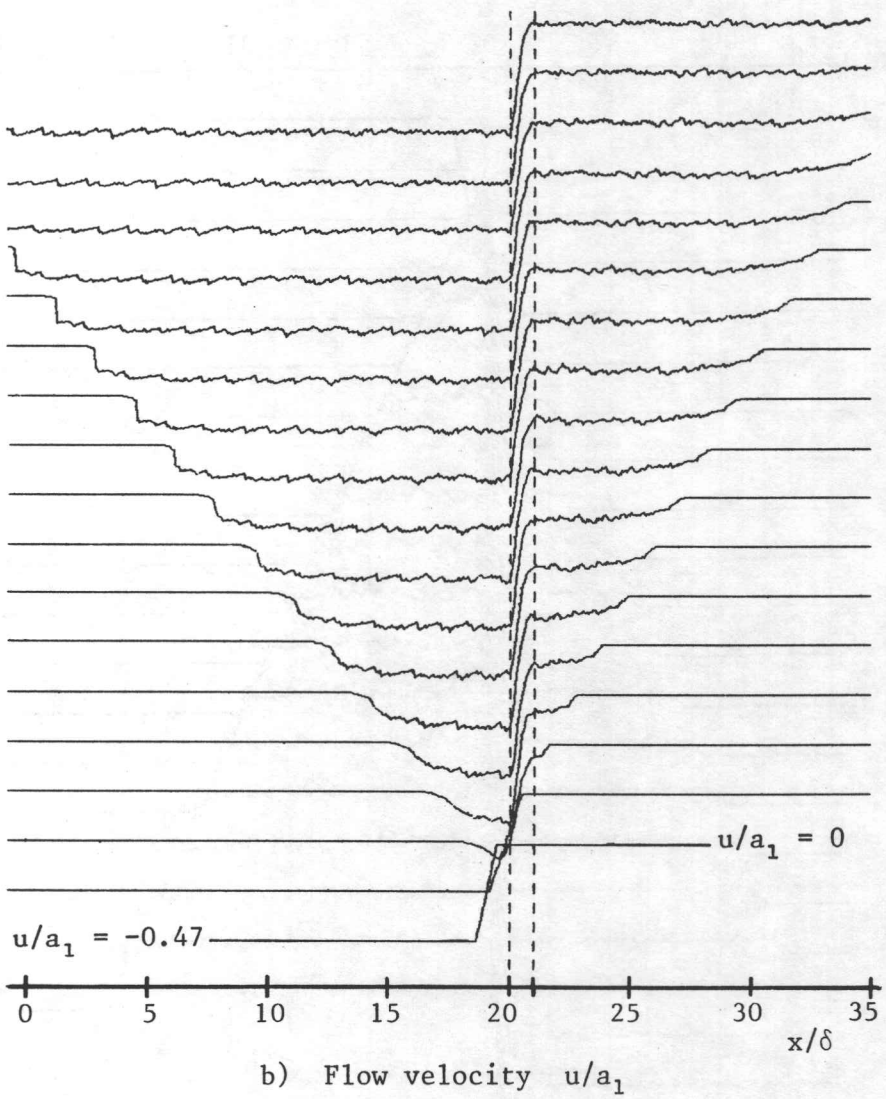

b) Flow velocity u/a_1

Fig. 13. Spatial distributions of pressure (a) and flow velocity (b) for the interaction of a rarefaction wave with an area enlargement ($p_2/p_1 = 0.50$, $S_d/S_u = 0.20$, $\Delta\tau = 1.14$, pattern A).

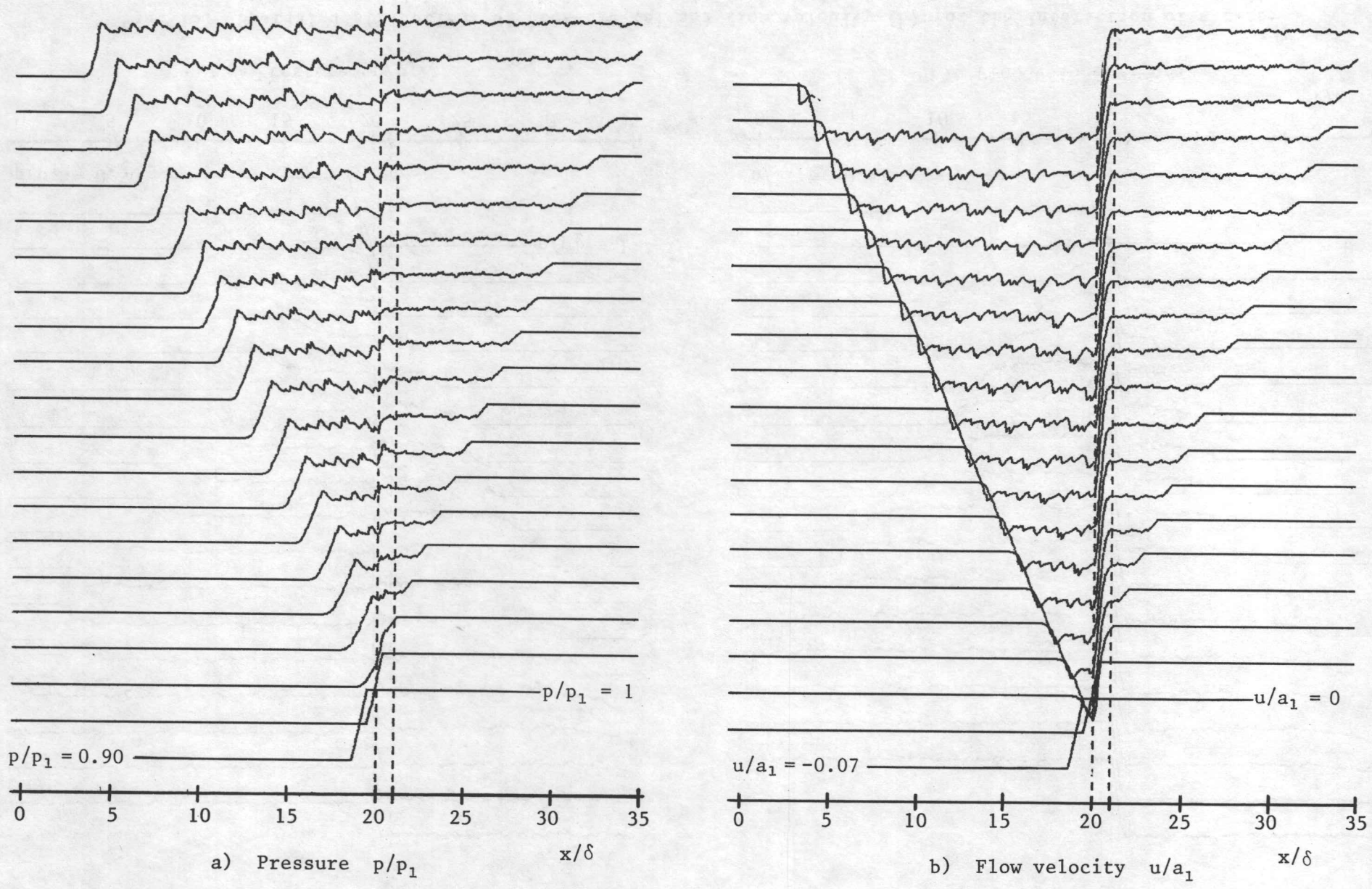

Fig. 14. Spatial distributions of pressure (a) and flow velocity (b) for the interaction of a rarefaction wave with an area enlargement ($p_2/p_1 = 0.90$, $S_d/S_u = 0.10$, $\Delta\tau = 0.88$, pattern A).

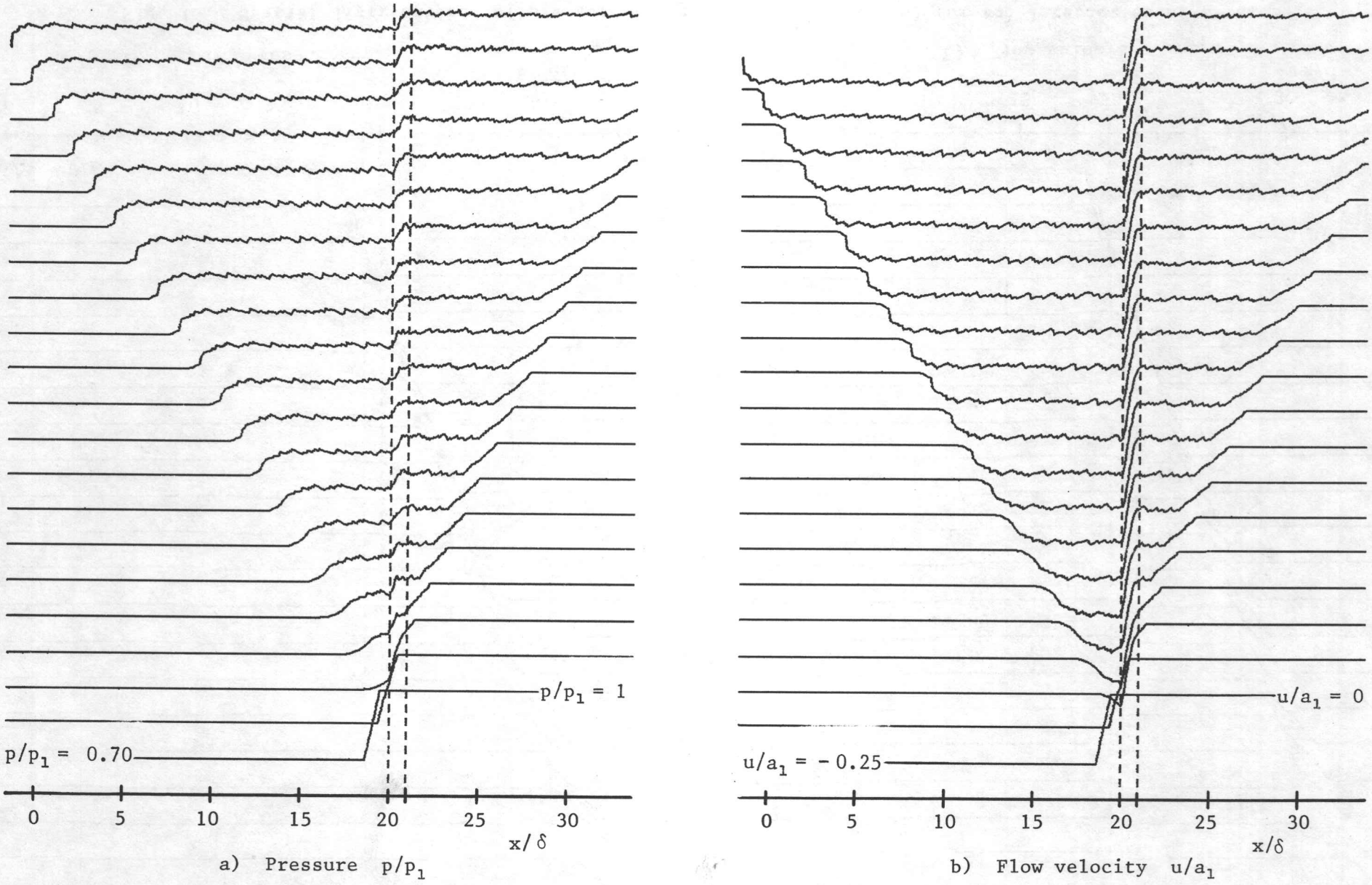

Fig. 15. Spatial distributions of pressure (a) and flow velocity (b) for the interaction of a rarefaction wave with an area enlargement ($p_2/p_1 = 0.70$, $S_d/S_u = 0.30$, $\Delta\tau = 0.97$, pattern A).

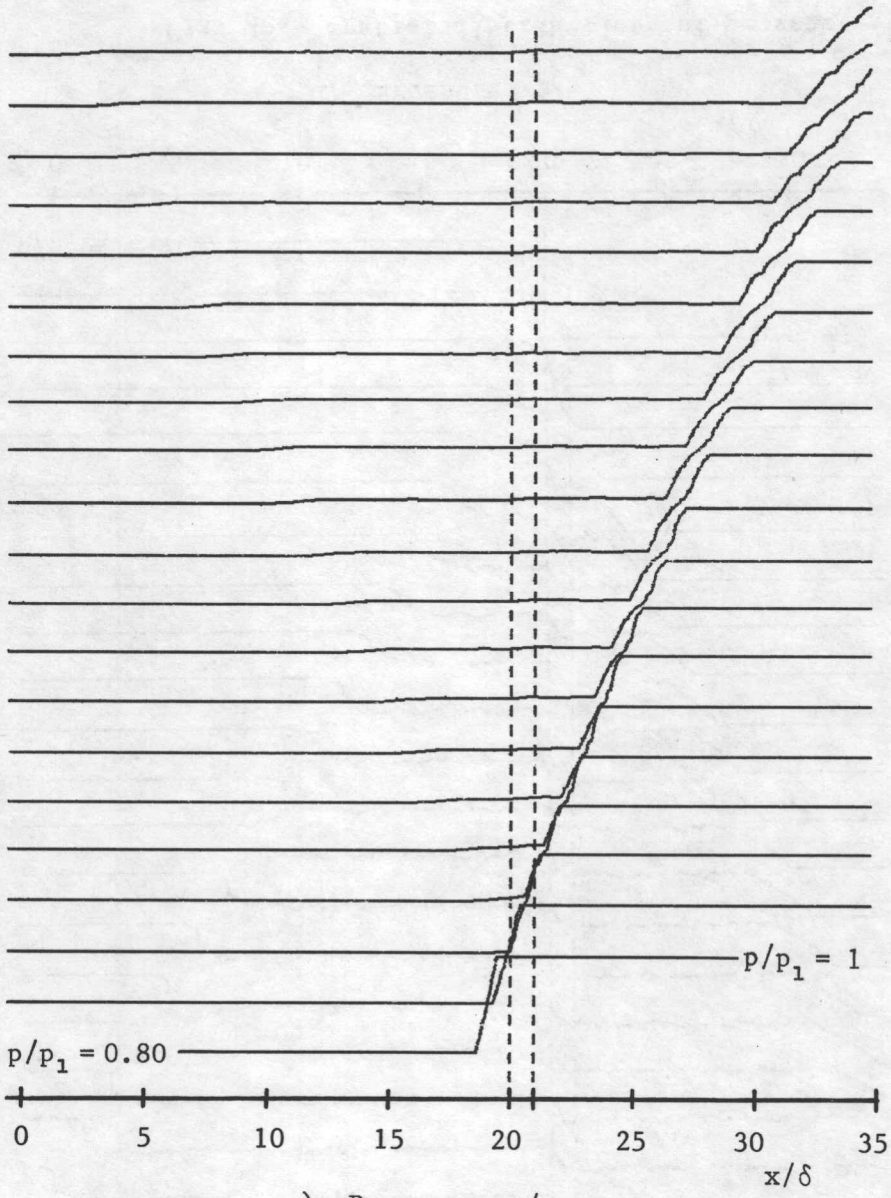

a) Pressure p/p_1

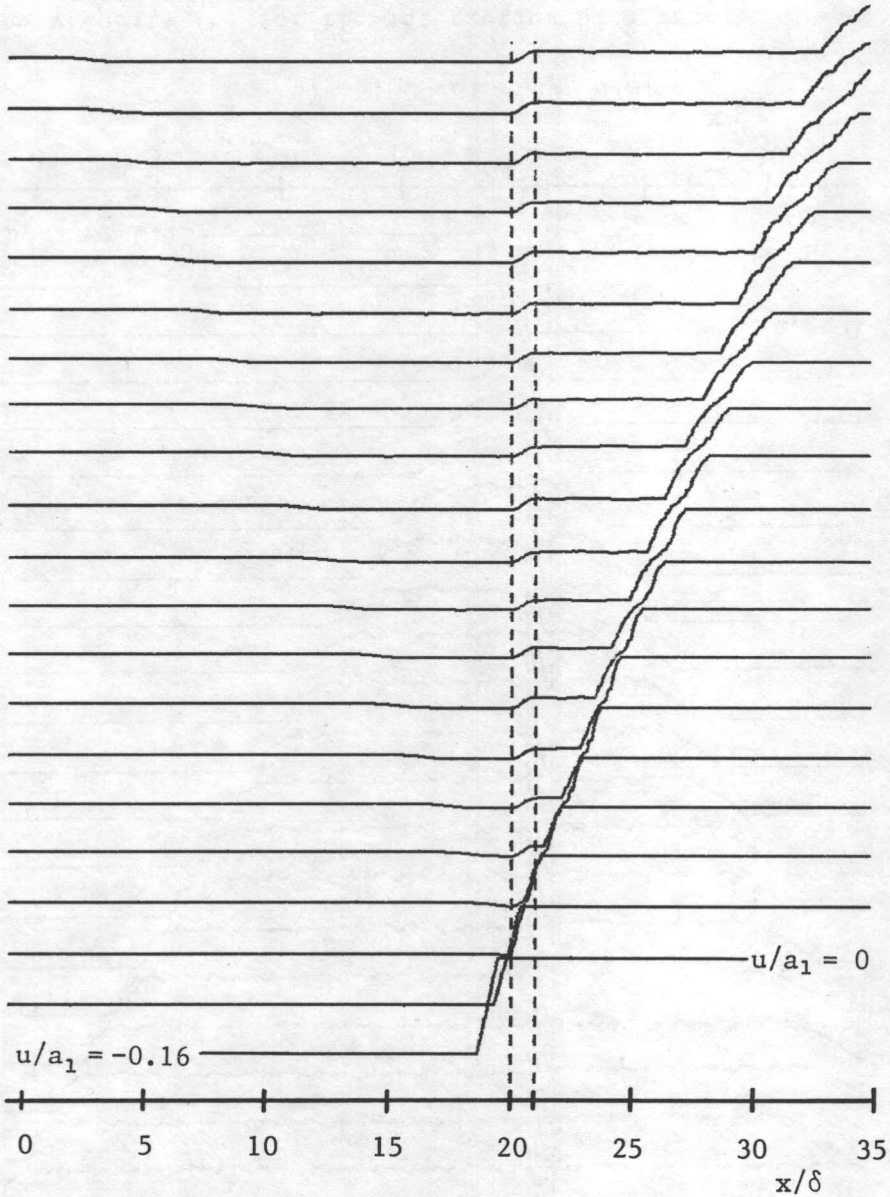

b) Flow velocity u/a_1

Fig. 16. Spatial distributions of pressure (a) and flow velocity (b) for the interaction of a rarefaction wave with an area enlargement ($p_2/p_1 = 0.80$, $S_d/S_u = 0.90$, $\Delta\tau = 0.88$, pattern A).

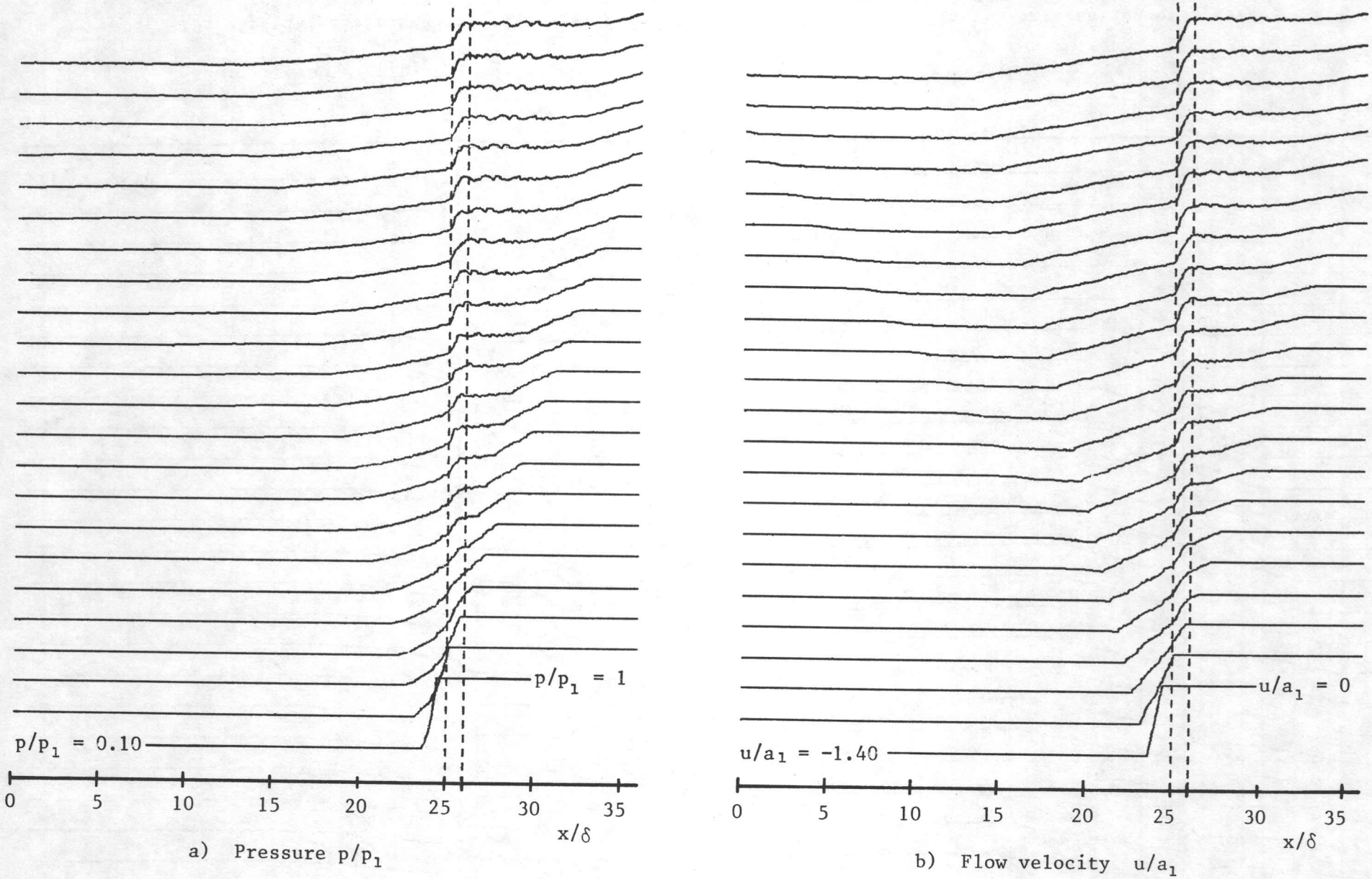

Fig. 17. Spatial distributions of pressure (a) and flow velocity (b) for the interaction of a rarefaction wave with an area enlargement ($p_2/p_1 = 0.10$, $S_d/S_u = 0.50$, $\Delta\tau = 0.67$, pattern B).

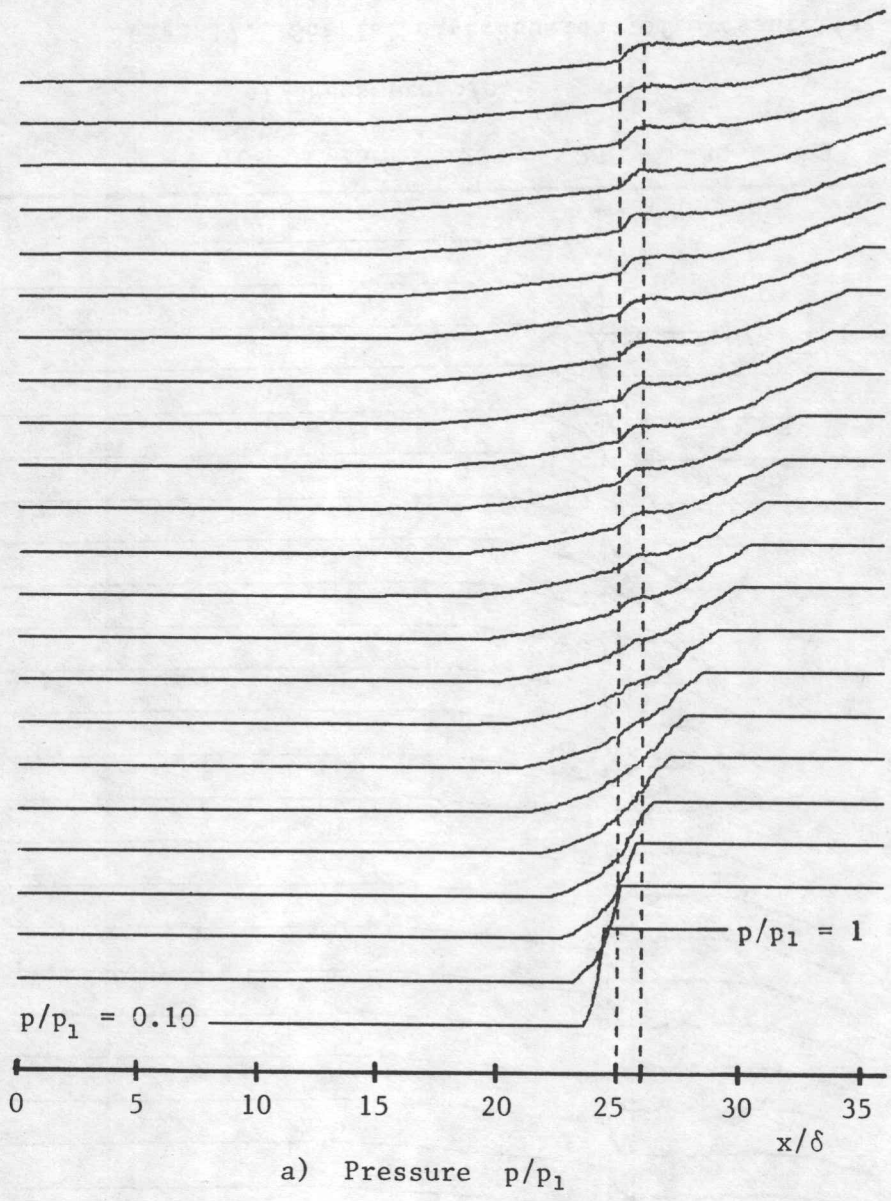

a) Pressure p/p_1

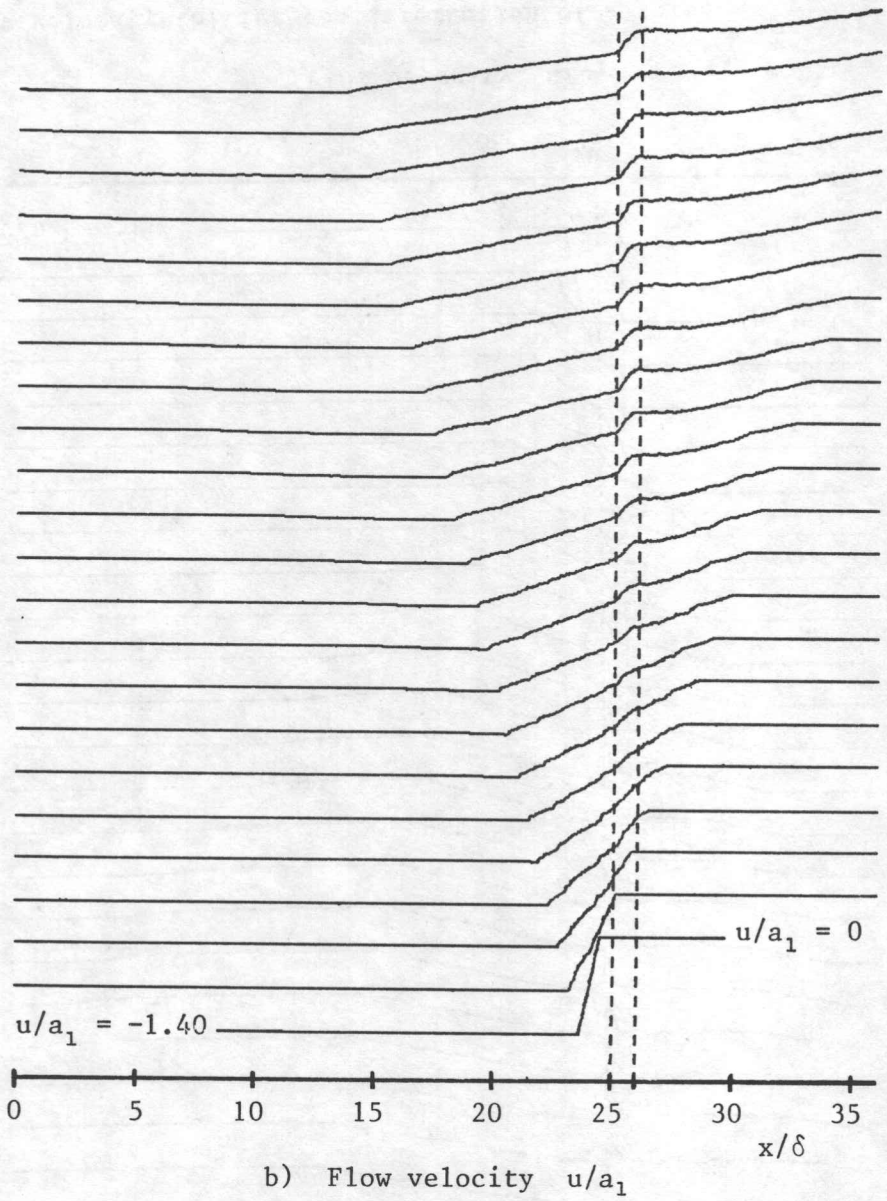

b) Flow velocity u/a_1

Fig. 18. Spatial distributions of pressure (a) and flow velocity (b) for the interaction of a rarefaction wave with an area enlargement ($p_2/p_1 = 0.10$, $S_d/S_u = 0.80$, $\Delta\tau = 0.67$, pattern B).

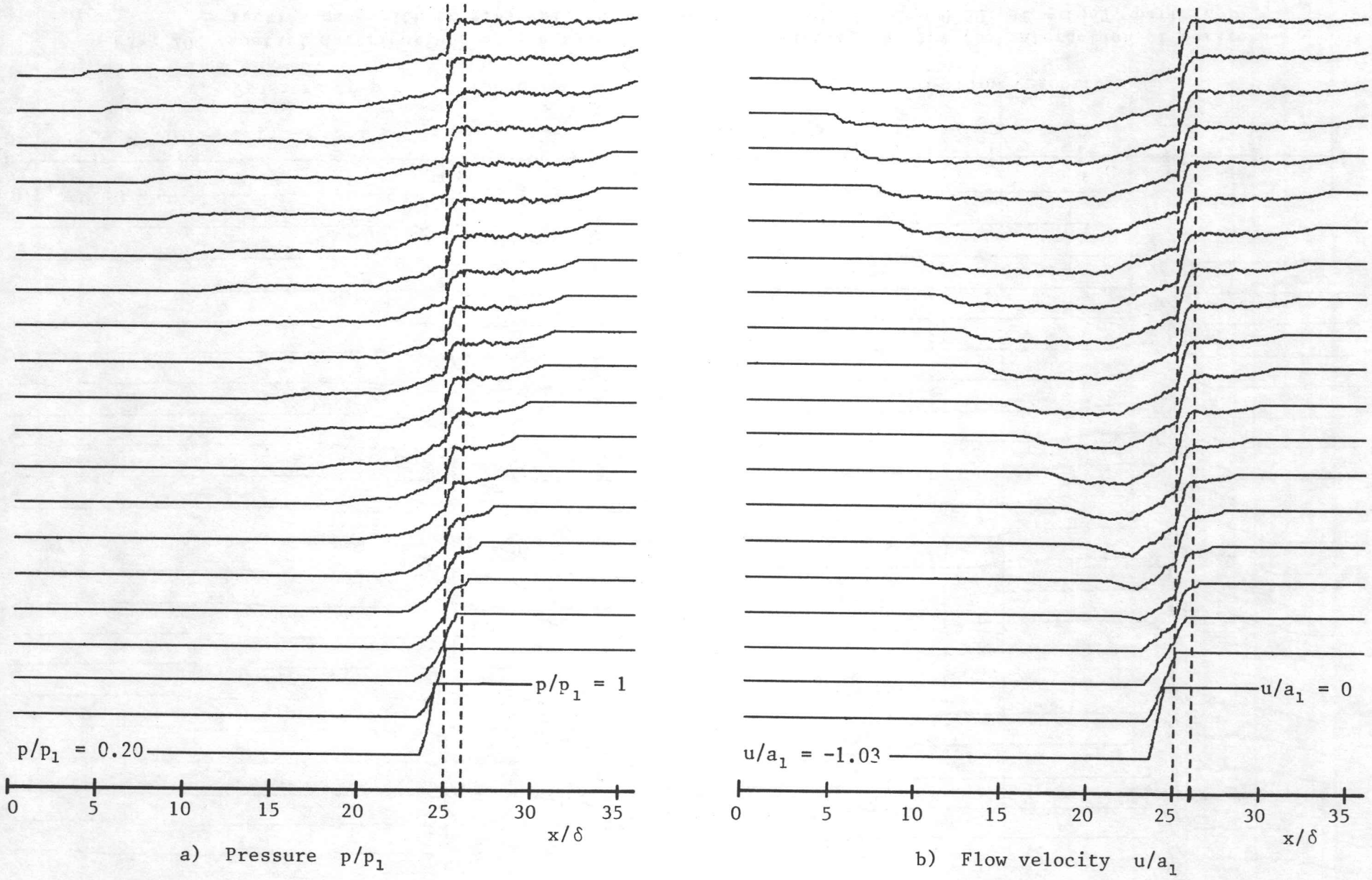

Fig. 19. Spatial distributions of pressure (a) and flow velocity (b) for the interaction of a rarefaction wave with an area enlargement ($p_2/p_1 = 0.20$, $S_d/S_u = 0.20$, $\Delta\tau = 0.77$, pattern B).

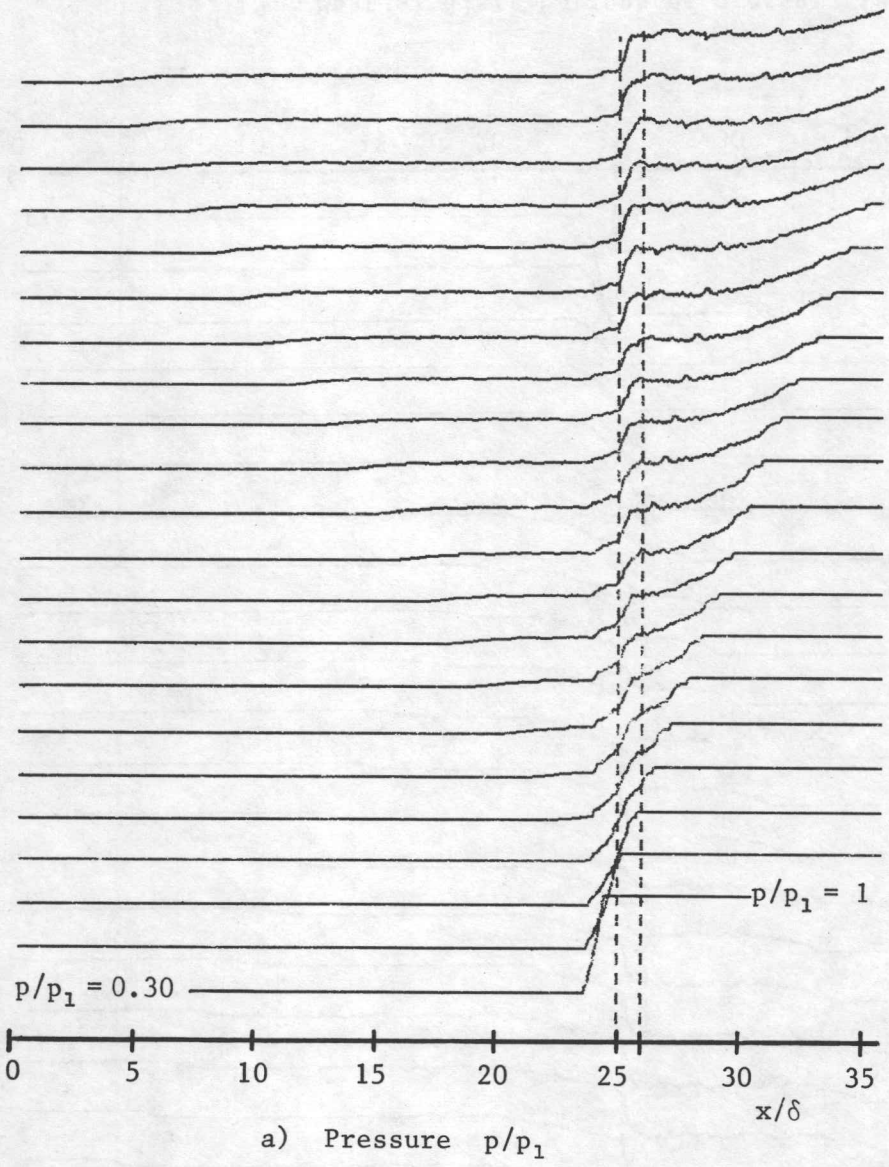

a) Pressure p/p_1

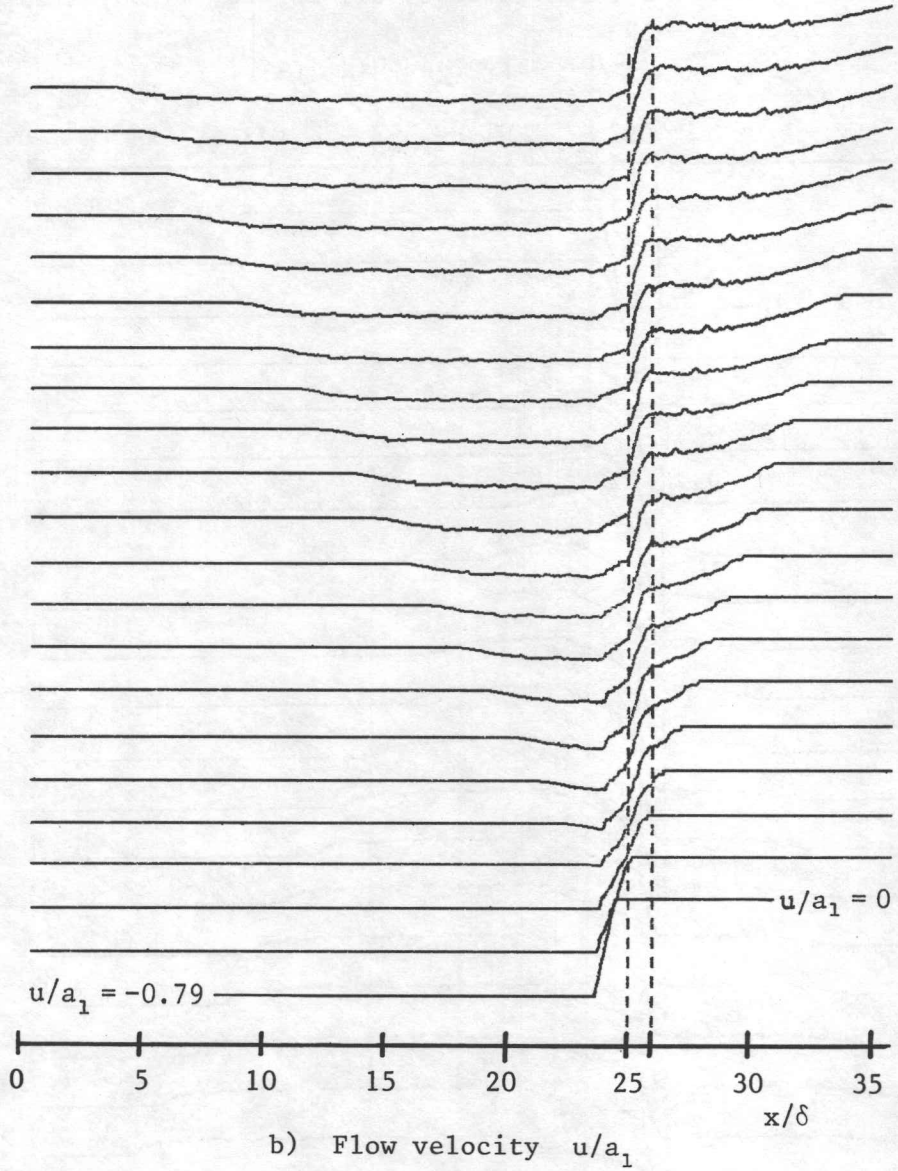

b) Flow velocity u/a_1

Fig. 20. Spatial distributions of pressure (a) and flow velocity (b) for the interaction of a rarefaction wave with an area enlargement ($p_2/p_1 = 0.30$, $S_d/S_u = 0.50$, $\Delta\tau = 0.67$, pattern B).

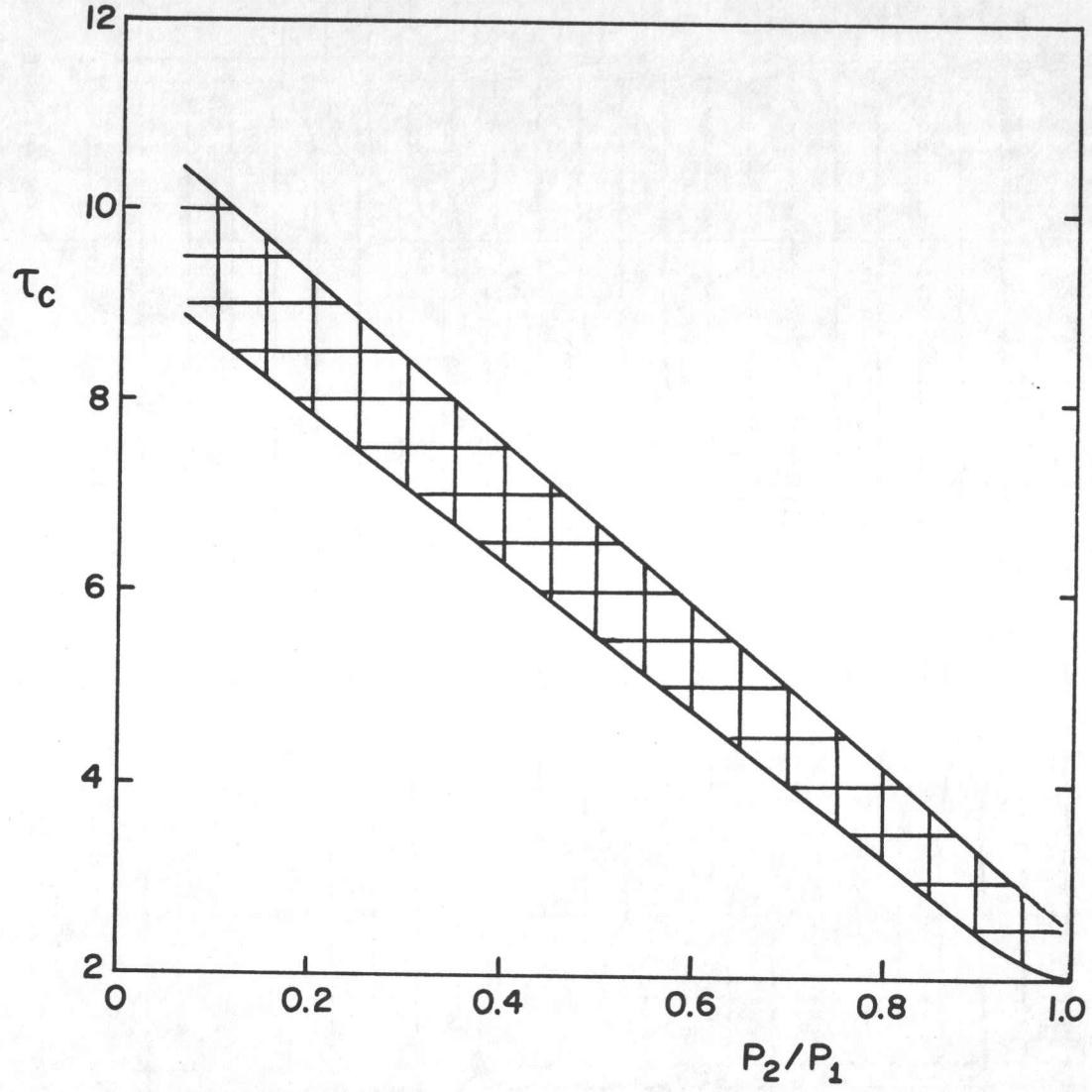

Fig. 21. Characteristic time $\tau_c = a_1 t_c/\delta$ versus incident rarefaction-wave strength p_2/p_1 for the initially nonstationary flow to eventually become almost quasi-steady (within 5%). These times lie in a band because they are slightly dependent on the area ratio S_d/S_u and also cannot be determined precisely from the numerical results.

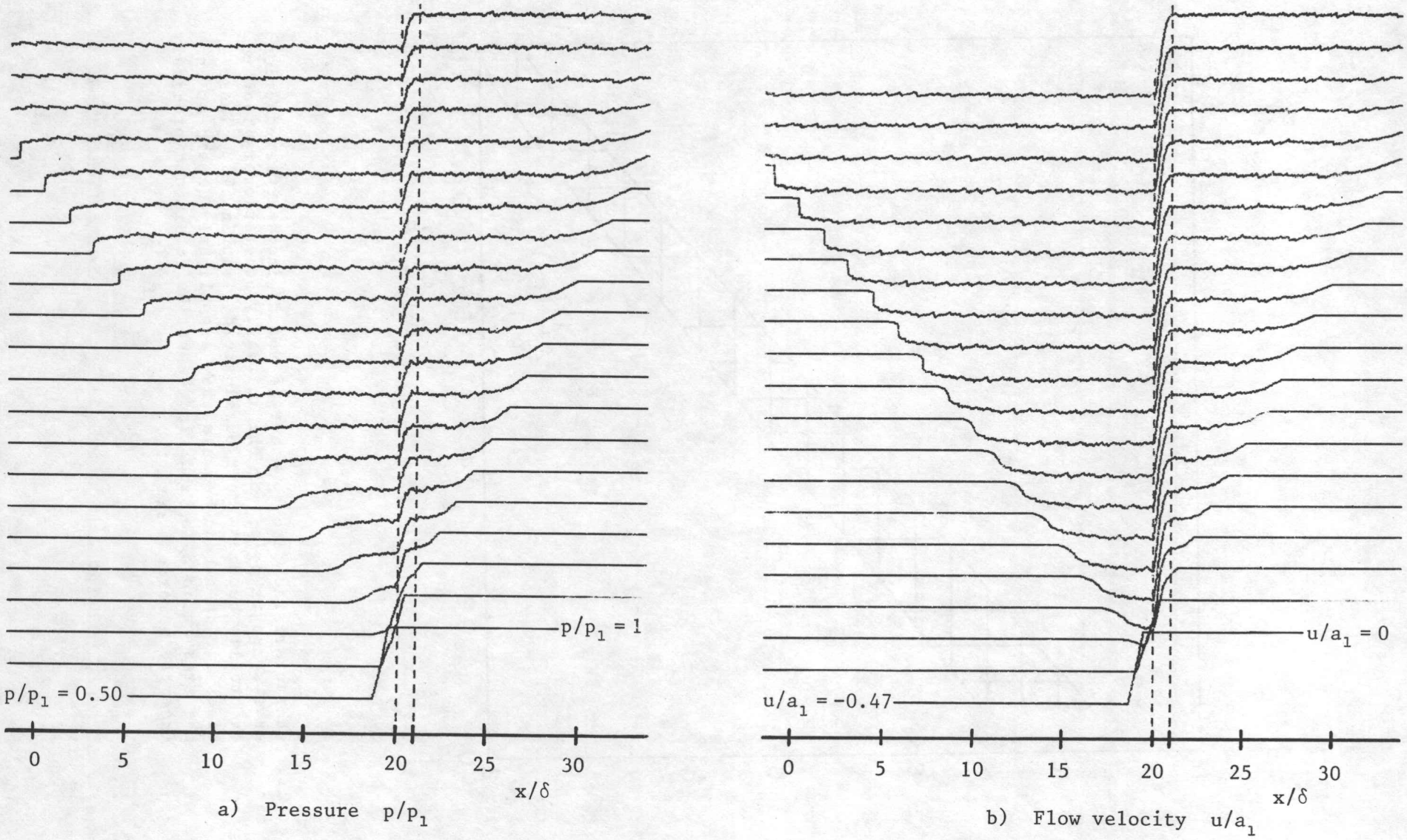

Fig. 22. Spatial distributions of pressure (a) and flow velocity (b) for the interaction of a rarefaction wave with an area enlargement ($p_2/p_1 = 0.50$, $S_d/S_u = 0.20$, $\Delta\tau = 1.15$, pattern A). Note that the number of grid zones was two-fold larger at 1440 for these numerical results.

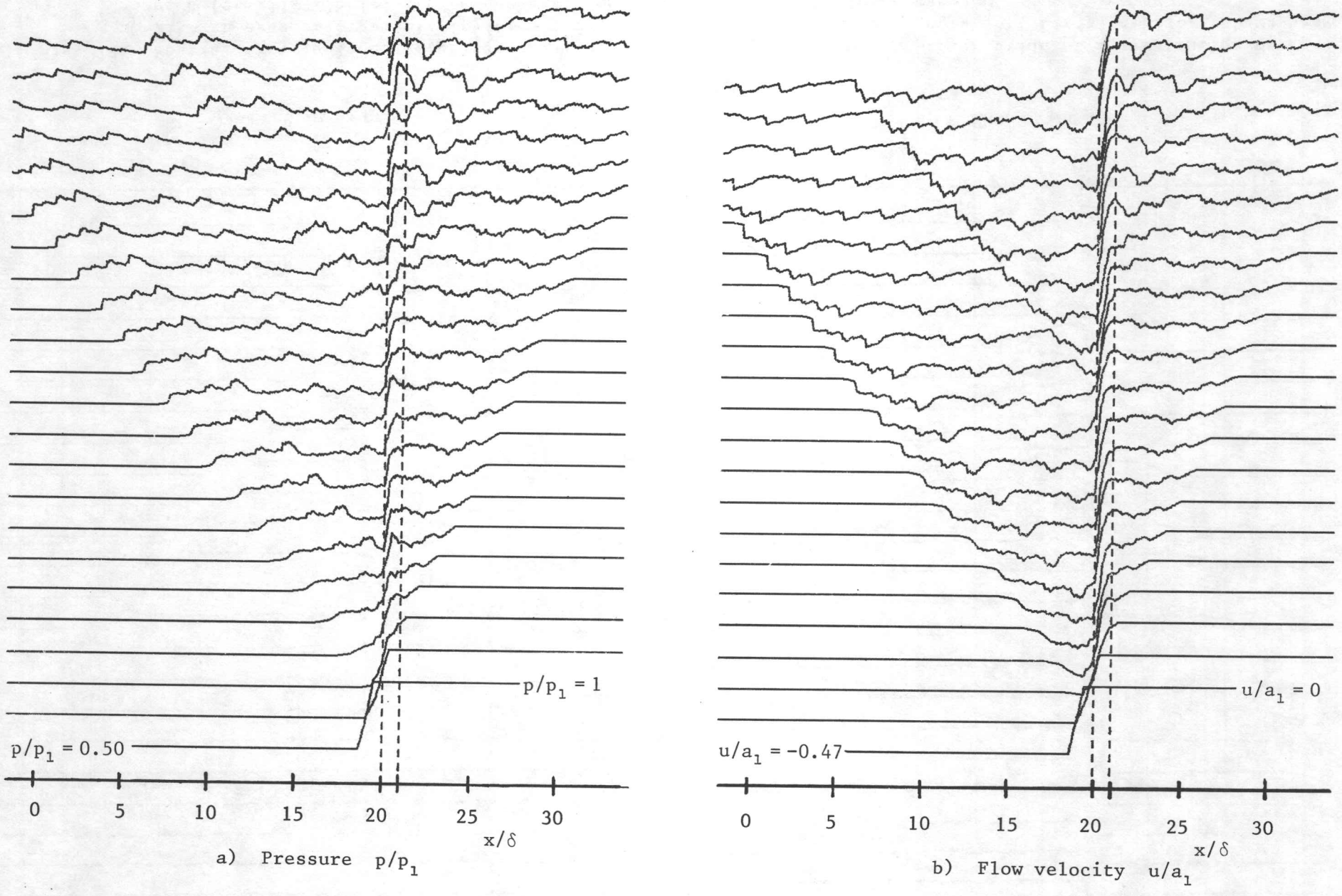

Fig. 23. Spatial distributions of pressure (a) and flow velocity (b) for the interaction of a rarefaction wave with an area enlargement ($p_2/p_1 = 0.50$, $S_d/S_u = 0.20$, pattern A). Note that the IMSL sampling scheme was used (random number sampling) and the number of grid zones was 720.

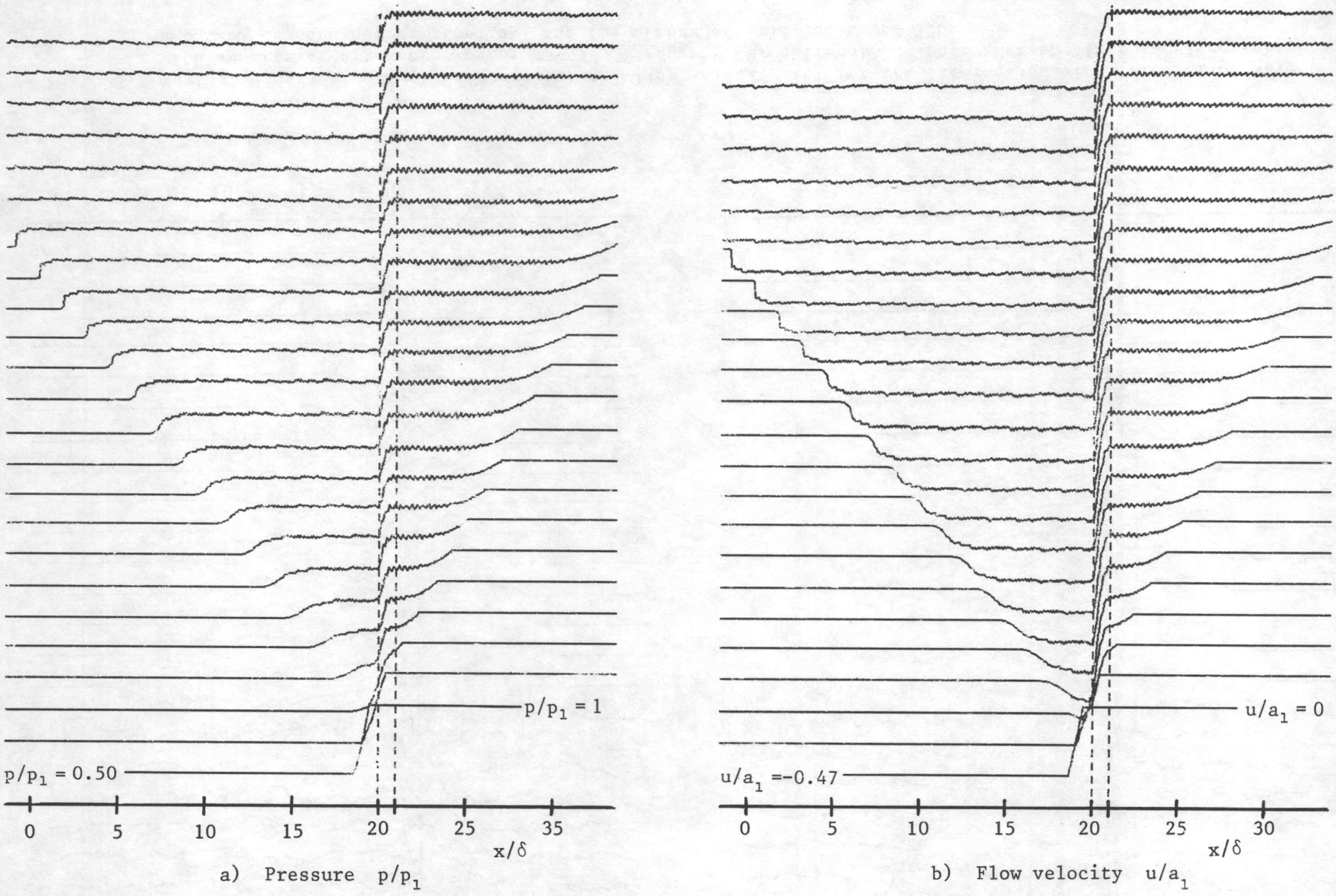

Fig. 24. Spatial distributions of pressure (a) and flow velocity (b) for the interaction of a rarefaction wave with an area enlargement ($p_2/p_1 = 0.50$, $S_d/S_u = 0.20$, pattern A). Note that Lax's sampling scheme was used (equidistributed random numbers) and the number of grid zones was 720.

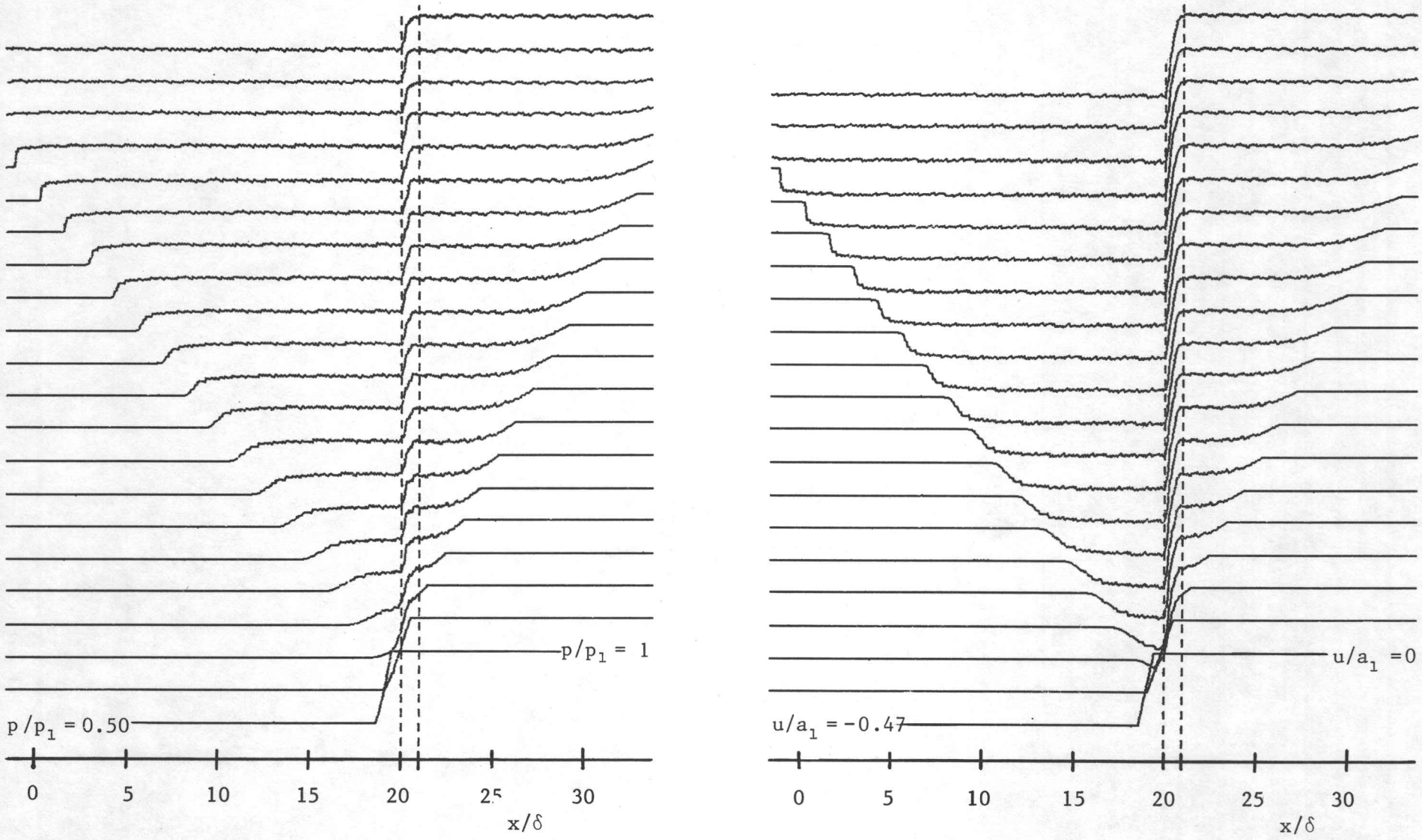

Fig. 25. Spatial distributions of pressure (a) and flow velocity (b) for the interaction of a rare faction wave with an area enlargement ($p_2/p_1 = 0.50$, $S_d/S_u = 0.20$, pattern A). Note that Van der Corput's sampling scheme was used (equidistributed random numbers) and the number of grid zones was 720.

APPENDIX A

COMPUTER PROGRAM LISTING OF THE QUASI-STEADY FLOW ANALYSIS

This computer program listing for the interaction of a rarefaction wave with an area enlargement includes two basic programs. For the first one the reflected wave from the interaction process is taken to be the standard case of a reflected shock wave. For the second one the reflected wave is taken to be a compression wave. Because the reflected wave is relatively weak, it is inconsequential as to which one is actually used to compute the quasi-steady flow properties, especially if the incident rarefaction-wave strength p_2/p_1 is greater than 0.01. The second program was used to verify this fact.

```
C-------------------------------------------------------------------
C--       RAREFACTION WAVE IMPINGING ON AN AREA ENLARGEMENT        --
C--                                                                --
C--         BY  P.M. OSTAFF,  O. IGRA,  AND  J.J. GOTTLIEB         --
C--                                                                --
C--                  CASE OF A REFLECTED SHOCK WAVE.               --
C-------------------------------------------------------------------
      IMPLICIT REAL*8(A-H,O-Z)
      REAL*8 M2, M3, M4, M5, M6, MS
      OPEN(UNIT=05,FILE='REFSHOC.DTA')
      OPEN(UNIT=06,FILE='PR:',RECL=132)
      N = 100
      IPAGE = 50
    1 READ(5,*) S56,G
      IF (S56) 1000, 5, 5
    5 CONTINUE
      G1 = (G-1.0D0)/2.0D0
      G2 = 2.0D0*G/(G-1.0D0)
      G3 = (G-1.0D0)/(G+1.0D0)
      G4 = 0.5D0*(G+1.0D0)/(G-1.0D0)
C------------------------------------------------------ PATTERN A ----
      DO 170 I=1,N
      M5 = - FLOAT(I)/FLOAT(N)
      CALL ARM (G, S56, M5, -1, M6)
      A61 = 1.0D0/(1.0D0 - G1*M6)
      P61 = A61**G2
      U61 = M6*A61
      A51 = A61 * (M6/(S56*M5))**G3
      U51 = M5*A51
      P51 = P61 * (A51/A61)**G2
      M4 = M5
      U41 = U51
      P41 = P51
      A41 = A51
      U31 = U41
      P31 = P41
      KCYC = 0
      P21 = P31
   20 KCYC = KCYC + 1
```

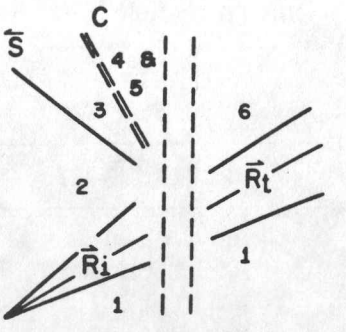

PATTERN A

```
      A21 = P21**(1.0D0/G2)
      F1 = G2*(A21 - 1.0D0) - G*U31
      F2 = DSQRT(P21*(P21 + P31/G3)/G2)
      F = F1 * F2 - A21*(P31 - P21)
      DF = F1*(P21 + G4*P31)/(G2*F2) + A21*(F2 + P21 - (P31-P21)/G2)/P21
      P21 = P21 - F/DF
      IF (1.0D-08 - DABS(F/DF)) 25, 25, 40
   25 IF (KCYC - 25) 20, 30, 30
   30 WRITE(6,35) F, DF, P21
   35 FORMAT ('   KCYC EXCEEDS 25     F  DF  P21', 3D15.5)
   40 P32 = P31/P21
      A21 = P21**(1.0D0/G2)
      A31 = A21 * DSQRT(P32*(1.0D0 + G3*P32)/(G3 + P32))
      M3 = U31/A31
      U21 = (A21 - 1.0D0)/G1
      M2 = U21/A21
      MS = - DSQRT((P32 - 1.0D0)*(G+1.0D0)/(2.0D0*G) + 1.0D0)
      IF (I-1) 120, 120, 130
  120 WRITE(6,121) S56, G
  121 FORMAT (1H1,/,' OSTAFF/IGRA/GOTTLIEB/RAREFACTION WAVE/AREA ENLARGE
     *MENT (R.S.)   S5/S6 =', F8.4, '      GAMMA =', F8.4, '       PATTE
     *RN A', //)
      IC = I + IPAGE/3
  122 WRITE(6,123)
  123 FORMAT ('    M6       U61      P61      A61       M5        U51
     *  P51      A51       M4        U41      P41      A41      P32')
      WRITE(6,124)
  124 FORMAT ('    M3       U31      P31      A31       M2        U21
     *  P21      A21                                            MS', /)
      GO TO 150
  130 IF (I-IC) 150, 135, 150
  135 WRITE(6,136) S56, G
  136 FORMAT (1H1,/, ' OSTAFF/IGRA/GOTTLIEB/RAREFACTION WAVE/AREA ENLARG
     *EMENT (R.S.)   S4/S3 =', F8.4, '    GAMMA =', F8.4, '    PATTERN A
     * CONTINUED', //)
      IC = IC + IPAGE/3
      GO TO 122
  150 WRITE(6,160) M6, U61, P61, A61, M5, U51, P51, A51, M4, U41, P41,
     * A41, P32
  160 FORMAT (F8.4, F9.4, 2F9.5, 2F10.5, 2F9.5, 2F10.5, 3F9.5)
  170 WRITE(6,180) M3, U31, P31, A31, M2, U21, P21, A21, KCYC, MS
  180 FORMAT (F8.4, F9.4, 2F9.5, 2F10.5, 2F9.5, I10, F37.5, /)
  500 CONTINUE
C------------------------------------------------ PATTERN B ----
      A51=A61*(-M6/S56)**G3
      P51=A51**G2
C-----------------------------------------
C     SPECIFY P45, 0<= P45 <= 1
C-----------------------------------------
      DP=0.01D0
      P45=1.0D0+DP
      DO 510 I=1,100
      P45=P45-DP
      A45=P45**(1.D0/G2)
      A41=A51*A45
      P41=P51*P45
```

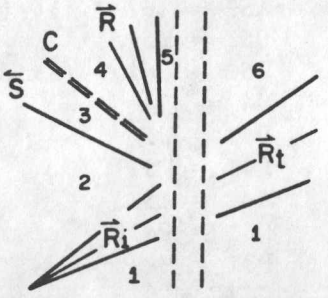

PATTERN B

```
      P31=P41
      U41=(1.D0/G1)*(-A51+A41)-A51
      M4=U41/A41
      U31=U41
      KCYC=0
      P21=P31
520   KCYC=KCYC+1
      A21=P21**(1.D0/G2)
      F1=G2*(A21-1.D0)-G*U31
      F2=DSQRT(P21*(P21+P31/G3)/G2)
      F=F1*F2-A21*(P31-P21)
      DF=F1*(P21+G4*P31)/(G2*F2)+A21*(F2+P21-(P31-P21)/G2)/P21
      P21=P21-F/DF
      IF(1.D-8 - DABS(F/DF))525,525,540
525   IF(KCYC-25)520,530,530
530   WRITE(6,535)F,DF,P21
535   FORMAT('    KCYC EXCEEDS 25      F  DF  P21',3D15.5)
540   P32=P31/P21
      A21=P21**(1.D0/G2)
      A31=A21*DSQRT(P32*(1.D0+G3*P32)/(G3+P32))
      M3=U31/A31
      U21=(A21-1.D0)/G1
      M2=U21/A21
      MS=-DSQRT((P32-1.D0)*(G+1.D0)/(2.D0*G)+1.D0)
      IF(I-1)620,620,630
620   WRITE(6,621)S56,G
621   FORMAT(1H1,/,' OSTAFF/IGRA/GOTTLIEB/RAREFACTION WAVE/AREA '
     * 'ENLARGEMENT (R.S.)   S5/S6 = ',F8.4,'      GAMMA = ',F8.4,
     * '       PATTERN B',//)
      IC=I+IPAGE/3
      WRITE(6,501)
501   FORMAT(1X,'SINCE M5=-1 THROUGHOUT THIS WAVE PATTERN, M6, A61,'
     * 'U61, U51, AND P61 REMAIN UNCHANGED (EQUAL TO THE LAST LINE '
     * 'IN PATTERN A, M5=-1')
622   WRITE(6,123)
      WRITE(6,124)
      GO TO 650
630   IF(I-IC)650,635,650
635   WRITE(6,636)S56,G
636   FORMAT(1H1,/,' OSTAFF/IGRA/GOTTLIEB/RAREFACTION WAVE/AREA '
     * 'ENLARGEMENT (R.S.)   S4/S3 =',F8.4,'    GAMMA =',F8.4,
     * '    PATTERN B CONTINUED',//)
C
      IC=IC+IPAGE/3
      GO TO 622
650   WRITE(6,160)M6,U61,P61,A61,M5,U51,P51,A51,M4,U41,P41,A41,P32
670   WRITE(6,180)M3,U31,P31,A31,M2,U21,P21,A21,KCYC,MS
510   CONTINUE
      GO TO 1
1000  STOP
      END
C-----------------------------------------------------------------------
      SUBROUTINE ARM(G,AR12,M1,N,M2)
C-----------------------------------------------------------------------
C     GIVEN THE INITIAL AREA RATIO AR12 AND FLOW MACH NUMBER
C     M1,THIS SUBROUTINE DETERMINES THE FLOW MACH NUMBER M2 BY
```

```
C     NEWTON'S ITERATION METHOD
C-----------------------------------------------------------------------
      IMPLICIT REAL*8(A-H,O-Z)
      REAL*8 M1,M2
      G1=(G-1.D0)/2.D0
      G2=(G+1.D0)/(2.D0*(G-1.D0))
      IF(N)5,10,10
5     M2=M1*AR12
      GO TO 15
10    M2=M1/AR12
15    KCYC=0
20    KCYC=KCYC+1
      F=(M1/M2)*AR12*((1.D0+G1*M2**2)/(1.D0+G1*M1**2))**G2-1.D0
      DF=(F+1.D0)*(2.D0*G1*G2*M2/(1.D0+G1*M2**2)-1.D0/M2)
      M2=M2-F/DF
      IF(1.D-8 - DABS(F/DF))25,25,40
25    IF(KCYC-125)20,30,30
30    WRITE(6,35)AR12,M1,M2
35    FORMAT('   KCYC EXCEEDS 125 ',/,4X,'   AR12   ','   M1   ',
     * '   M2   ',/,1X,3F10.3/)
40    RETURN
      END
C
C
C-----------------------------------------------------------------------
C--       RAREFACTION WAVE IMPINGING ON AN AREA ENLARGEMENT           --
C--                                                                   --
C--         BY  P.M. OSTAFF,  O. IGRA,  AND  J.J. GOTTLIEB           --
C--                                                                   --
C--              CASE OF A REFLECTED COMPRESSION WAVE.                --
C-----------------------------------------------------------------------
      IMPLICIT REAL*8(A-H,O-Z)
      REAL*8 M2, M3, M4, M5, M6, MS
      OPEN(UNIT=05,FILE='REFCOMP.DTA')
      OPEN(UNIT=06,FILE='PR:',RECL=132)
      N = 100
      IPAGE = 50
    1 READ(5,*) S56,G
      IF (S56) 1000, 5, 5
    5 CONTINUE
      G1=(G-1.)/2.
      G2=2.*G/(G-1.)
      G3=(G-1.)/(G+1.)
C------------------------------------------------- PATTERN A ----
      I=0
      DO 10 IN=-1,-100,-1
      M5=DFLOAT(IN)*0.01D0
      I=I+1
      CALL ARM(G,S56,M5,-1,M6)
      A61=(2./(G-1.))/(2./(G-1.)-M6)
      U61=(2./(G-1.))*(A61-1.)
      P61=A61**(2.*G/(G-1.))
      A51=A61*(M6/(M5*S56))**((G-1.)/(G+1.))
      P51=A51**(2.*G/(G-1.))
      A41=A51
      A31=A51
```

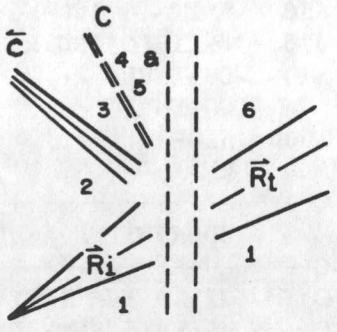

PATTERN A

```
      M3=M5
      M4=M5
      P41=P51
      P31=P51
      A21=0.5*(A41+1.)+((G-1.)/4.)*M5*A51
      P21=A21**((2.*G)/(G-1.))
      U51=M5*A51
      U41=U51
      U31=U41
      P32=P31/P21
      U21=(A21-1.)/G1
      M2=U21/A21
      MS=-DSQRT((P32-1.)*(G+1.)/(2.*G)+1.)
      KCYC=0
      IF (I-1) 120, 120, 130
  120 WRITE(6,121) S56, G
  121 FORMAT (1H1, /, ' OSTAFF/IGRA/GOTTLIEB/RAREFACTION WAVE/AREA ENLAR
     *GEMENT (R.S.)   S5/S6 =', F8.4, '      GAMMA =', F8.4, '      PAT
     *TERN A', //)
      IC = I + IPAGE/3
  122 WRITE(6,123)
  123 FORMAT ('    M6       U61      P61      A61       M5       U51
     *  P51      A51       M4       U41      P41      A41      P32')
      WRITE(6,124)
  124 FORMAT ('    M3       U31      P31      A31       M2       U21
     *  P21      A21                                          MS', /)
      GO TO 150
  130 IF (I-IC) 150, 135, 150
  135 WRITE(6,136) S56, G
  136 FORMAT (1H1,/, ' OSTAFF/IGRA/GOTTLEB/RAREFACTION WAVE/AREA ENLARGE
     *MENT (R.S.)   S5/S6 =', F8.4, '    GAMMA =', F8.4, '    PATTERN A
     *CONTINUED', //)
      IC = IC + IPAGE/3
      GO TO 122
  150 WRITE(6,160) M6, U61, P61, A61, M5, U51, P51, A51, M4, U41, P41,
     * A41, P32
  160 FORMAT (F8.4, F9.4, 2F9.5, 2F10.5, 2F9.5, 2F10.5, 3F9.5)
  170 WRITE(6,180) M3, U31, P31, A31, M2, U21, P21, A21, KCYC, MS
  180 FORMAT (F8.4, F9.4, 2F9.5, 2F10.5, 2F9.5, I10, F37.5, /)
   10 CONTINUE
C------------------------------------------------ PATTERN B ----
      A51=A61*(-M6/S56)**G3
      P51=A51**G2
C-------------------------------------------------
C     SPECIFY P45, 0<= P45 <= 1
C-------------------------------------------------
C     A61,U61,M6,A51,P51 RETAINS VALUE WHEN M5=-1
C-------------------------------------------------
      I=0
      DO 20 IN=95,5,-1
      P45=DFLOAT(IN)*0.01
      I=I+1
      A45=P45**((G-1.)/(2.*G))
      A41=A51*P45**((G-1.)/(2.*G))
      A31=A41
      P41=P45*P51
```

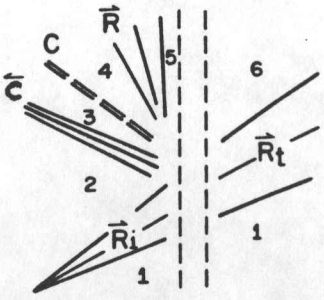

PATTERN B

```
      P31=P41
      M4=(2./(G-1.))-((G+1.)/(G-1.))*(A51/A41)
      M3=M4
      A21=0.5*(A31+1.)+((G-1.)/4.)*M3*A31
      P21=A21**((2.*G)/(G-1.))
      U41=M4*A41
      U31=U41
      P32=P31/P21
      U21=(A21-1.)/G1
      M2=U21/A21
      MS=-DSQRT((P32-1.)*(G+1.)/(2.*G)+1.)
      IF(I-1)620,620,630
620   WRITE(6,621)S56,G
621   FORMAT(1H1,/,'    IGRA/GOTTLIEB   RAREFACTION WAVE/AREA '
     * 'ENLARGEMENT (R.S.)   S5/S6 = ',F8.4,'      GAMMA = ',F8.4,
     * '       PATTERN B',//)
      IC=I+IPAGE/3
      WRITE(6,501)
501   FORMAT(1X,'SINCE M5=-1 THROUGHOUT THIS WAVE PATTERN, M6, A61,'
     * 'U61, U51, AND P61 REMAIN UNCHANGED (EQUAL TO THE LAST LINE '
     * 'IN PATTERN A, M5=-1')
622   WRITE(6,123)
      WRITE(6,124)
      GO TO 650
630   IF(I-IC)650,635,650
635   WRITE(6,636)S56,G
636   FORMAT(1H1,/,'  IGRA/GOTTLIEB   RAREFACTION WAVE/AREA '
     * 'ENLARGEMENT (R.S.)   S5/S6 =',F8.4,'    GAMMA =',F8.4,
     * '    PATTERN B CONTINUED',//)
      IC=IC+IPAGE/3
      GO TO 622
650   WRITE(6,160)M6,U61,P61,A61,M5,U51,P51,A51,M4,U41,P41,A41,P32
670   WRITE(6,180)M3,U31,P31,A31,M2,U21,P21,A21,KCYC,MS
20    CONTINUE
      GO TO 1
1000  STOP
      END
```

APPENDIX B

DIFFERENT ALGORITHMS FOR GENERATING RANDOM NUMBERS

Four different random-number schemes or algorithms are now presented and discussed in this appendix, for application in the random-choice method (RCM). The names that were given to these sampling schemes in the main body of this report are:

i) Chorin's sampling scheme,

ii) IMSL sampling scheme,

iii) Modified Lax sampling scheme,

iv) Van der Corput's sampling scheme.

Each of these schemes will now be considered, but not in the order that they appear in this list. Then, some graphical illustrations of how the random numbers vary are presented for interest.

IMSL Sampling Scheme

The IMSL sampling scheme for generating random numbers is in the extensive collection of mathematical and statistical subroutines written in the language FORTRAN that have been collected and published for sale by the International Mathematical and Statistical Libraries (IMSL), Incorporated.[B1] Although this library with its sampling algorithm is readily available for use with numerous different computers, the actual source listing of the computer program for this sampling scheme or the method of computer implementation is protected by copyright laws and not available to users. As a consequence, the source listing or method of implementation is unknown to the authors.

The only information available to the user is that given in the IMSL notes along with the description and examples of how to use the sampling scheme. The IMSL random number algorithm having the call statement GGUBFS(SEED)[B1] produces pseudo-random numbers that are suppose to be uniform over the interval from zero to unity with a very small standard deviation, provided that many random numbers are used. This was carefully checked and found to be true. In fact, of all random-number algorithms that were checked, the IMSL scheme proved to be best for producing the most truly random numbers. There is no doubt that the values were drawn from a random number generator implemented on the computer, probably with some variance reduction technique, but without stratification or modification of the random number. If this is true, then it would be a simple random sampling method. However, random numbers from random sampling are known to be not equidistributed as required or, more correctly, as desired for use in the RCM, in the sense discussed by both Chorin[B2] and Colella.[B3-B4] Hence, it should not be expected to be a good random number generator for the RCM.

Chorin's Sampling Scheme

Chorin's basic method[B2] is outlined here. In his method there are three parameter for which values have to be selected. Let k_1 and k_2 be two mutually

prime numbers with $k_1 > k_2$. For example, let $k_1 = 11$ and $k_2 = 7$. Now consider the sequence of integers that is given by the following expession

$$n_{i+1} = \{n_i + k_2\} \bmod \{k_1\},$$

for which the first number n_0 is specified initially. For example, let us take $n_0 = 2$, and note that it must be less than k_1. For the three specified values of $n_0 = 2$, $k_1 = 11$ and $k_2 = 7$, the sequence of numbers would therefore follow as presented below.

$$\begin{aligned}
n_0 &= 2 \\
n_1 &= \{k_2 + n_0\} \bmod \{k_1\} = 9 \\
n_2 &= \{k_2 + n_1\} \bmod \{k_1\} = 5 \\
n_3 &= \{k_2 + n_2\} \bmod \{k_1\} = 1 \\
n_4 &= \{k_2 + n_3\} \bmod \{k_1\} = 8 \\
n_5 &= \{k_2 + n_4\} \bmod \{k_1\} = 4 \\
n_6 &= \{k_2 + n_5\} \bmod \{k_1\} = 0 \\
n_7 &= \{k_2 + n_6\} \bmod \{k_1\} = 7 \\
&\cdots \\
&\cdots \\
n_{i+1} &= \{k_2 + n_i\} \bmod \{k_1\} = .
\end{aligned}$$

[Note that we can also have $n_{i+1} = \{k_2 + n_i\} \bmod \{k_1\} = k_2 + n_i$ if $k2 + n_i < k_1$ or $n_{i+1} = \{k_2 + n_i\} \bmod \{k_1\} = k_2 + n_i - k_1$ if $k2 + n_i \geq k_1$.] Based on the above sequence of integers, a modified sequence of fairly good equidistributed random numbers θ_i in the range of $-1/2$ to $+1/2$ is given by the following expression

$$\theta_i = [(n_i + \eta_i)/k_1] - 1/2,$$

for which η_i is another set of random numbers in the range from zero to unity (0 to 1). This second set of random numbers is generated by random sampling, such as the IMSL random sampling scheme.

In our studies the second or other set of random numbers η_i is given by an algorithm contained in the following FORTRAN statements

```
      SUBROUTINE RANDU (IX, IY, YFL)
      IY = IX*65539
      IF (IY) 5, 6, 6
    5 IY = IY + 2147483647 + 1
    6 YFL = IY
      YFL = YFL*0.4656613E-09
      IX = IY
      RETURN
      END
```

for which IX = 123456789 initially and YFL = η_i. For IX = 123456789, the first six random numbers from this scheme are 0.774670, 0.130622, 0.811695, 0.694577, 0.862203, and 0.922028, which lie in the range from 0 to 1. The other set of

FORTRAN statements that we have employrd to get the set of random number θ_i are given as follows:

```
K1 = 11
K2 =  7
NU =  2
IX = 123456789
NU = MOD(K2 + NU, K1)
CALL RANDU (IX, IY, YFL)
SI = (YFL + FLOAT(NU))/FLOAT(K1) - 0.5
```

In these statements SI = θ_i, YFL = η_i, NU = n_i, k1 = k_1 and k2 = k_2. The first six random numbers for SI or θ_i are 0.388606, -0.033580, -0.335300, 0.290416, -0.057982, and -0.416179, which lie in the range from -1/2 to +1/2.

Chorin's random-number algorithm just presented is based primarily on a standard deviation reduction technique. Note that his procedure modifies a set of random numbers, to make them nonrandom and become more equidistributed. His method produces stratified random numbers, which are not quite equidistributed random numbers. His stratified random numbers should be much better for the RCM than the previously described IMSL random numbers, but there are also two better ones that will now be introduced.

Modified Lax Sampling Scheme

Lax[B5] proposed a sampling scheme for use in solving hyperbolic equations, which is probably due to earlier work by Richtmeyer and Ostrowski. It is a simple sampling scheme defined by $\theta_i = \{r^{1/2}\} \bmod \{1\}$, where θ_i is the random number in the range of 0 to 1, and r is an integer which is not the square of another integer. This scheme has subsequently been modified and it is given by $\theta_i = \{i\ r^{1/2}\} \bmod \{1\}$, where i takes on the integer values of 1, 2, 3, . , etc. In FORTRAN language, the following statement in double precision is used to get the set random numbers θ_i,

```
SI  =  DMOD(DFLOAT(I)*DSQRT(2.0D0), 1.0D0) - 0.5D0,
```

where SI = θ_i and I = i. The subtraction of 1/2 has been inserted so that the random numbers cover the range -1/2 to +1/2. The first six numbers of this sequence are -0.085786, 0.328427, -0.257359, 0.156854, -0.428932, and -0.014719.

The modified Lax set of random numbers is a nonrandom equidistributed sequence, which should be better for use with the RCM than Chorin's sampling scheme because they are equidistributed, as required for better computational results.[B2-B4]

Van der Corput's Sampling Scheme

Van der Corput's sampling scheme,[B6] which is also given in the book by Hammersley and Handscomb,[B7] is also discussed by Colella.[B3-B4] Suppose that the natural numbers are expressed in the scale of notation with a radix equal to 2, so that

$$n = \sum_{k=0}^{m} i_k\, 2^k .$$

This is also the binary expansion of the number sequence n = 1, 2, 3, . , etc, where i is a binary number that equal only 0 and 1. Then, a set of random numbers θ_i can be obtained by simply writing the digits of these numbers in their reverse order, preceded by a point. This results in the following series

$$\theta_n = \sum_{k=0}^{m} i_k \, 2^{-(k+1)} .$$

The method of getting the sequence of random numbers from the above equations might seem to be a little unclear. In order to clearly illustrate the manner in which this sequence is constructed, the first few elements of the various sequences are written down for convenience.

n (decimal)	i_k (binary)	θ_n (binary)	θ_n (decimal)
1	1_2	0.1_2	0.5000
2	10_2	0.01_2	0.2500
3	11_2	0.11_2	0.7500
4	100_2	0.001_2	0.1250
5	101_2	0.101_2	0.6250
6	110_2	0.011_2	0.3750
7	111_2	0.111_2	0.8750
8	1000_2	0.0001_2	0.0625
9	1001_2	0.1001_2	0.5625
10	1010_2	0.0101_2	0.3125

The decimal numbers n are first changed into the binary numbers i_k. Then these binary numbers are reversed and a point or decimal is put in the front to get θ_n as binary numbers. Finally, these binary numbers are converted back into decimal numbers, yielding θ_n in decimal notation, having the range from 0 to 1.

We can also note that $\theta_n < 0.5$ if n is even, and $\theta_n > 0.5$ if n is odd, but always covering the range from 0 to 1. Also, we have $(k/4) \leq \theta_n < (\{k+1\}/4)$ if $n = j_k \bmod (4)$, with k = 1, 2, and 4, where $j_0 = 0$, $j_1 = 2$, $j_2 = 1$, and $j_3 = 3$.

The FORTRAN statements that we use in applying the Van der Corput sampling scheme are given below for interest.

```
      IE = (1, 2, 3, . . . , etc.)
      MRND = 0
      RNDM = 0.D0
  201 MRND = MRND + 1
      MD = MOD(IE, 2**MRND)
      IF (MD .EQ. 0) GO TO 201
      RNDM = RNDM + 1.D0/2.D0**MRND
      IE = IE - MD
      IF (IE .EQ. 0) GO TO 202
      GO TO 201
  202 RNDM = RNDM - 0.5D0
```

In the above statements, RNDM = θ_n, and the random number that now has a range

from -1/2 to +1/2. The first seven random numbers are 0.000000, -0.250000, 0.250000, -0.375000, 0.125000, -0.125000, and finally 0.375000.

This Van der Corput sampling sequence, like all of them with a radix different than 2, are equidistributed.[B3-B4] Hence, for use with the RCM, Van der Corput's equidistributed sampling scheme should be much better than the first IMSL sampling scheme, better than Chorin's stratified sampling scheme, and probably equivalent to Lax's equidistributed sampling scheme. In fact, Van der Corput's sampling scheme should be slightly superior to Lax's sampling scheme, because it produces a slightly smaller error in the location of moving fronts like shock waves.[B3-B4]

Graphical Results for the Four Different Random Number Schemes

Four sets of graphical results from the sampling schemes of IMSL, Chorin, Lax, and Van der Corput are presented in Figs. B1 to B4. In each graph the random number value is plotted versus the n^{th} random number. The horizontal scale is in arbitrary units, to spread out the 400 random numbers for clarity.

Random numbers from the IMSL sampling scheme are spread out or distributed in an irregular or random manner in Fig. B1, without any apparent pattern, as one might expect, although some successive values are clustered more than one might expect. For Chorin's sampling scheme, the stratified random numbers in Fig. B2 are still quite spread out or distributed in an irregular or random manner, although there is now no marked clustering. One would be hard pressed to find some repetitive pattern in Chorin's results, although this would be easier done for his results than those from the IMSL sampling scheme.

Equidistributed random numbers from Lax's sampling scheme are markedly repetitive with an easily recognized pattern, and those from Van der Corput's sampling scheme are also similarly repetitive but slightly less so, as can be seen from the results given in Fig. B3 and 4, respectively. The primary reason for this behavior is that they are equidistributed. This particular type of behavior of equidistributed nonrandom numbers is desirable or needed for the RCM, in order to get good numerical results with less superposed numerical noise, holding all other things constant. This is verified by the numerical results given and discussed in section 3.3.2 in the main body of this report.

References for Appendix B

B1. Anon., 'International Mathematical and Statistical Library', International Mathematical and Statistical Libraries, Incorporated, Customer Relations, Sixth Floor, NBC Building, 7500 Bellaire Boulevard, Houston, Texas, U.S.A., June 1982.

B2. Chorin, A.J., 'Random Choice Solution of Hyperbolic Systems,' Journal of Computational Physics, Vol. 22, No. 4, pp. 517-533, December 1976.

B3. Colella, 'Glimm's Method for Gas Dynamics,' Society for Industrial and Applied Mathematics, Journal of Scientific and Statistical Computing, Vol. 3, No. 1, March 1982.

B4. Colella, P., 'An Analysis of the Effect of Operator Splitting and the Sampling Procedure on the Accuracy of Glimm's Method,' Report No.

LBL-8874, Lawrence Berkeley Laboratory, Physics, Computer Science and Mathematics Division, University of California, Berkeley, California, U.S.A., December 1978.

B5. Lax, P.D., 'Hyperbolic Systems of Equations and Computing,' Society for Industrial and Applied Mathematics, Review 11, pp. 7-19, 1969.

B6. Van der Corput, 'Verteilungsfunktionen,' Proc. Kon. Adad. Wet., Vol. 38, pp. 813-821 and pp. 1058-1066, Amsterdam, 1935.

B7. Hammersley, J.M. and Handscomb, D.C., 'Monte Carlo Methods,' Methuen and Company Limited, London, 1975.

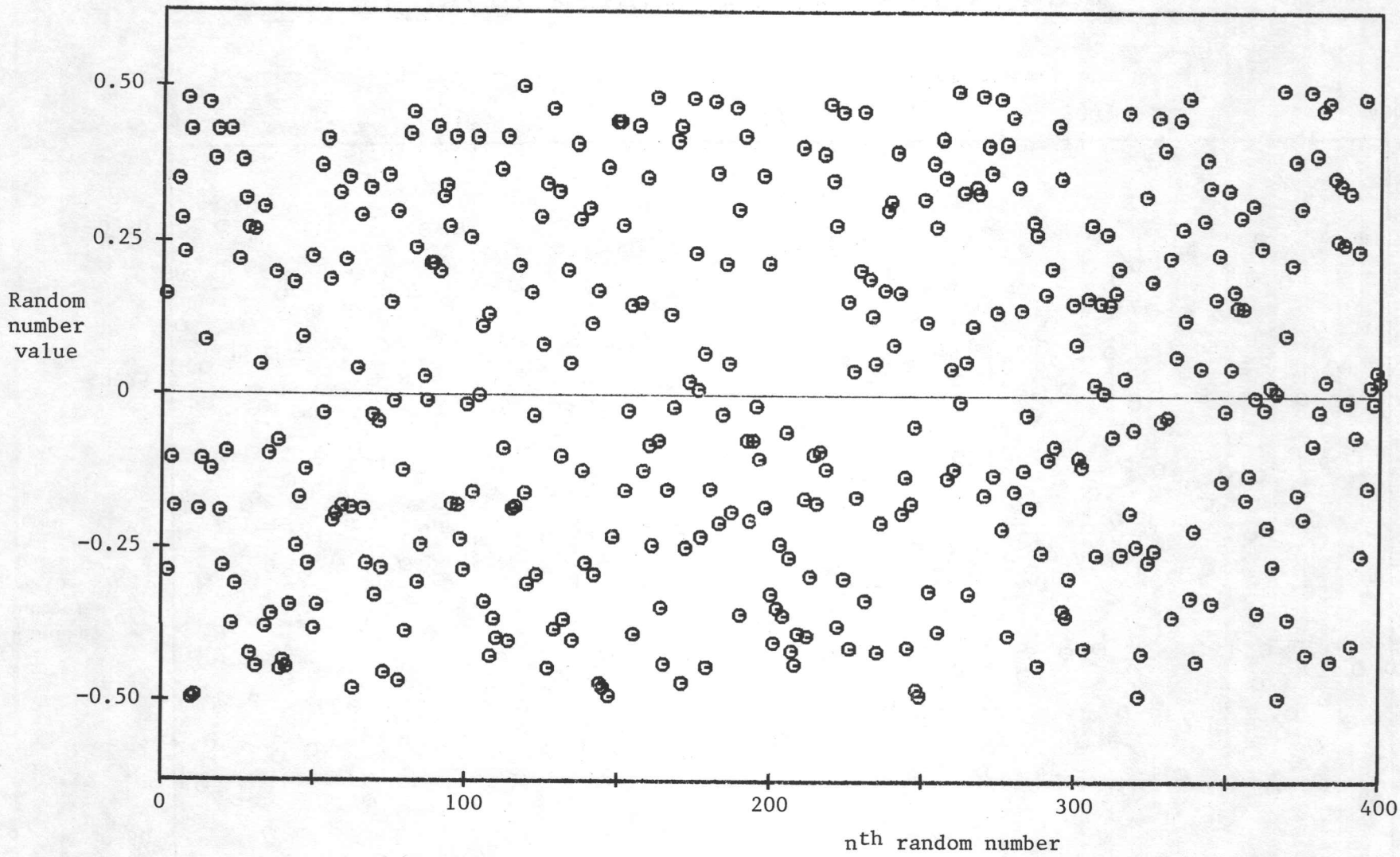

Fig. B1. Random number values in the range of -1/2 to +1/2 from the IMSL sampling scheme.

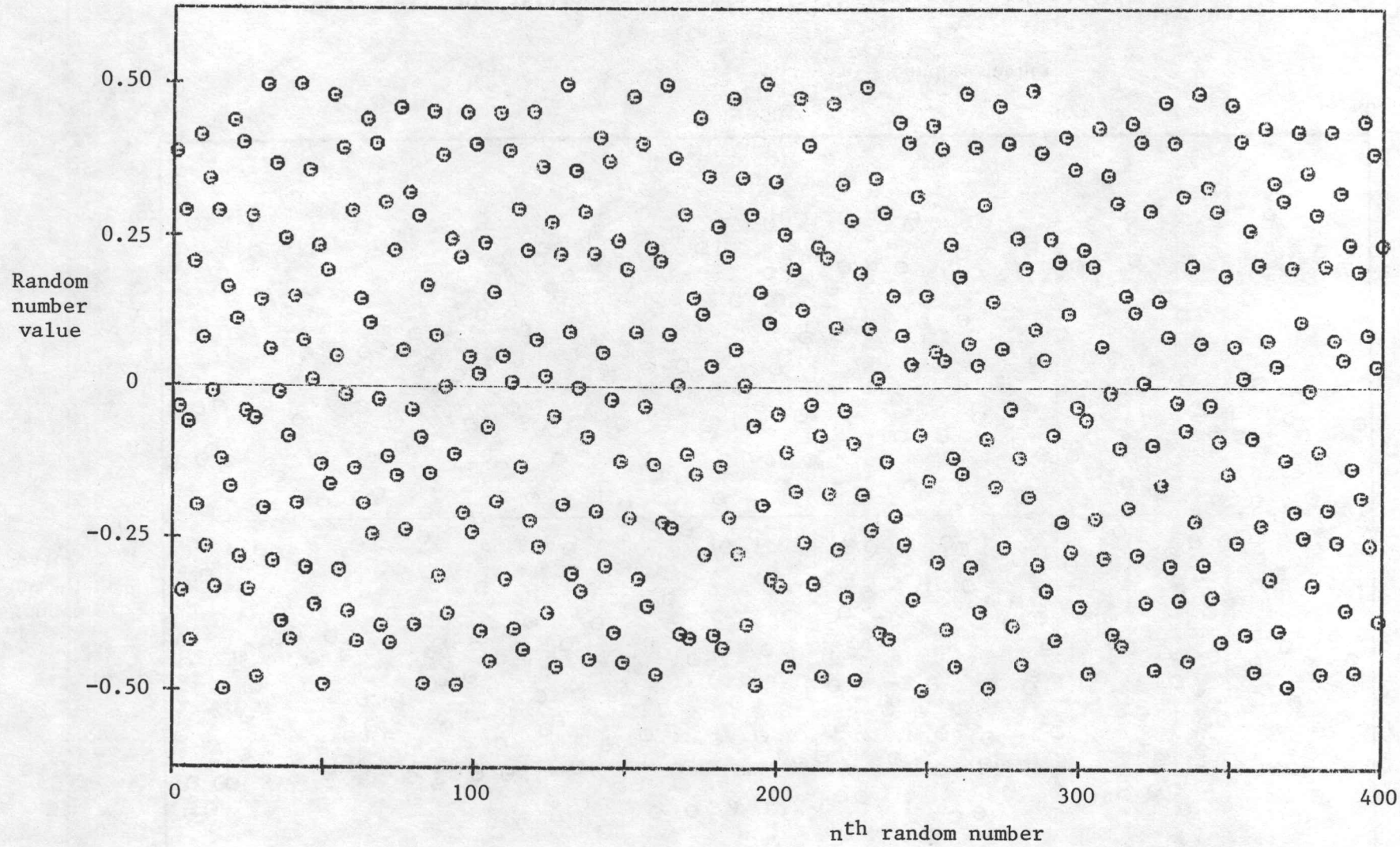

Fig. B2. Stratified random number values in the range of −1/2 to +1/2 from Chorin's sampling scheme.

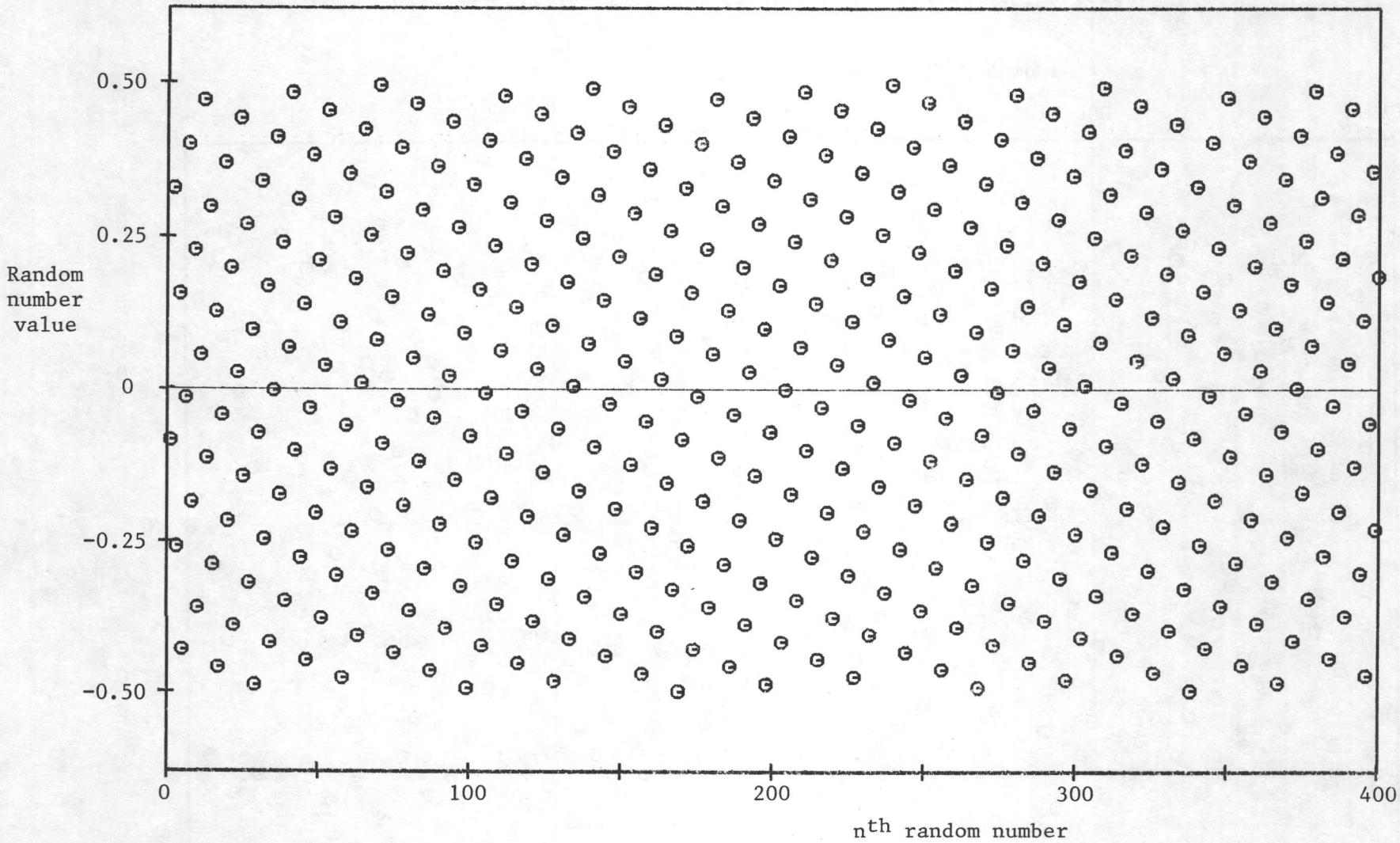

Fig. B3. Equidistributed random number values in the range of -1/2 to +1/2 from Lax's sampling scheme.

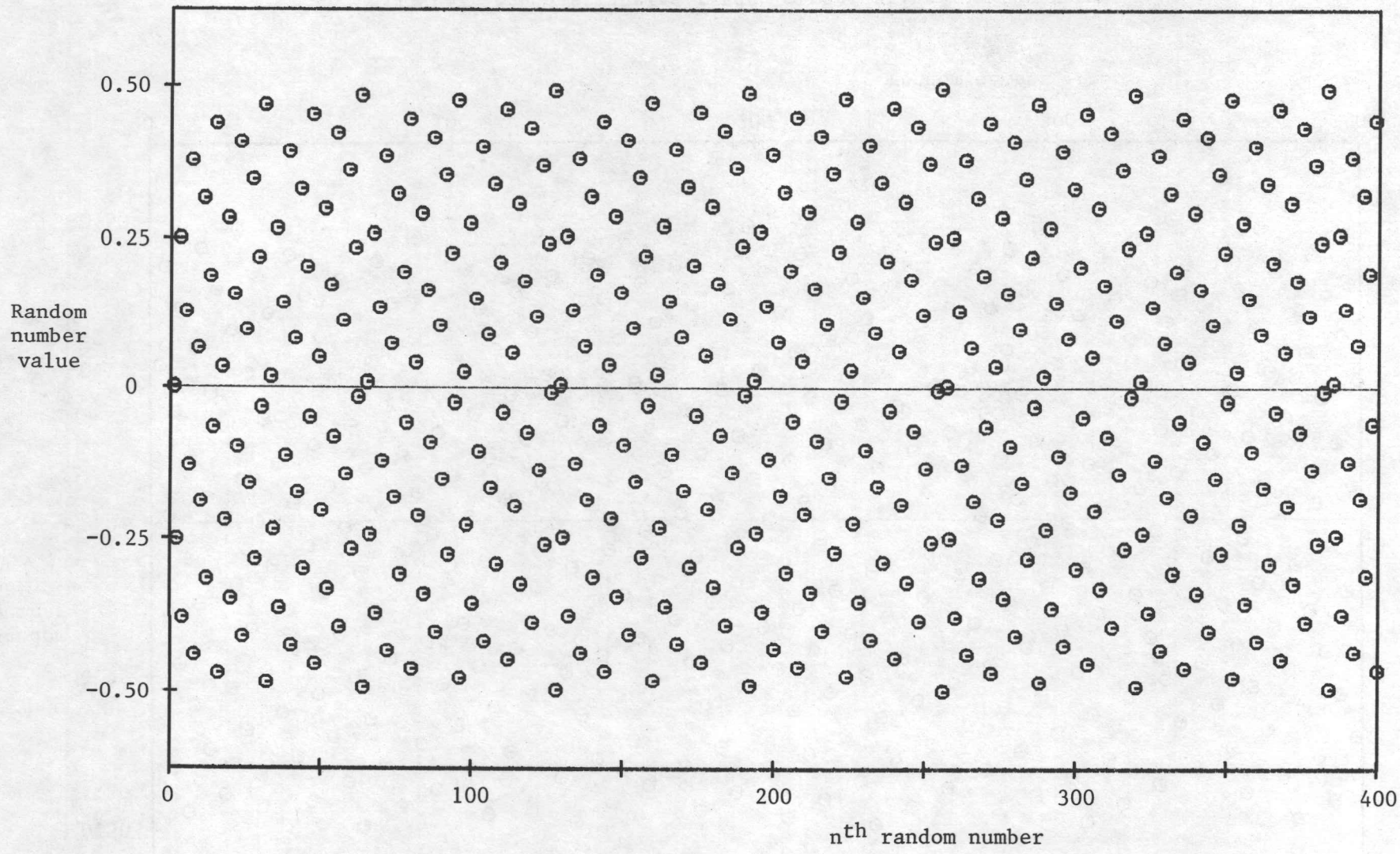

Fig. B4. Equidistributed random number values in the range of -1/2 to +1/2 from Van der Corput's sampling scheme.

UTIAS Report No. 273

University of Toronto, Institute for Aerospace Studies (UTIAS)
4925 Dufferin Street, Downsview, Ontario, Canada, M3H 5T6

AN ANALYTICAL AND NUMERICAL STUDY OF THE INTERACTION OF RAREFACTION WAVES WITH AREA CHANGES IN DUCTS
PART 2: AREA ENLARGEMENTS

Igra, O., Gottlieb, J. J., Saito, T.

1. Rarefaction wave 2. Duct flows 3. Flow through area change

I. Igra, O., Gottlieb, J. J., Saito, T. II. UTIAS Report No. 273

The interaction of a rarefaction wave with a gradual monotonic area enlargement of finite length in a duct or pipe is studied both analytically and numerically. A quasi-steady flow analysis that is analytical for an inviscid flow of a perfect gas is presented first, to obtain asymptotic solutions for the flow at late times, after all transient disturbances from the interaction process have subsided. Analytical results are given and discussed for the boundary between the two possible asymptotic wave patterns that are predicted and the corresponding asymptotic strengths of the transmitted, reflected and other waves, all as a function of both the incident rarefaction-wave strength and area-enlargement ratio. This was done for both perfect diatomic gases and air with $\gamma = 7/5$ and perfect monatomic gases with $\gamma = 5/3$. Finally, numerical results obtained by employing the new random choice method to solve the nonstationary equations of motiona are presented and discussed for the complete unsteady rarefaction-wave interaction with the area enlargement, for numerous different combinations of rarefaction-wave strengths and area-enlargement ratios. These results show clearly how the transmitted, reflected and other waves develop and evolve with time, until they eventually attain constant strengths at late times, in good agreement with the quasi-steady flow predictions for the asymptotic wave patterns.

Available copies of this report are limited. Return this card to UTIAS, if you require a copy.

UTIAS Report No. 273

University of Toronto, Institute for Aerospace Studies (UTIAS)
4925 Dufferin Street, Downsview, Ontario, Canada, M3H 5T6

AN ANALYTICAL AND NUMERICAL STUDY OF THE INTERACTION OF RAREFACTION WAVES WITH AREA CHANGES IN DUCTS
PART 2: AREA ENLARGEMENTS

Igra, O., Gottlieb, J. J., Saito, T.

1. Rarefaction wave 2. Duct flows 3. Flow through area change

I. Igra, O., Gottlieb, J. J., Saito, T. II. UTIAS Report No. 273

The interaction of a rarefaction wave with a gradual monotonic area enlargement of finite length in a duct or pipe is studied both analytically and numerically. A quasi-steady flow analysis that is analytical for an inviscid flow of a perfect gas is presented first, to obtain asymptotic solutions for the flow at late times, after all transient disturbances from the interaction process have subsided. Analytical results are given and discussed for the boundary between the two possible asymptotic wave patterns that are predicted and the corresponding asymptotic strengths of the transmitted, reflected and other waves, all as a function of both the incident rarefaction-wave strength and area-enlargement ratio. This was done for both perfect diatomic gases and air with $\gamma = 7/5$ and perfect monatomic gases with $\gamma = 5/3$. Finally, numerical results obtained by employing the new random choice method to solve the nonstationary equations of motiona are presented and discussed for the complete unsteady rarefaction-wave interaction with the area enlargement, for numerous different combinations of rarefaction-wave strengths and area-enlargement ratios. These results show clearly how the transmitted, reflected and other waves develop and evolve with time, until they eventually attain constant strengths at late times, in good agreement with the quasi-steady flow predictions for the asymptotic wave patterns.

Available copies of this report are limited. Return this card to UTIAS, if you require a copy.

UTIAS Report No. 273

University of Toronto, Institute for Aerospace Studies (UTIAS)
4925 Dufferin Street, Downsview, Ontario, Canada, M3H 5T6

AN ANALYTICAL AND NUMERICAL STUDY OF THE INTERACTION OF RAREFACTION WAVES WITH AREA CHANGES IN DUCTS
PART 2: AREA ENLARGEMENTS

Igra, O., Gottlieb, J. J., Saito, T.

1. Rarefaction wave 2. Duct flows 3. Flow through area change

I. Igra, O., Gottlieb, J. J., Saito, T. II. UTIAS Report No. 273

The interaction of a rarefaction wave with a gradual monotonic area enlargement of finite length in a duct or pipe is studied both analytically and numerically. A quasi-steady flow analysis that is analytical for an inviscid flow of a perfect gas is presented first, to obtain asymptotic solutions for the flow at late times, after all transient disturbances from the interaction process have subsided. Analytical results are given and discussed for the boundary between the two possible asymptotic wave patterns that are predicted and the corresponding asymptotic strengths of the transmitted, reflected and other waves, all as a function of both the incident rarefaction-wave strength and area-enlargement ratio. This was done for both perfect diatomic gases and air with $\gamma = 7/5$ and perfect monatomic gases with $\gamma = 5/3$. Finally, numerical results obtained by employing the new random choice method to solve the nonstationary equations of motiona are presented and discussed for the complete unsteady rarefaction-wave interaction with the area enlargement, for numerous different combinations of rarefaction-wave strengths and area-enlargement ratios. These results show clearly how the transmitted, reflected and other waves develop and evolve with time, until they eventually attain constant strengths at late times, in good agreement with the quasi-steady flow predictions for the asymptotic wave patterns.

Available copies of this report are limited. Return this card to UTIAS, if you require a copy.

UTIAS Report No. 273

University of Toronto, Institute for Aerospace Studies (UTIAS)
4925 Dufferin Street, Downsview, Ontario, Canada, M3H 5T6

AN ANALYTICAL AND NUMERICAL STUDY OF THE INTERACTION OF RAREFACTION WAVES WITH AREA CHANGES IN DUCTS
PART 2: AREA ENLARGEMENTS

Igra, O., Gottlieb, J. J., Saito, T.

1. Rarefaction wave 2. Duct flows 3. Flow through area change

I. Igra, O., Gottlieb, J. J., Saito, T. II. UTIAS Report No. 273

The interaction of a rarefaction wave with a gradual monotonic area enlargement of finite length in a duct or pipe is studied both analytically and numerically. A quasi-steady flow analysis that is analytical for an inviscid flow of a perfect gas is presented first, to obtain asymptotic solutions for the flow at late times, after all transient disturbances from the interaction process have subsided. Analytical results are given and discussed for the boundary between the two possible asymptotic wave patterns that are predicted and the corresponding asymptotic strengths of the transmitted, reflected and other waves, all as a function of both the incident rarefaction-wave strength and area-enlargement ratio. This was done for both perfect diatomic gases and air with $\gamma = 7/5$ and perfect monatomic gases with $\gamma = 5/3$. Finally, numerical results obtained by employing the new random choice method to solve the nonstationary equations of motiona are presented and discussed for the complete unsteady rarefaction-wave interaction with the area enlargement, for numerous different combinations of rarefaction-wave strengths and area-enlargement ratios. These results show clearly how the transmitted, reflected and other waves develop and evolve with time, until they eventually attain constant strengths at late times, in good agreement with the quasi-steady flow predictions for the asymptotic wave patterns.

Available copies of this report are limited. Return this card to UTIAS, if you require a copy.